NAVAL POSTGRADUATE SCHOOL
Monterey, California

THESIS

CEAREX AMBIENT NOISE DATA MEASURED
NORTHEAST OF SVALBARD

by

John David Cousins

March, 1991

Thesis Co-Advisors: Robert H. Bourke
Robert S. Pritchard

Approved for public release; distribution is unlimited.

T256217

Unclassified
SECURITY CLASSIFICATION OF THIS PAGE

REPORT DOCUMENTATION PAGE

Form Approved
OMB No 0704-0188

1a REPORT SECURITY CLASSIFICATION: UNCLASSIFIED	1b RESTRICTIVE MARKINGS
2a SECURITY CLASSIFICATION AUTHORITY	3 DISTRIBUTION / AVAILABILITY OF REPORT
2b DECLASSIFICATION / DOWNGRADING SCHEDULE	
4 PERFORMING ORGANIZATION REPORT NUMBER(S)	5 MONITORING ORGANIZATION REPORT NUMBER(S)
6a NAME OF PERFORMING ORGANIZATION: Naval Postgraduate School; 6b OFFICE SYMBOL (If applicable): Code 35	7a NAME OF MONITORING ORGANIZATION: Naval Postgraduate School
6c. ADDRESS (City, State, and ZIP Code): Monterey, CA 93943-5000	7b ADDRESS (City, State, and ZIP Code): Montery, CA 93943-5000
8a. NAME OF FUNDING / SPONSORING ORGANIZATION; 8b OFFICE SYMBOL (If applicable)	9 PROCUREMENT INSTRUMENT IDENTIFICATION NUMBER
8c. ADDRESS (City, State, and ZIP Code)	10 SOURCE OF FUNDING NUMBERS: PROGRAM ELEMENT NO; PROJECT NO; TASK NO; WORK UNIT ACCESSION NO

11 TITLE (Include Security Classification)
CEAREX AMBIENT NOISE DATA MEASURED NORTHEAST OF SVALBARD

12 PERSONAL AUTHOR(S)
Cousins, John David

13a TYPE OF REPORT	13b TIME COVERED	14 DATE OF REPORT (Year, Month, Day)	15 PAGE COUNT
Master's Thesis	FROM _____ TO _____	March 1991	132

16 SUPPLEMENTARY NOTATION

17 COSATI CODES			18 SUBJECT TERMS (Continue on reverse if necessary and identify by block number)
FIELD	GROUP	SUB-GROUP	CEAREX, Ambient Noise, Arctic Ambient Noise, Svalbard

19 ABSTRACT (Continue on reverse if necessary and identify by block number)

Ambient Noise measurements made northeast of Svalbard from two omni-direction hydrophones, deployed at 60 and 90 m beneath the ice, were acquired as the research vessel Polarbjoern drifted southward from 11 October to 18 November 1988. The ambient noise data as well as the accompanying meteorological and ice motion data were collected as part of the Coordinated Eastern Arctic Experiment, CEAREX. The ambient noise measurements were composed of one and a half minute samples that were averaged hourly to provide a 38-day time series at 10, 31.5, and 100 Hz. Higher frequencies were considered valid only above the median level due to high system electronic noise. Measurements were obtained in deep and shallow water (100 m) as the ship drifted generally southwestward with the ice pack towards the Svalbard Archipelago. The ambient noise time series were correlated with hourly-averaged wind, air temperature, and ice motion data in order to determine its association with the major noise

20 DISTRIBUTION / AVAILABILITY OF ABSTRACT	21 ABSTRACT SECURITY CLASSIFICATION	
☒ UNCLASSIFIED/UNLIMITED ☐ SAME AS RPT ☐ DTIC USERS	Unclassified	
22a NAME OF RESPONSIBLE INDIVIDUAL: Dr. Robert H. Bourke	22b TELEPHONE (Include Area Code): (408) 646 - 3270	22c OFFICE SYMBOL: OCBf

DD Form 1473, JUN 86 — Previous editions are obsolete — S/N 0102-LF-014-6603

SECURITY CLASSIFICATION OF THIS PAGE
Unclassified

generating mechanisms. Both visual and numerical comparisons between the ambient noise and the environmental parameters revealed significant correlations. The two primary forces operating on the ice pack were the wind stress and 12-hour tidal/ inertial oscillations. When either of these forces opposed the mean direction of ice motion, there was increased convergence and higher levels of ambient noise were experienced. The mean ambient noise levels northeast of Svalbard were 20-30 dB higher than typical central Arctic basin values due to the active ridging encountered immediately north of the Svalbard Archipelago. These noise levels compare favorably with other active ridging regions or dynamically active regions such as the marginal ice zone.

Approved for public release; distribution is unlimited.

CEAREX AMBIENT NOISE DATA MEASURED NORTHEAST OF SVALBARD

by

John D. Cousins
Lieutenant, United States Navy
B.S., Pennsylvania State University, 1983

Submitted in partial fulfillment
of the requirements for the degree of

MASTER OF SCIENCE IN METEOROLOGY AND PHYSICAL OCEANOGRAPHY

from the

NAVAL POSTGRADUATE SCHOOL
March 1991

TK563
C756783
C.1

ABSTRACT

Ambient noise measurements made northeast of Svalbard from two omni-directional hydrophones, deployed at 60 and 90 m beneath the ice, were acquired as the research vessel *Polarbjoern* drifted southward from 11 October to 18 November 1988. The ambient noise data as well as the accompanying meteorological and ice motion data were collected as part of the Coordinated Eastern Arctic Experiment, CEAREX. The ambient noise measurements were composed of one and a half minute samples that were averaged hourly to provide a 38-day time series at 10, 31.5, and 100 Hz. Higher frequencies were considered valid only above the median level due to high system electronic noise. Measurements were obtained in deep and shallow water (<100 m) as the ship drifted generally southwestward with the ice pack towards the Svalbard Archipelago. The ambient noise time series were correlated with hourly-averaged wind, air temperature, and ice motion data in order to determine its association with the major noise generating mechanisms. Both visual and numerical comparisons between the ambient noise and the environmental parameters revealed significant correlations. The two primary forces operating on the ice pack were the wind stress and 12-hour tidal/inertial oscillations. When either of these forces opposed the mean direction of ice motion, there was increased convergence and higher levels of ambient noise were experienced. The mean ambient noise levels northeast of Svalbard were 20-30 dB higher than typical central Arctic basin values due to the active ridging encountered immediately north of the Svalbard Archipelago. These noise levels compare favorably with other active ridging regions or dynamically active regions such as the marginal ice zone.

TABLE OF CONTENTS

I. INTRODUCTION 1

A. PURPOSE 1

B. OBJECTIVES 1

C. BACKGROUND 2

D. ORGANIZATION 7

II. DATA COLLECTION 8

A. AMBIENT NOISE MEASUREMENTS 9

B. AMBIENT NOISE PROCESSING 11

C. METEOROLOGICAL MEASUREMENTS 14

III. DATA ANALYSIS 16

A. AMBIENT NOISE SPECTRUM 16

1. Time Series Analysis 16

2. Hourly Autocorrelations 29

B. METEOROLOGICAL ANALYSIS 31

1. Wind Data 31

2. Temperature Data 39

C. ICE MOTION ANALYSIS 43

IV. CROSS-CORRELATIONS 52

A. ICE MOTION FORCING FUNCTIONS 52
B. WIND and ICE MOTION 57
1. Wind Speed and Ice Speed 57
2. Wind Direction and Ice Direction 60
C. WIND SPEED and AMBIENT NOISE 65
D. ICE SPEED and AMBIENT NOISE 67
E. TEMPERATURE and AMBIENT NOISE 72
F. FREQUENCY COMPARISONS 74

V. EVENT ANALYSIS 77
A. MOTION vs AMBIENT NOISE 77
B. AMBIENT NOISE vs. WIND SPEED 83
C. WARMING vs. COOLING TRENDS 85
D. ANALYSIS OF SHALLOW WATER RIDGING ENVIRONMENT . 86
1. Time Series Analysis 86
2. Cross-correlations 94
E. SHALLOW vs. DEEP WATER AMBIENT NOISE 103
F. STANDARD DEVIATION COMPARISONS 105

VI. SUMMARY, CONCLUSION, AND RECOMMENDATIONS . . . 110
A. SUMMARY 110
B. CONCLUSIONS 111
C. RECOMMENDATIONS 113
D. LIST OF REFERENCES. 115
E. INITIAL DISTRIBUTION LIST. 118

LIST OF TABLES

1. STATISTICAL INFORMATION FOR THE FREQUENCIES OF 10, 31.5, AND 100 HZ (JULIAN DAYS 285-323).....21

2. SUMMARY OF HOURLY AVERAGED WIND DIRECTION DATA SORTED INTO 30 DEGREE SECTORS BY FREQUENCY AND PERCENT.....33

3. STATISTICAL DATA FOR WIND SPEED, TEMPERATURE, AND ICE SPEED. CALCULATED FROM HOURLY AVERAGED DATA.....35

4. AMBIENT NOISE RECORDED DURING NORTHERLY AND SOUTHERLY ICE MOTION FOR THE FREQUENCIES OF 10, 31.5, AND 100 HZ.....79

5. STATISTICAL INFORMATION FOR THE FREQUENCIES OF 10, 31.5, 100, 315, 630, AND 1000 HZ (JULIAN DAYS 317-324).....90

LIST OF FIGURES

1.1 Drift track of the Research Vessel *Polarbjoern* from Julian Day 260 to 330 (16 September-25 November).....6

2.1 Plot of electronic system "self noise" spectrum.....10

2.2 31.5 Hz ambient noise time series plotted with data averaged over intervals from 15 minutes to 24 hours....12

3.1 Hourly-averaged time series for 10, 31.5, and 100 Hz.....17

3.2 Hourly-averaged ambient noise time series for 315, 630, and 1000 Hz.....18

3.3 Measured and composite ambient noise spectra for frequencies from 10 to 1000 Hz.....20

3.4 Comparison of spectral slopes from 38-day composite, 38-day 95th percentile, 7-day shallow water, and slopes derived from two previous ambient noise studies by Bradley (1986) and Urick (1975).....22

3.5 The mean and standard deviations for frequencies from 10 to 100 Hz.....23

3.6 Comparison of Pritchard's Barents Sea spectrum with deep water spectra acquired from other ice-covered regions by Lewis and Denner (1987), Makris and Dyer (1986), and Urick (1975).....25

3.7 Comparison of Pritchard's Barents Sea spectrum with spectra obtained from other dynamically active regions.....27

3.8 NOAA-10 imagery of the region northeast of Svalbard....28

3.9 Autocorrelations for frequencies of 10, 31.5, and 100 Hz.....30

3.10 Frequency histogram of true wind direction.....32

3.11 Frequency histogram of wind speed.....34

3.12 Three dimensional frequency histogram of wind speed and wind direction.....36

3.13 Time series of hourly-averaged wind speed that was recorded from 11 October to 18 November 1988 (Julian day 285-323) onboard the *Polarbjoern*.....37

3.14 Autocorrelation of hourly-averaged wind speed.....38

3.15 Frequency histogram of temperature 40

3.16 Time series of hourly-averaged temperatures that were measured onboard the *Polarbjoern* from 11 October to 18 November 1988 (Julian days 285-323).....41

3.17 An autocorrelation of hourly-averaged temperature.....42

3.18 Time series of hourly interpolated ice speed and U & V-components of ice speed from 11 October to 18 November 1988 (Julian days 285-323).....44

3.19 Frequency histogram of hourly-averaged ice speed.....45

3.20 Hourly-averaged ice motion (direction and speed) for Julian days 300 and 301 (26-27 October 1988).....47

3.21 Autocorrelation of hourly-averaged ice speed.....48

3.22 Cross-correlations of U & V components of ice speed....51

4.1 Hourly-averaged time series of ice speed from 11 October to 18 November 1988 (Julian days 285-323)...54

4.2 Hourly-averaged time series of wind speed and ice speed for Julian days 307-318.....56

4.3 Cross-correlations between the 38-day wind speed and ice speed records.....58

4.4 Hourly-averaged wind and ice motion (direction and speed) time series for Julian days 285-323.....61

4.5 Hourly-averaged wind and ice motion (speed and direction) time series for Julian days 300-302.....63

4.6 Hourly-averaged wind and ice motion (speed and direction) time series for Julian days 288-301.....64

4.7 Cross-correlations between wind speed and ambient noise for frequencies of 10, 31.5, and 100 Hz.....66

4.8 Cross-correlations between ice speed and ambient noise for frequencies of 10, 31.5, and 100 Hz.....69

4.9 Hourly-averaged time series for wind speed, ice speed, and 10 Hz (Julian days 307-318).....71

4.10 Cross-correlations between temperature and ambient noise for frequencies of 10, 31.5 and 100 Hz.....73

4.11 Cross-correlations between the hourly-averaged 10, 31.5, and 100 Hz time series.....75

5.1 Spectral plot comparing the ambient noise levels recorded during northerly and southerly ice motion.....78

5.2 Spectral plots comparing ambient noise levels for northerly and southerly motion in during two different periods of the record.....81

5.3 Spectral plots comparing the ambient noise at different wind speeds from 0 to 20 m/s.....84

5.4 Spectral plots comparing the ambient noise levels recorded during a warming trend and a cooling trend....87

5.5 Hourly-averaged time series of wind and temperature that display the relationship between warming and cooling trends and wind direction.....88

5.6 Hourly-averaged time series for wind speed, ice speed, and temperature on Julian days 317-324.....89

5.7 Median ambient noise levels in a region of active ridging north of Kvitoya for Julian days 317-324.....91

5.8 Hourly-averaged ambient noise time series for frequencies of 10, 31.5, 100, 315, 630, and 1000 Hz....92

5.9 Cross-correlations of 7-day wind speed and ambient noise time series for 10, 31.5, 100, 315, 630, and 1000 Hz during Julian days 317-324 (12-19 November)....95

5.10 Comparison between 38-day and 7-day cross-correlations of wind speed and ambient noise (10, 31.5, 100 Hz).....97

5.11 Cross-correlations of 7-day ice speed and ambient noise time series for 10, 31.5, 100, 315, 630, and 1000 Hz during Julian days 317-324 (12-19 November)....98

5.12 Comparison of 38-day and 7-day cross-correlations of ice speed and ambient noise (10, 31.5, 100 Hz).....99

5.13 Cross-correlations between 7-day hourly averaged 1/3 octave bands measured during Julian days 317-324.....101

5.14 Comparison of 38-day and 7-day 1/3 octave band cross-correlations (10 Hz/31.5 Hz, 31.5 Hz/100 Hz, and 10 Hz/100 Hz).....102

5.15 Comparison of deep water (days 284-291), shallow water (days 317-324), and composite (days 285-323) spectral plots.....104

5.16 Variations in ambient noise standard deviations with increasing wind speed near Bermuda and Fiji.....107

5.17 Comparison of ambient noise standard deviations in ice covered waters northeast of Svalbard.....108

5.18 Comparison of standard deviations during periods of high ambient noise (days 317-324) and low ambient noise (days 304-312).....109

I. INTRODUCTION

A. PURPOSE

Although numerous Arctic ambient noise studies have been conducted, many of them were simple descriptions of the observed ambient noise level. Where additional analysis needs to be concentrated is in the determination of the actual forcing functions involved in ambient noise generation. The underlying physics involved in the generation of ambient noise in ice covered regions must be understood before effective noise prediction algorithms and models can be developed.

B. OBJECTIVES

One of the primary objectives of this study was to analyze the ambient noise record in the region northeast of Svalbard. This in itself is a significant accomplishment given the paucity of shallow water ambient noise experiments that have been conducted in the Arctic and the absence of detailed studies in this region in the past. The bulk of the previous ambient noise experiments have been conducted in the deep waters of the central Arctic.

Another objective of this study was to determine the relative association of several expected forcing functions to the observed under-ice ambient noise. Wind speed and direction, air temperature, and ice motion (both speed and direction) were analyzed for their effect on ambient noise.

C. BACKGROUND

In order to lay the foundation for subsequent ambient noise discussions, a brief review of previous Arctic ambient noise studies will be conducted.

Arctic ambient noise is a composite of many different noise sources. Dyer (1983) divided the ambient noise spectrum into a number of spectral sectors and identified the major sources of ambient noise within each sector. The major noise sources he identified were flow noise, cable strum, ice action, and thermal cracking.

In the frequency range from 0.1 to 0.5 Hz, the quasi-static velocity fluctuations in the flow past the hydrophone (flow noise) was responsible for the majority of the ambient noise. In the spectral sector from 0.5 to 10 Hz, currents and eddies have the potential of inducing oscillations in the hydrophone cables. These oscillations are known as cable strum and, if present, can effectively mask the noise levels in this frequency spectrum. Thus, these lower frequencies are very susceptible to masking by instrument related noise. When the frequency spectrum is not contaminated by cable strum, it generally displays a broad spectral peak that lies between 10 and 20 Hz. Dyer attributes this noise (which dominates the 1-100 Hz range) to "ice action" which is composed of a number of different processes that occur when ice is placed under stress and fails. The final noise generating mechanism described by

Dyer is that of atmospheric cooling which results in increased ambient noise due to thermal cracking.

Thermal cracking was first described in detail by Milne (1972). During cooling trends, heat loss at the surface of the ice results in greater cooling than that found in the interior of the ice. The surface of the ice contracts more than the interior resulting in increased tensile stress. This stress is released through surface-tension cracks that are exhibited in the ambient noise spectrum as broad maxima in the 60-1000 Hz range. In a more recent study, Makris and Dyer (1986) showed that while the atmospheric cooling is a high correlate of mid-frequency noise, it is considerably less important at low frequencies.

As described above, Dyer attributed the peak ambient noise to ice action that resulted from increased stress. One of the primary sources of stress on the Arctic ice pack is the wind. Thorndike and Colony (1982) and Serreze (1989) revealed that approximately 70 percent of the variance in daily ice motion is accounted for by the geostrophic wind and that a similar relationship is demonstrated with the surface wind. Large-scale correlations of the atmospheric pressure field (Green and Buck, 1978) generally show a higher correlation with ambient noise than local wind measurements because a large portion of the wind generated noise is derived from distant sources.

Lewis and Denner (1987a) found that during the summer the highest correlation with low frequency ambient noise was with ice speed. During the fall and winter ice interactions such as ridging and rafting become the dominant sources of ambient noise. In his analysis of ambient noise measurements that were collected in the Beaufort Sea during AIDJEX, Pritchard (1984) also discovered that ridging was the single largest source of ambient noise in the winter. Average noise levels between 80-97 dB have been measured in regions of active ridging in the central Arctic (Buck and Wilson, 1986).

In measurements of the spatial and temporal coherency of ambient noise in the Beaufort Sea, Lewis and Denner (1987a) revealed e-folding length scales of several hundred kilometers and time scales of 10-30 hours. Given the strong relationship between wind speed and ambient noise discussed earlier, it is not surprising that the spatial coherence for ambient noise coincides with the scale size of synoptic weather systems.

The lack of previous ambient noise measurements in the region northeast of Svalbard, and in ice-covered shallow water in general, provided little information with which this study could be directly compared. Two studies were found which were relevant. Mean ambient noise levels of 83 dB at 20 Hz and 69.3 dB at 100 Hz were obtained from unclassified portions of the AEAS Arctic ambient noise data base (Bradley and Hartley, 1986) for winter conditions in the region northeast of Svalbard. The data base also contained standard deviations of

5.2 and 2.5 dB for the frequencies of 20 Hz and 100 Hz, respectively. In a separate study, Poffenburger and Bourke (1987) analyzed ambient noise data from drifting buoys in the Eurasian Basin. One buoy, which passed several hundred kilometers to the north of Svalbard, provided measurements with which the deep water portion of this study could be compared. Median ambient noise levels of 71 dB and 63 dB were collected at 10 and 100 Hz, respectively, and a temporal coherence of about 1.5 days was observed.

D. CEAREX

All of the meteorological, acoustical, and ice motion data utilized in this study were collected on board the research vessel *Polarbjoern* during the fall of 1988, as part of the Coordinated Eastern Arctic Experiment, CEAREX. The *Polarbjoern* was accompanied by the icebreaker *USCG Northwind* and first entered the polar ice pack during the early days of September 1988. The *Polarbjoern* was allowed to freeze into the ice on 16 September at 82°41′N 32°26′E (Pritchard, 1989).

The *Polarbjoern* drifted to the southeast towards the islands of Franz Joseph Land and Ostrov Viktoriya (Figure X) for the first 30 days before shifting to a southwesterly drift on 16 October (Julian day 290). This southwesterly drift carried the ship between the islands of Kvitoya and Nordaustlandet during the last week of November. All CEAREX related drift operations were completed by mid-January 1989.

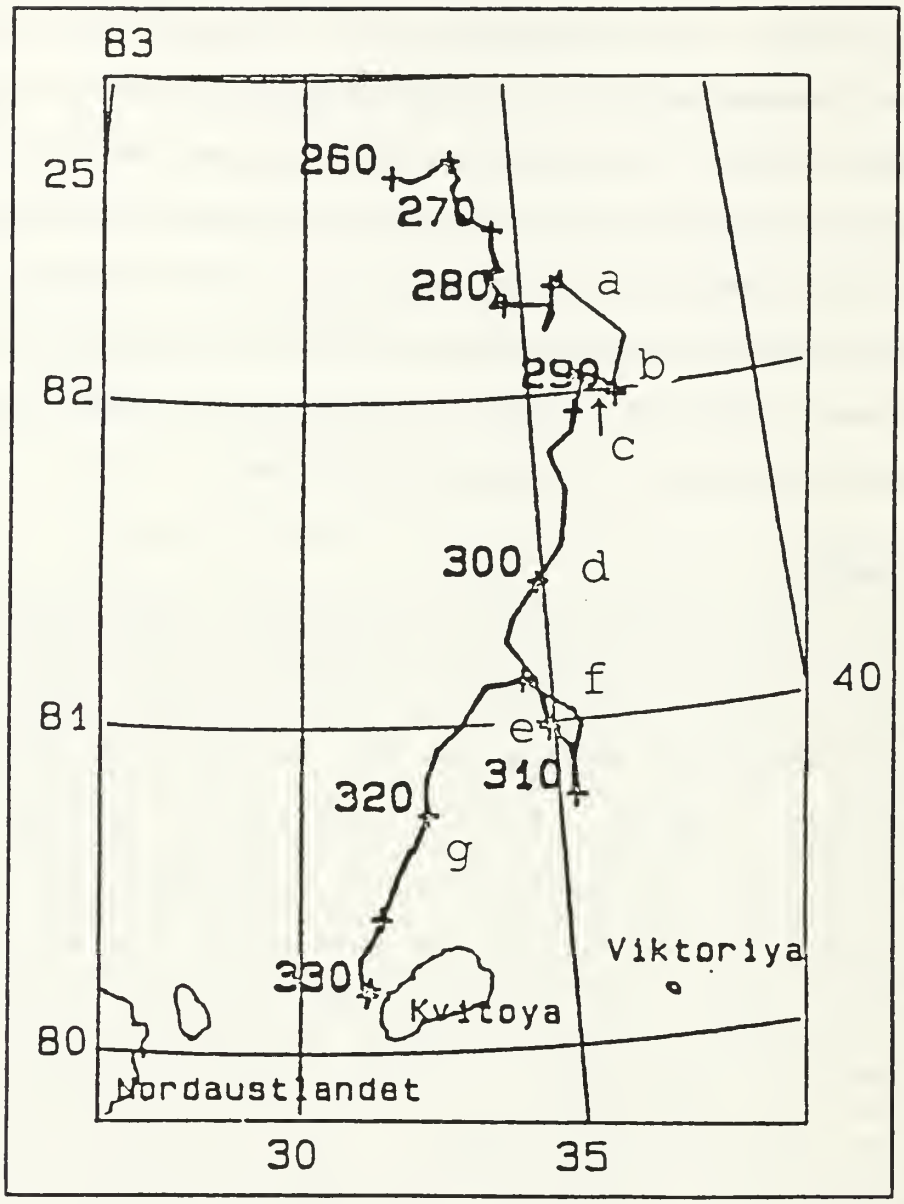

Figure 1.1 Drift track of the Research Vessel *Polarbjoern* from Julian Day 260 to 330 (16 September-25 November 1988) (from Pritchard, 1989).

E. ORGANIZATION

The remainder of this thesis is organized in a manner similar to the way in which this study was conducted; data collection, analysis, correlation, and then conclusions. Chapter II examines the various means by which the ambient noise and environmental data were collected and initially processed. In Chapter III the analysis of the different parameters is conducted. This includes time series analysis, autocorrelations, and simple statistical computations. The actual comparison and cross-correlation of the 38-day ambient noise and environmental data sets are conducted in Chapter IV. A more detailed analysis of the relationship between the ambient noise, wind, ice motion, and air temperature are described in Chapter V. This chapter divides the record into specific events in order to obtain a more detailed look at the various influences on ambient noise. Chapter VI summarizes the results and conclusions of this thesis and makes recommendations for future research.

II. DATA COLLECTION

Ambient noise, ice motion, and meteorological data were obtained from a region in the Barents Sea, northwest of Svalbard. The data sets used in this analysis were compiled over a six week period as the *Polarbjoern*, and the flow in which she was frozen, drifted southwards from 11 October to 18 November 1988. Figure 1.1 shows the trajectory of the ship drift. As the *Polarbjoern* approached the island of Kvitoya, extreme ridging and fracturing of the ice pack forced the removal of the tethered hydrophones from the ice due to the repeated disconnection of the instrumentation cables.

Six discrete frequencies 10, 31.5, 100, 315, 630, and 1000 Hz, were initially chosen for analysis. Subsequent investigation revealed that the higher frequencies were significantly masked by system "self noise" during relatively quiet periods. Therefore, the majority of this study will be focused on the three lowest frequencies: 10, 31.5, and 100 Hz. Additional emphasis will be placed on the extremely high ambient noise levels and ridging conditions encountered during the last week of the drift period before the floe began to break-up.

A. AMBIENT NOISE MEASUREMENTS

As summarized by Pritchard (1989), ambient noise data were obtained via two calibrated omni-directional hydrophones that were tethered beneath the ice at depths of 60 and 90 m. The hydrophones were deployed approximately 1 km from the *Polarbjoern*. The hydrophone output was amplified and then transferred through a shielded instrumentation cable, through a low-pass Butterworth filter with an adjustable corner frequency, and then through an A/D interface board in a Compaq 386/20 computer.

A LOFAR computer program (Prada, 1986) provided a real time, interactive capability to acquire and display the ambient noise time series and their spectra. The system was initially designed to process frequencies below 500 Hz, but when unexpectedly high noise levels were discovered at 630 and 1000 Hz, a decision was made to attempt to record these frequencies. Since the anti-aliasing filter was set at approximately half of the frequency maximum, the initial processing frequency maximum was increased from 512 Hz to as high as 8192 Hz. This increase allowed the collection of non-aliased noise data up to about 4 kHz (Pritchard, personal communication, 1991).

The system's electronic or "self noise" was estimated by disconnecting the hydrophone and measuring the resulting signal. The "system" then consisted of the shielded instrumentation cable, the anti-aliasing filter, the A/D

converter, and the computer. The system's self noise was determined on 6 November while the maximum frequency was set at 2048 Hz and the anti-aliasing filter was set at 1400 Hz (Pritchard, 1989). The spectrum of the "system self noise" is shown in Figure 2.1. Note that the spectrum is relatively constant 72 dB (re uPa²/Hz) across the frequency spectrum. The high level of the system self noise is believed to be the result of dynamic range limitations (36 dB) in the 12-bit A/D converter. The 36 dB dynamic range was sufficient for the low

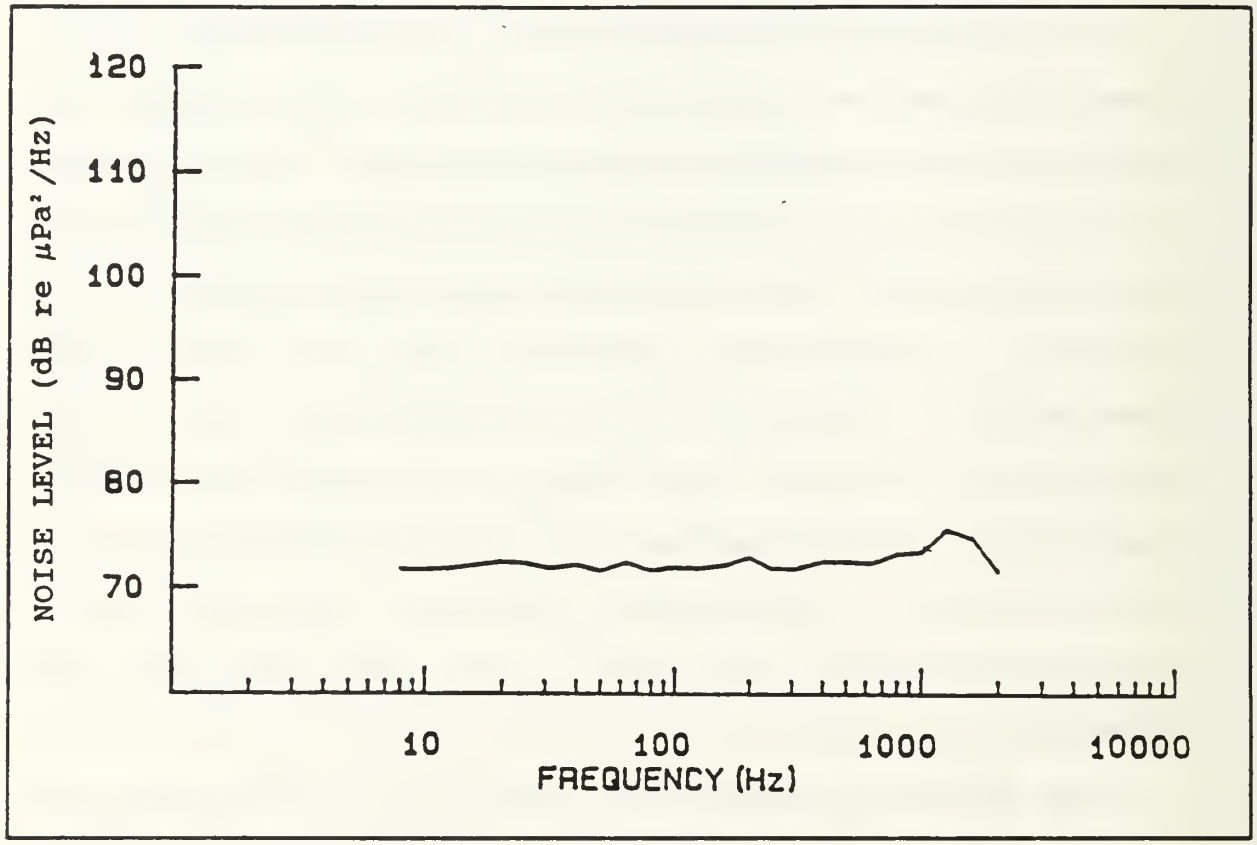

Figure 2.1 An electronic system "self noise" level of about 72 dB (re $\mu Pa^2/Hz$) was measured when the hydrophone was disconnected from the rest of the ambient noise acquisition system (from Pritchard, 1989).

frequency noise spectrum (< 500 Hz) initially planned for but was not broad enough to contain the low noise levels associated with the higher frequencies. For reasons that have yet to be determined, this relatively high level of system self noise occasionally decreased for periods from several hours to several days at a time, dropping by as much as 10 dB, thus allowing the collection of low amplitude signals.

B. AMBIENT NOISE PROCESSING

The ambient noise data were further processed via a fast fourier transform (FFT) and then averaged in order to obtain the most representative results possible. As described by Pritchard (personal communication, 1991), a fast fourier transform was performed on blocks of 1024 data points as they were received from the hydrophone. Once 128 FFTs were summed and then averaged, this provided one processed data point approximately every 1.5 minutes. Using a maximum processing frequency of 512 Hz, approximately 50 percent of the data collection period was used to sample ambient noise while the other 50 percent was spent processing the data.

Ambient noise time series were plotted with raw and averaged data in order to examine the effect of the different scales of forcing. The effects of averaging the ambient noise record at various intervals from 15 minutes to 24 hours may be observed in Figure 2.2. Averaging intervals of 15 minutes, one hour, and three hours provide a reasonably good

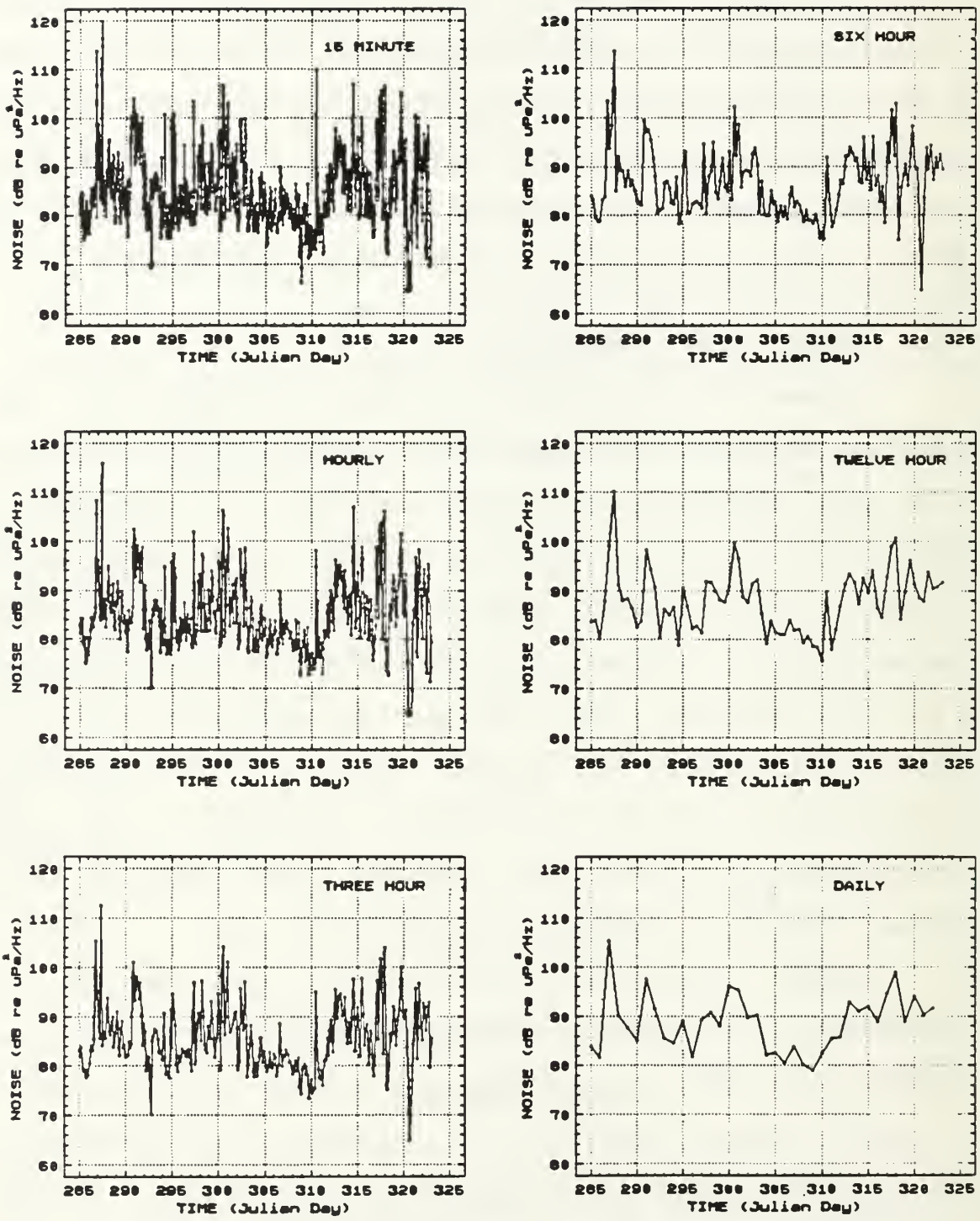

Figure 2.2 31.5 Hz ambient noise time series plotted with data averaged over intervals from 15 minutes to 24 hours.

representation of the high frequency fluctuations. When the data were averaged over intervals greater than the tidal/inertial Nyquist frequency (6 hours), these oscillations were quickly smoothed from the record.

All ambient noise and environmental data utilized in this study were ultimately averaged over one hour intervals. This averaging was performed in order to remove unwanted high frequency fluctuations, facilitate data processing, and to provide a data base with uniform time intervals.

One of the major objectives of this study was to determine what the major forcing functions for ambient noise were in the region northeast of Svalbard. In accomplishing this, it was deemed essential that variations in the ambient noise record greater than 4-6 hours be resolvable. This time scale was established in order to include the highly influential tidal/inertial oscillations often encountered in this region. Thus by averaging the data over a one hour interval, all high frequency fluctuations that were not germane to this study were removed while still meeting the 4 hour resolution criteria.

The sheer number of observations taken also required some sort of averaging in order to reduce the amount of time required to complete even relatively simple numerical operations. Averaging was also conducted in order to improve data presentation. The large number of observations could not

be handled by some plotting programs and presented a cluttered appearance on others.

The final reason for averaging was to provide a complete data set with uniform time intervals. With the same one hour time interval present in all meteorological, ice motion, and ambient noise data sets, comparisons and correlations could be more easily accomplished.

C. METEOROLOGICAL MEASUREMENTS

Meteorological data used in this experiment were obtained using a Coastal Climate WeatherPak Meteorological Station. Details concerning instrumentation and data accuracy can be obtained from the CEAREX/POLARBJOERN METEOROLOGY ATLAS (Lackman et al.,1989). The instruments were positioned forward of the *Polarbjoern's* bow mast at a height of 14 m above sea level. The air temperature data are considered accurate to within 1.0°C; wind speed and direction are accurate to within 0.3 m/s and 10 degrees. Due to the location of the wind gauges, errors may be slightly larger when winds were from directly astern. This was a rare occurrence due to the ship's heading and the predominantly northerly winds experienced during the experiment. Only relatively small corrections were required to compensate for the ship's motion. Meteorological observations were based on ten minute vector averages collected every ten minutes. These ten minute values were then averaged to obtain the hourly data

used in this analysis (Davidson and Guest, personal communication, 1991).

D. ICE MOTION MEASUREMENTS

Ice motion data for this study was based on position and velocity analysis conducted by McPhee (1988). The navigational information from which McPhee derived his analysis came principally from SATNAV and ARGOS buoy positions. Figure 1.1, the drift track of the *Polarbjoern* from Julian day 260-330, was computed from daily interpolated positional information that smoothed all high frequency oscillations. All other ice speed and ice direction data were derived from hourly interpolated measurements.

III. DATA ANALYSIS

A. AMBIENT NOISE SPECTRUM

1. Time Series Analysis

The hourly-averaged ambient noise time series for 10, 31.5, and 100 Hz are presented in Figure 3.1. There are two obvious time scales on which the noise levels vary. The high frequency fluctuations vary rapidly with several 30-40 dB peak-to-peak oscillations common within a 24 hour period. These high frequency variations are then superimposed on a more slowly varying background signal that changes on a 2-10 day time scale. Both the high and low frequency variations are evident at all three frequencies but tend to be of lesser magnitude at higher frequencies and during relatively quiet periods.

The hourly-averaged time series for 315 Hz, 630 Hz, and 1000 Hz are presented in Figure 3.2. As discussed earlier, a system electronic noise was relatively steady at 72 dB across all sampled frequencies thus making it more significant at these higher frequencies where the noise amplitudes are smaller. During relatively quiet periods, such as Julian days 302-305 and 311-312, the system electronic noise served as a "floor" below which the true ambient noise level could not be determined. The overall result was the contamination of the

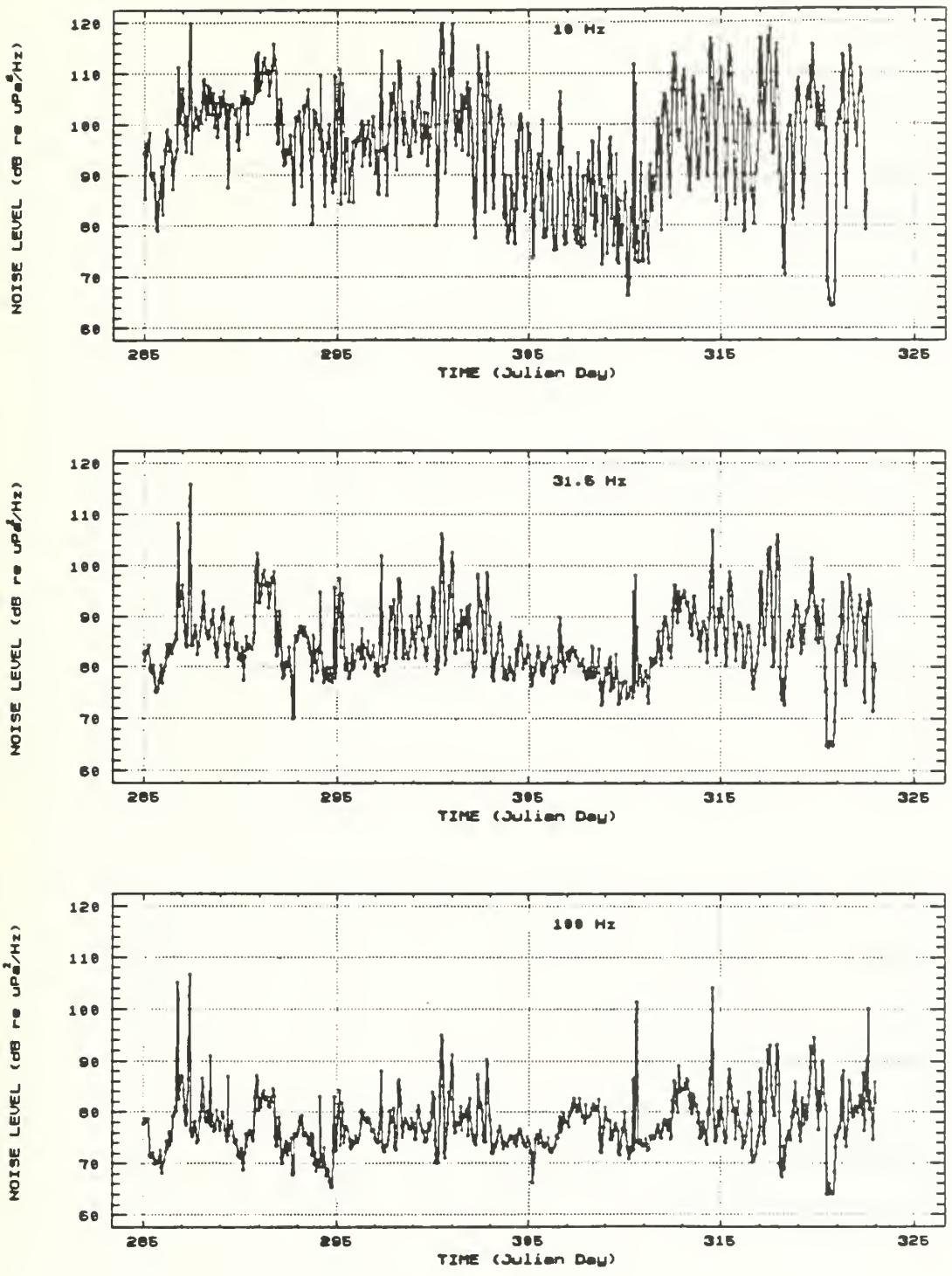

Figure 3.1 Hourly-averaged time series for 10, 31.5, and 100 Hz. High frequency oscillations (30-40 dB) are superimposed on a slowly varying backgound signal.

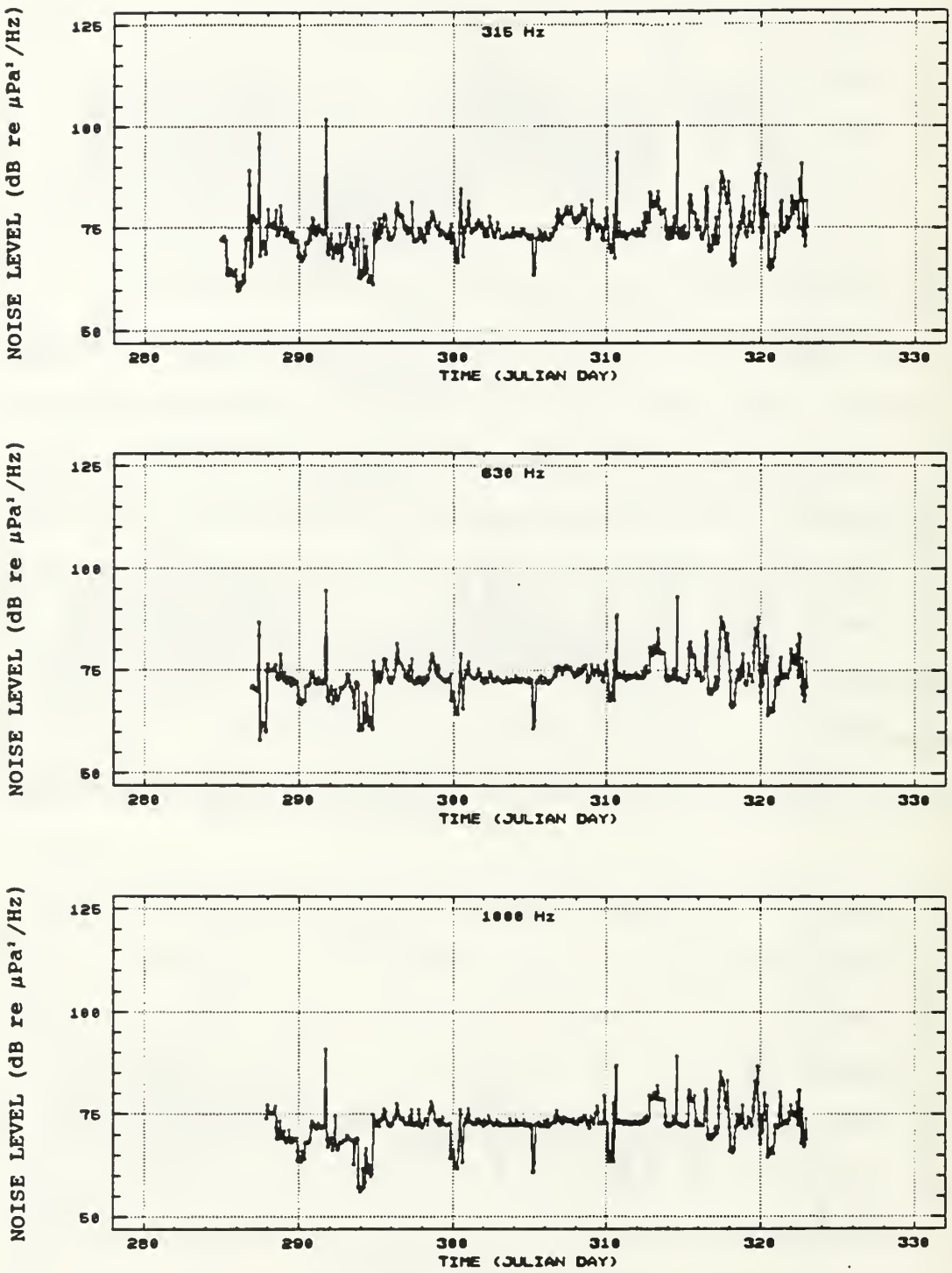

Figure 3.2 Hourly-averaged ambient noise time series for 315, 630, and 1000 Hz. A 72 dB electronic noise "floor" contaminated the noise record during quiet periods.

high frequency record up to at least the fiftieth percentile values.

Instead of discarding the entire high frequency record, the high amplitude portions of the record which were not contaminated were used to generate a composite high frequency spectrum. This composite frequency spectrum was constructed by analyzing the apparently uncontaminated sections of the ambient noise record (i.e., 10-1000 Hz), by examining the distribution of data points above the "floor", and by making comparisons with other dynamic high ambient noise environments. The aliased and composite values for the median ambient noise frequency spectrum are plotted in Figure 3.3. The largest adjustment was at 1000 Hz where the median value was depressed by 4 dB. The process by which this composite spectrum was generated will be discussed more fully below.

During the last week of data collection, days 317-323, the high ambient noise associated with local ridging elevated spectrum levels above the system self noise. During this 7-day period, the slopes of the median and ninety-fifth percentile were similar to that of the ninety-fifth percentile determined from the complete record, days 285-323. Thus, these slopes (7-day median and the 38-day ninety-fifth percentile) were used to construct a composite spectrum for the higher frequencies: 315, 630, and 1000 Hz. The 38-day ninety-fifth percentile, the 7-day median, and the composite

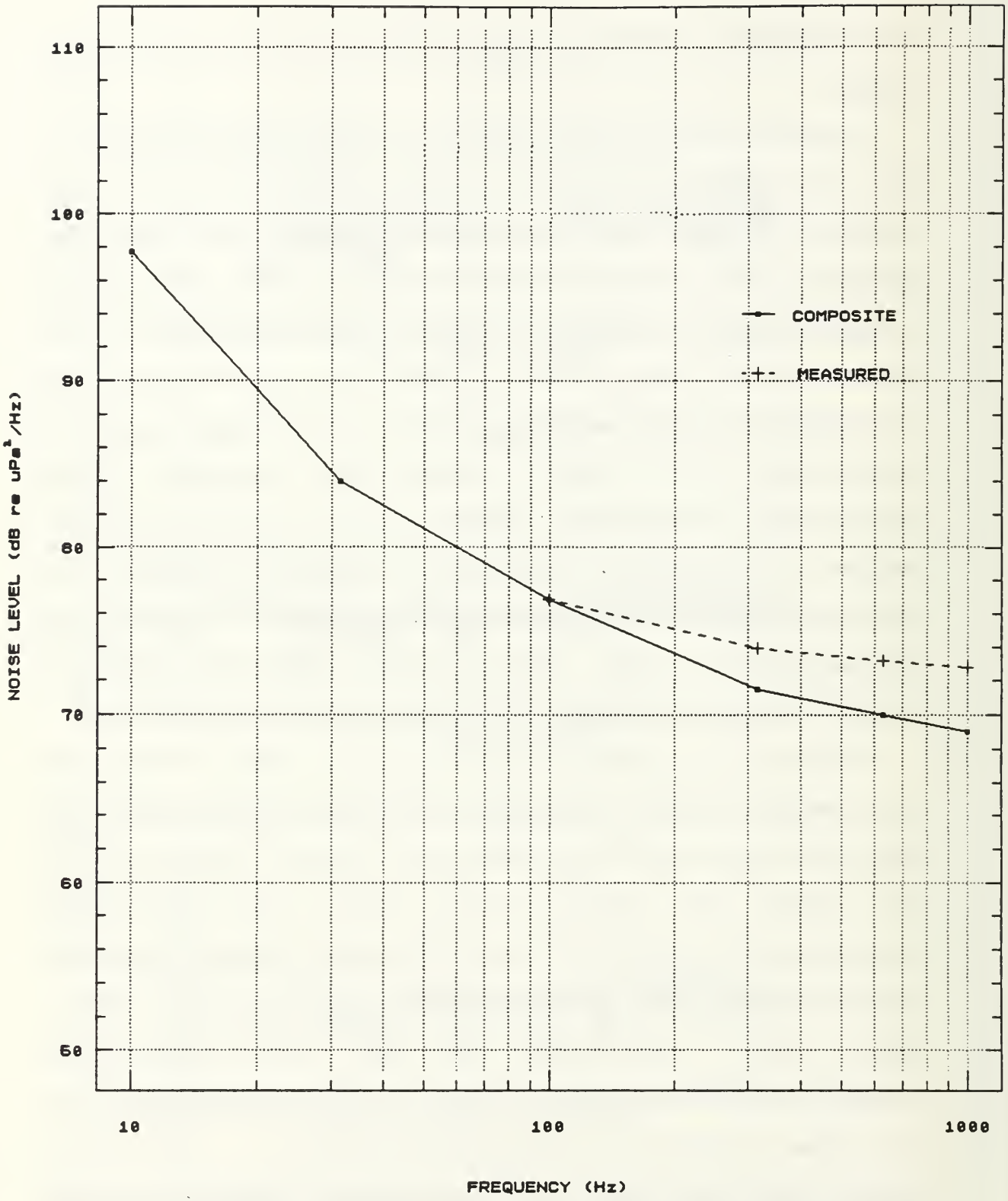

Figure 3.3 Measured and composite ambient noise spectra for frequencies from 10 to 1000 Hz.

median spectrum can be compared with measurements from other high ambient noise environments in Figure 3.4. The composite frequency spectrum compares quite favorably with previous ambient noise studies conducted by Bradley (1986) and Urick (1975). Thus the composite slope obtained from unaliased portions of the record will be used in subsequent high frequency discussions in this paper.

TABLE 1. STATISTICS FOR 10, 31.5, AND 100 HZ

VARIABLE	10 Hz	31.5 Hz	100 Hz
SAMPLE SIZE	901	913	913
MEDIAN	97.7	84.0	76.8
MEAN	96.3	85.1	77.8
STANDARD DEVIATION	10.9	7.1	5.7
MAXIMUM	124.1	125.8	114.6
MINIMUM	64.3	64.4	63.9

Table 1 contains statistical information concerning the amplitude of the noise level for the three uncontaminated frequencies for Julian days 285-323. One notes that both the mean and standard deviations decrease with increasing frequency (Figure 3.5). The mean spectrum decreases from 96.3

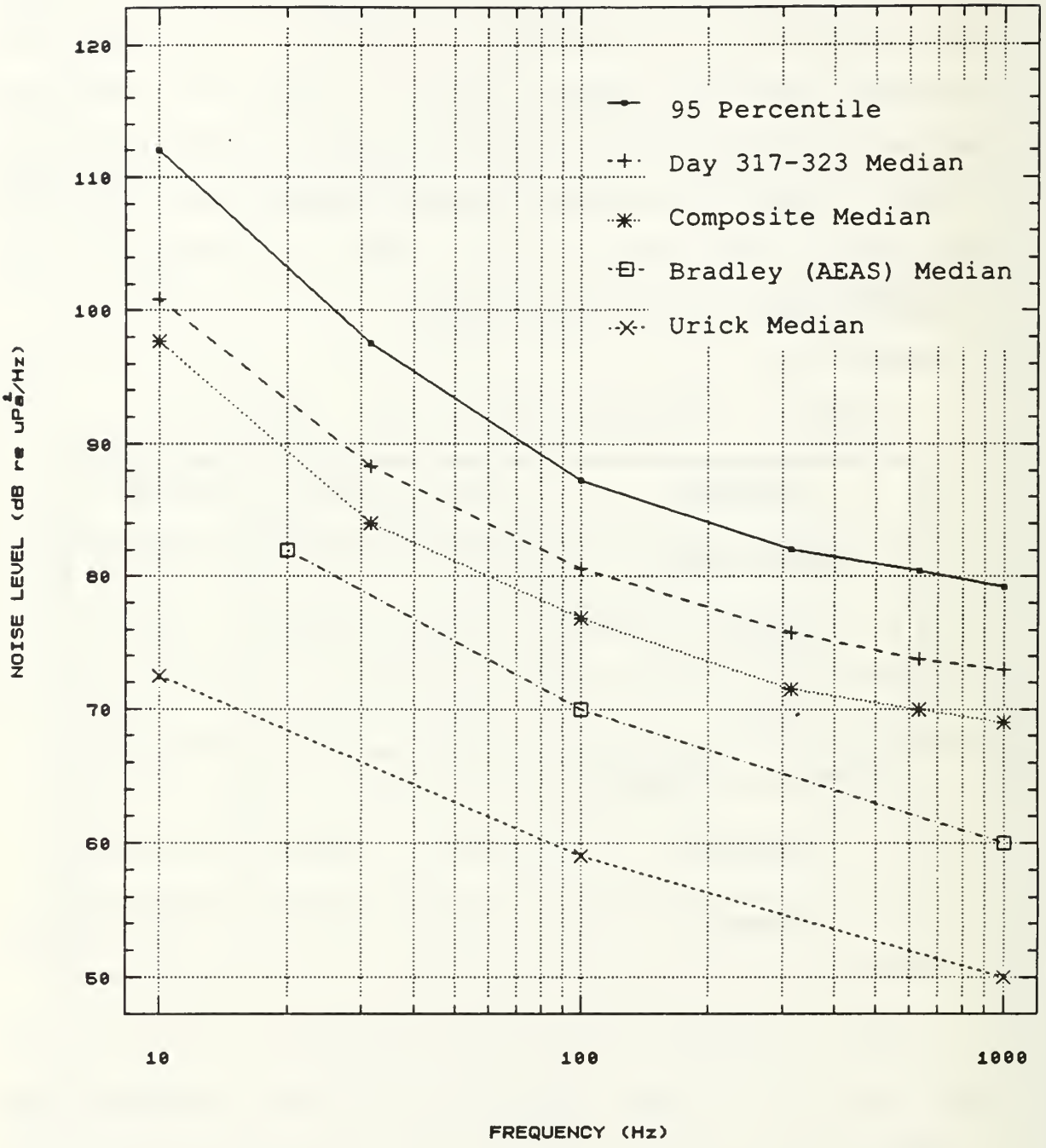

Figure 3.4 Spectral slopes from 38-day composite, 38-day 95th percentile, 7-day shallow water, and slopes derived from two previous ambient noise studies by Bradley (1986) and Urick (1975) compare quite favorably.

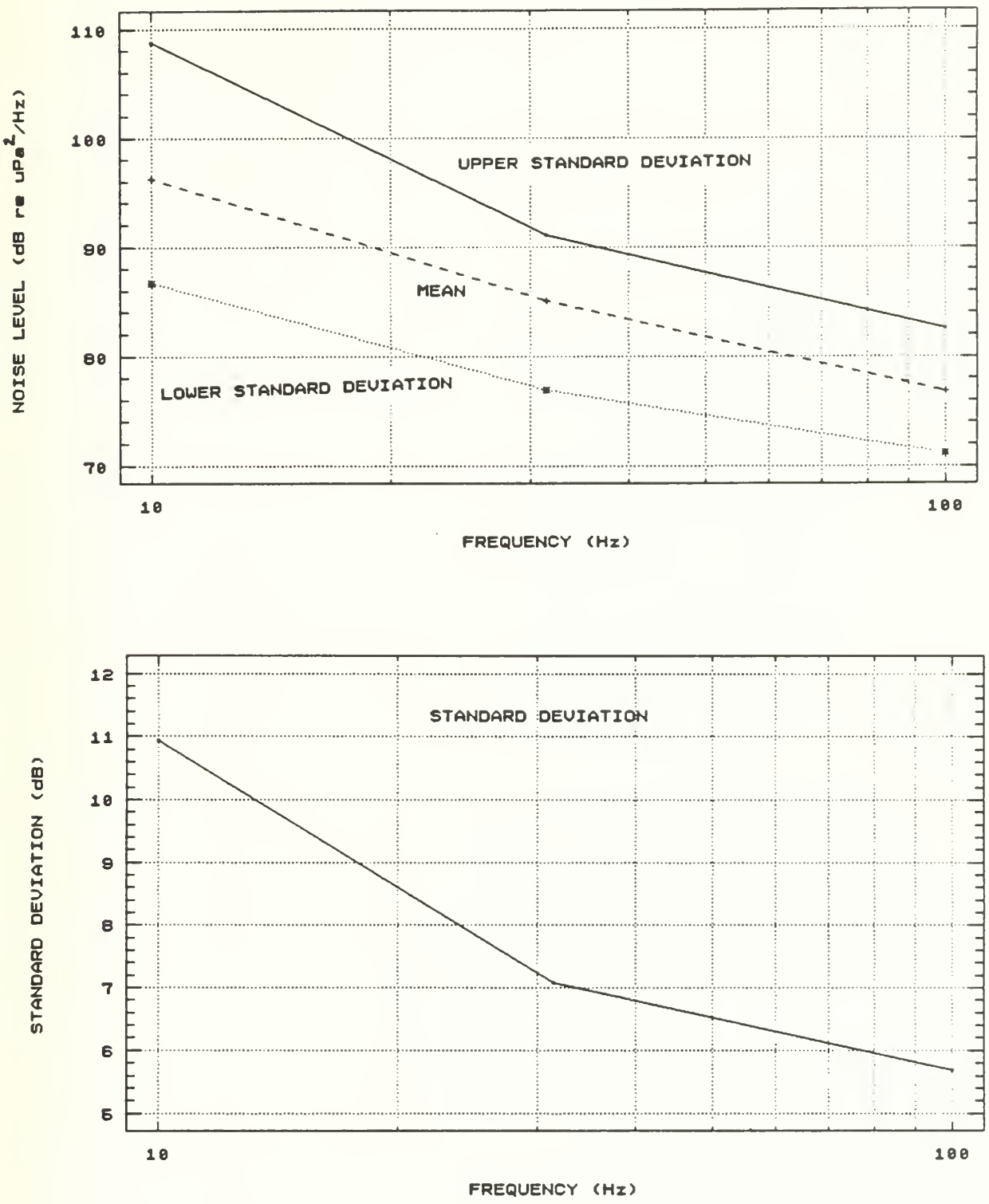

Figure 3.5 The mean and standard deviations for frequencies from 10 to 100 Hz decrease with increasing frequency.

dB at 10 Hz to 77.8 dB at 100 Hz with a relatively steep slope of 6.2 dB per octave.

The standard deviation provides a useful measure of the variability of the noise level for a given frequency. Figure 3.5 (bottom) presents the standard deviation for the frequency range 10-100 Hz. The majority of the ambient noise record, the portion within one standard deviation of the mean, lies within a 22 dB window at 10.0 Hz and decreases to only 11.4 dB at 100 Hz. The large difference in the standard deviation between 10 and 100 Hz may indicate that different noise generation mechanisms are predominant at each of these frequencies. Bannister et al. (1979) reported that different levels of standard deviation were indicative of different ambient noise regimes.

When the 38-day Barents Sea ambient noise spectrum is compared to other deep water spectra from ice covered regions, it becomes readily apparent that the Barents Sea spectra are significantly noisier. Figure 3.6 shows the comparison between the ambient noise spectra from the central Arctic, the Beaufort Sea, and Barents Sea. The central Arctic spectrum was derived from ice camp data collected in April, 1982 (Makris and Dyer, 1986). The Beaufort Sea spectrum was created from drifting buoy measurements in 1975-1976 during the Arctic Ice Dynamics Joint Experiment, AIDJEX (Lewis and Denner, 1987a) and the last spectrum (Urick, 1975) was derived from a composite of many under ice ambient noise measurements.

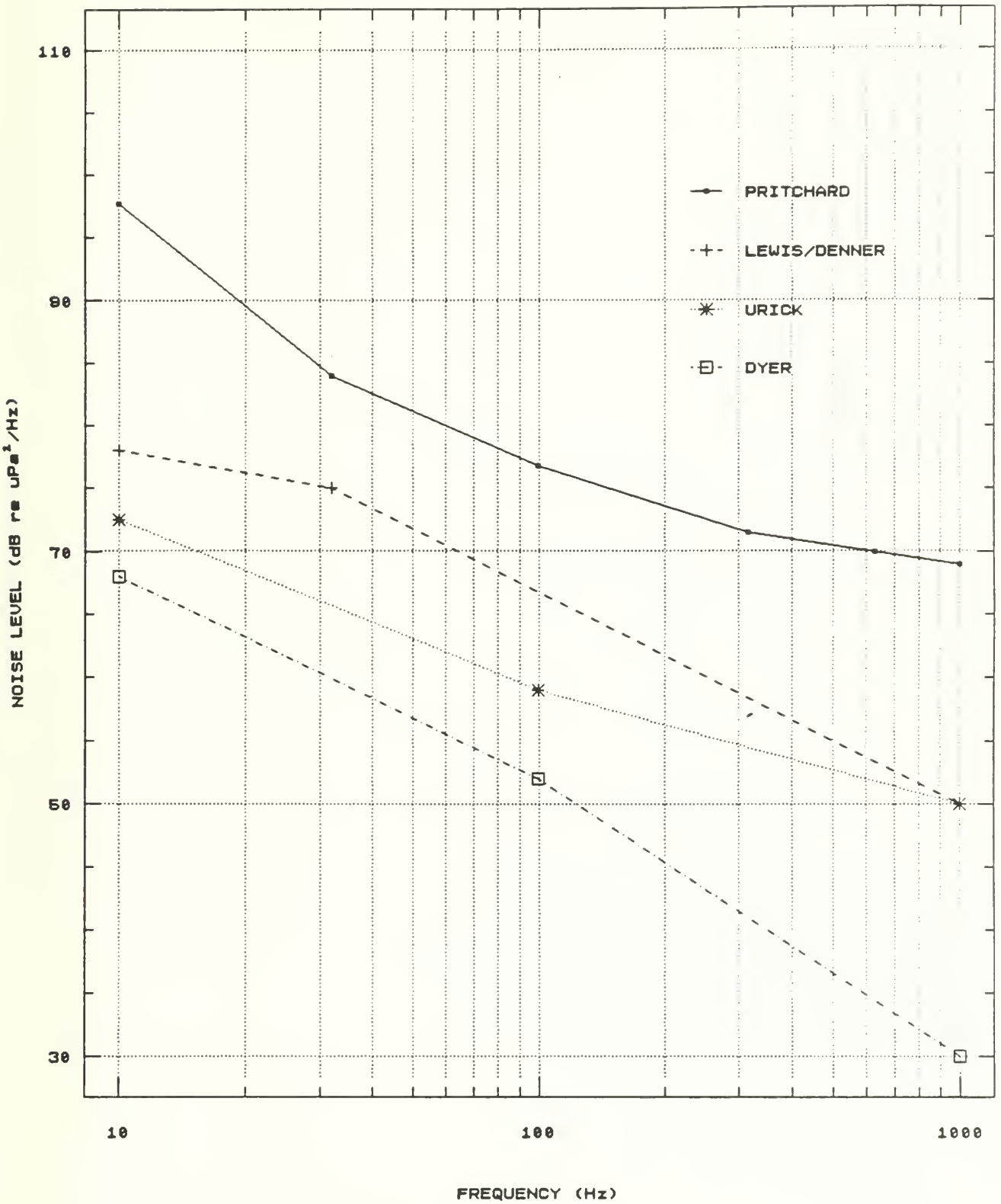

Figure 3.6 Pritchard's Barents Sea spectrum is significantly noisier than deep water spectra acquired from other ice-covered regions by Lewis and Denner (1987), Makris and Dyer (1986), and Urick (1975).

While the large amplitude of the Barents Sea ambient noise spectrum may initially appear disturbing when compared with these central Arctic measurements, further investigation reveals similarities with spectra obtained from other dynamically active Arctic regions (Figure 3.7). These active regions include spectra obtained during active ridging events from Buck and Wilson (1986) and Buck and Green (1979) as well as studies conducted in the marginal ice zone (Johannessen, 1988; Diachok and Winokur, 1974). When compared with these similarly noisy locations or events, the Barents Sea spectrum falls within the middle of the spectra illustrating that intense noise generating mechanisms are present in this area.

The Barents Sea noise data were obtained from a region where the ice was undergoing extreme convergence due to its close proximity to land. The winds during this period were predominantly from the north, driving the ice southwards from the deep waters of the central Arctic into the relatively shallow waters of the Barents Shelf, wherein local ridging occurred when the southerly moving ice encountered the unyielding islands of Kvitoya, Viktoriya, and Nordaustlandet. Figure 1.1 depicts the southward drift of the *Polarbjoern* towards these islands from Julian day 260 to 330. During the *Polarbjoern's* drift southwards, the ice pack, when viewed on a macro-scale, was experiencing large scale divergence. Remote sensing imagery from the NOAA-10 polar orbiter (Figure

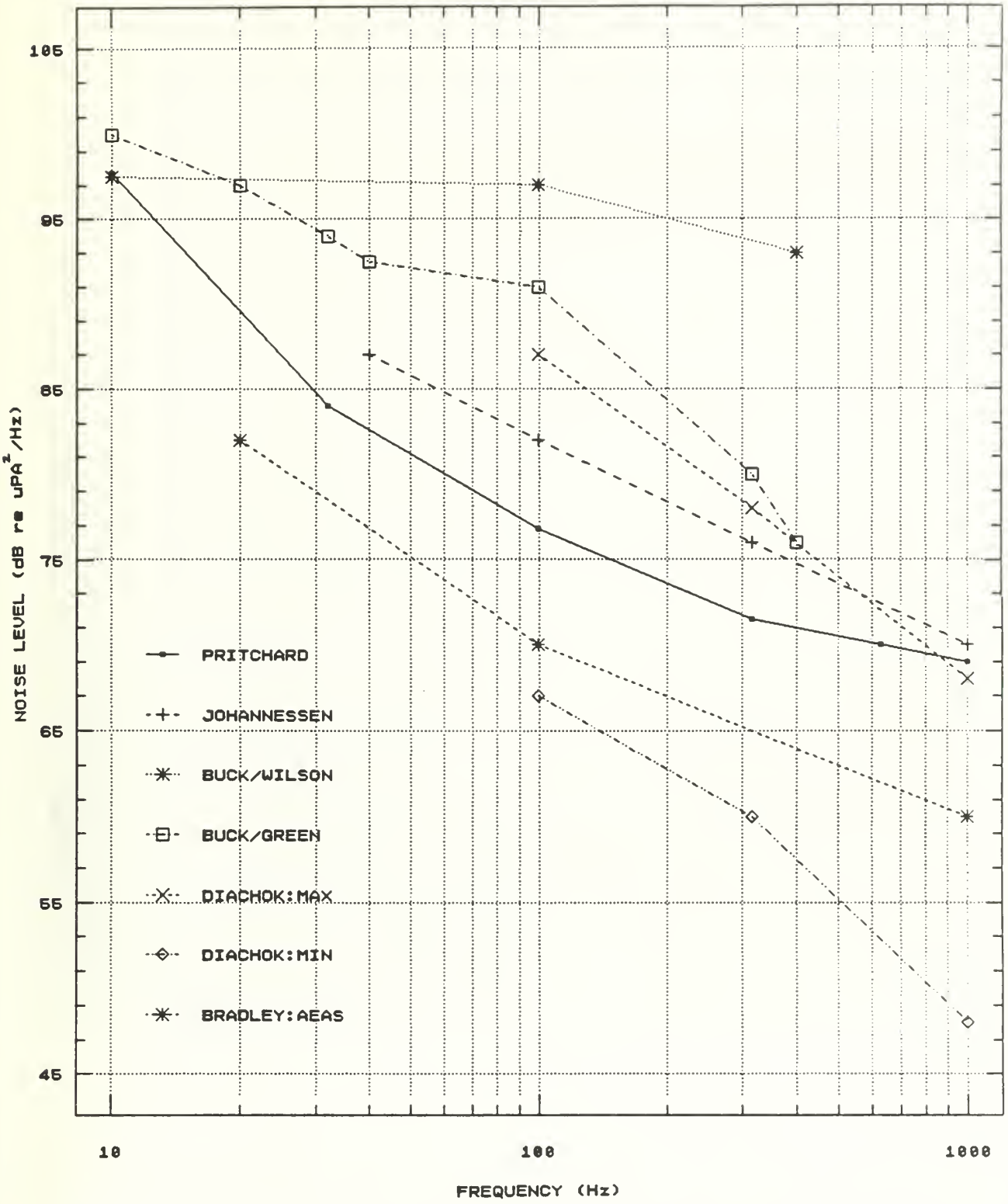

Figure 3.7 Pritchard's Barents Sea spectrum compares favorably to spectra obtained from other dynamically active regions. Buck and Wilson (1986) and Buck and Green's (1979) spectra were derived from regions of active ridging. Johannessen's (1988) and Diachok and Winokur's (1974) spectra were obtained from the MIZ.

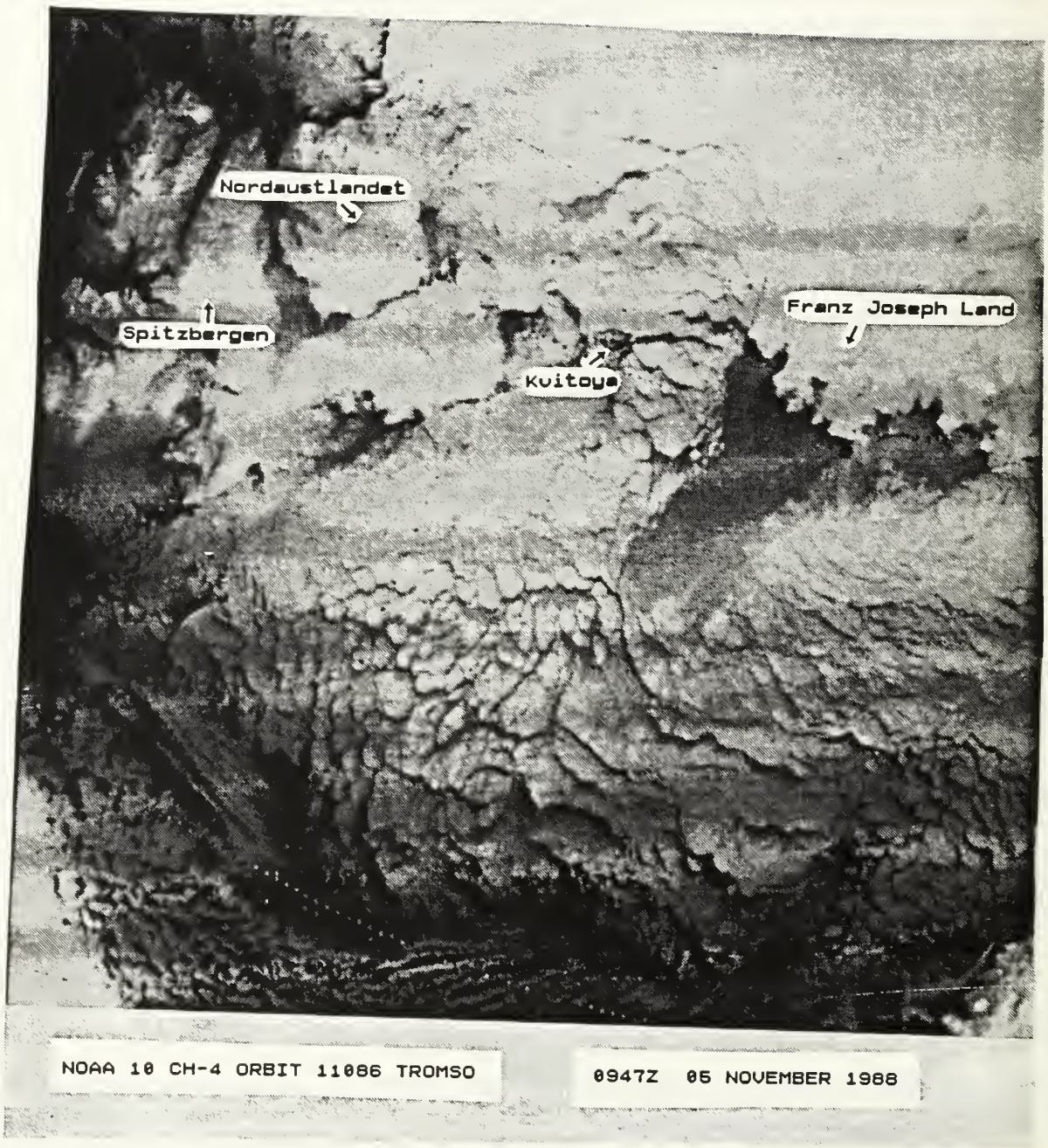

Figure 3.8 NOAA-10 imagery of the region northeast of Svalbard. Large scale divergence of Arctic ice pack is revealed as an extensive network of polynyas and fractures arching from Nordaustlandet to Franz Joseph Land.

3.8) reveals this divergence as an extensive network of polynyas and fractures arching from Nordaustlandet to Franz Joseph Land. This arch of fractures was formed by the convergence of the Arctic ice pack onto the islands which act as the supporting pillars. The southward moving ice pack diverges once it moves past the arch.

However, on a more local scale, extensive convergence was taking place in the vicinity of the Svalbard Archipelago. During the last two weeks of data collection, when the ship was within 100 km of the islands, ridging and shearing were extremely active in the vicinity of the ship (Pritchard, personal conversation, 1991). This resulted in the repeated separation of the hydrophones from the instrumentation cables and necessitated their eventual removal from the ice pack.

2. Hourly Autocorrelations

Autocorrelations were performed on the hourly-averaged frequencies from 10 to 100 Hz. Figure 3.9 shows the autocorrelations for 10, 31.5, and 100 Hz. A strong 12 hour periodicity is evident at these lower frequencies that may be attributed to tidal/inertial oscillations. These oscillations will be addressed more fully in the ice motion section. At 10 Hz, the 12 hour periodicity is clearly observed with a lag of up to 60 hours. The dashed lines represent twice the large lag errors for each coefficient and display a value of about

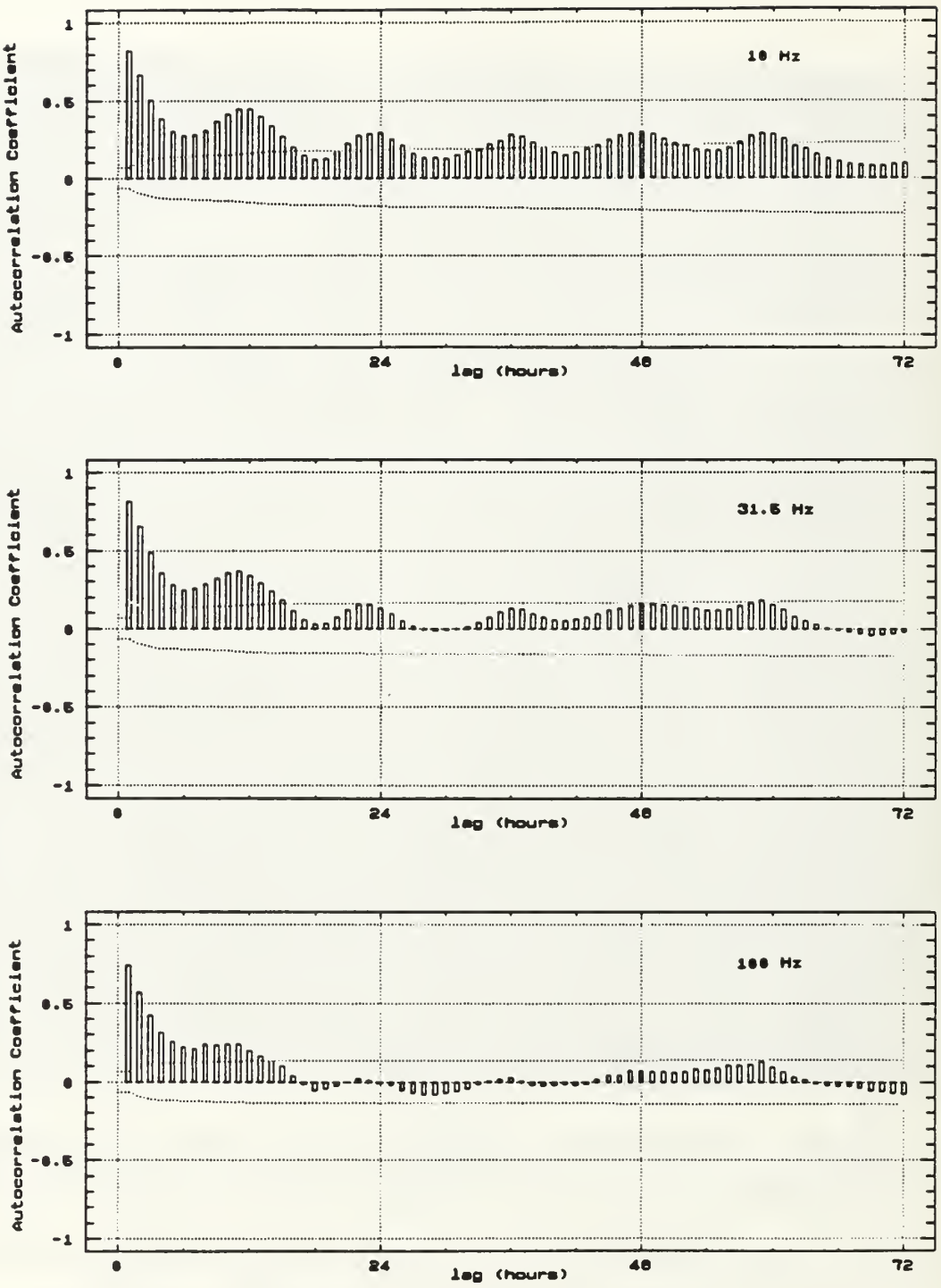

Figure 3.9 Autocorrelations for frequencies of 10, 31.5, and 100 Hz display a 12-hour periodicity.

0.2. The temporal coherence of the noise can be estimated from the e-folding time (time for the signal to be reduced to e^{-1} of its peak value or about 0.37). At 10 Hz the e-folding time is about 4 hours. The 31.5 Hz autocorrelation also demonstrates a significant 12 hour periodicity and is similar in shape to the 10 Hz autocorrelation but beyond a 24 hour lag displays a considerably lower correlation coefficient. The 100 Hz autocorrelation shows the least correlation. Beyond 12 hours the correlation becomes statistically insignificant. The e-folding time is about 3 hours. When the autocorrelations for 10, 31.5, and 100 Hz are compared, it appears that the temporal coherence of the noise field decreases with increasing frequency.

B. METEOROLOGICAL ANALYSIS

1. Wind Data

Throughout the duration of this study, the wind remained predominantly from the north. Figure 3.10 is a frequency histogram of the true wind direction and Table 2 gives the numerical and relative frequency of wind direction in 30 degree sectors. The wind was from 300 to 060 degrees for more than three quarters of all observations and was within 30 degrees of true north for more than half of the period.

The wind speed varied from a high of 18 m/sec during high wind periods to near zero during calm periods. The overall

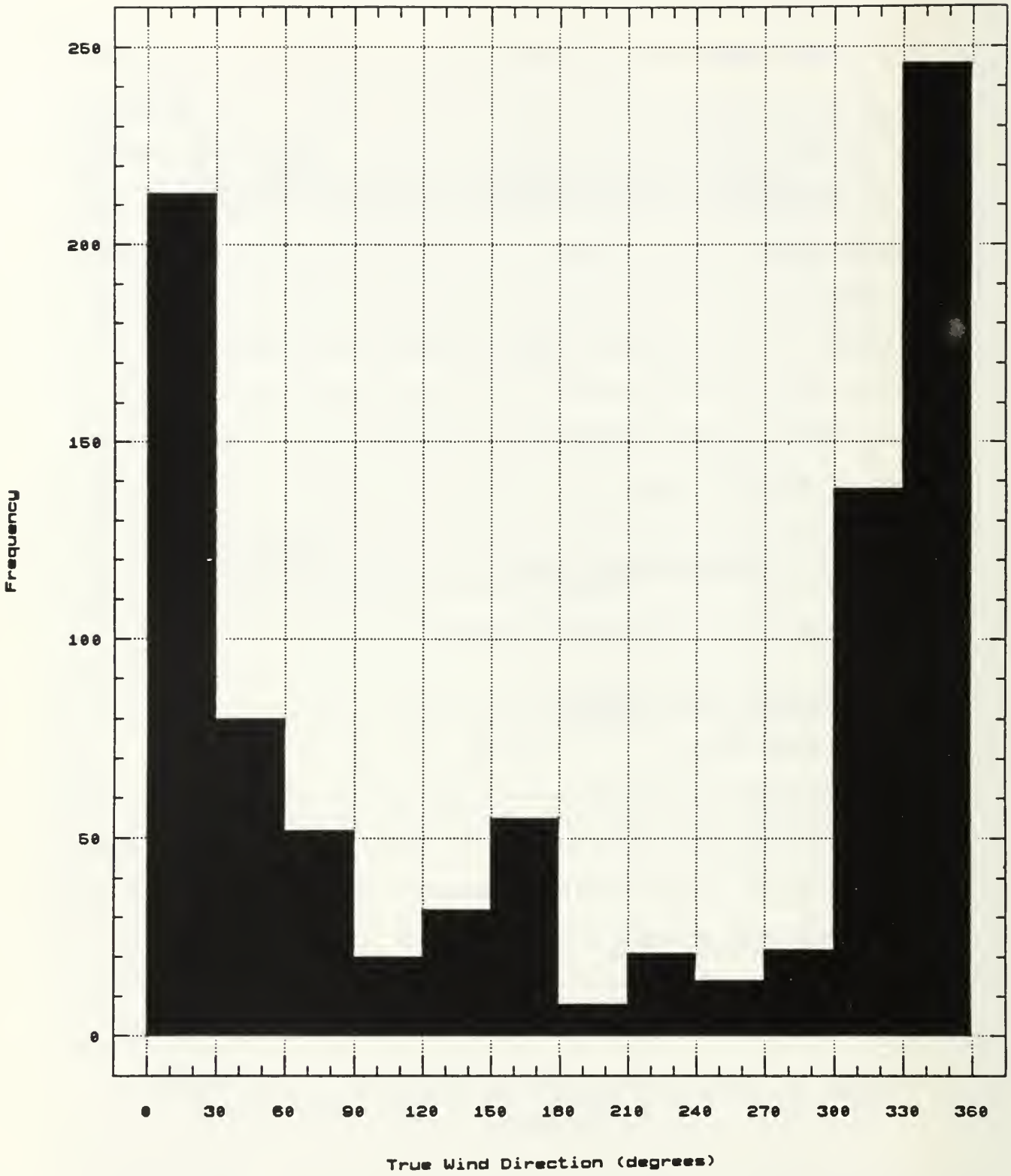

Figure 3.10 Frequency histogram of true wind direction reveals that the wind was predominantly from the north.

mean wind speed was 7.2 m/sec with a standard deviation of 3.4 m/sec. Table 3 displays basic wind speed statistics and a histogram of wind speeds is displayed in Figure 3.11. Thus

TABLE 2. SUMMARY OF HOURLY AVERAGED WIND DIRECTION DATA SORTED INTO 30 DEGREE SECTORS BY FREQUENCY AND PERCENT.

DEGREES	FREQUENCY	PERCENT
270-300	23	25.2
300-330	142	15.5
330-360	242	26.5
000-030	218	23.9
030-060	81	8.9
060-090	53	5.8
090-120	20	2.2
120-150	33	3.6
150-180	57	6.2
180-210	9	1.0
210-240	21	2.3
240-270	14	1.5

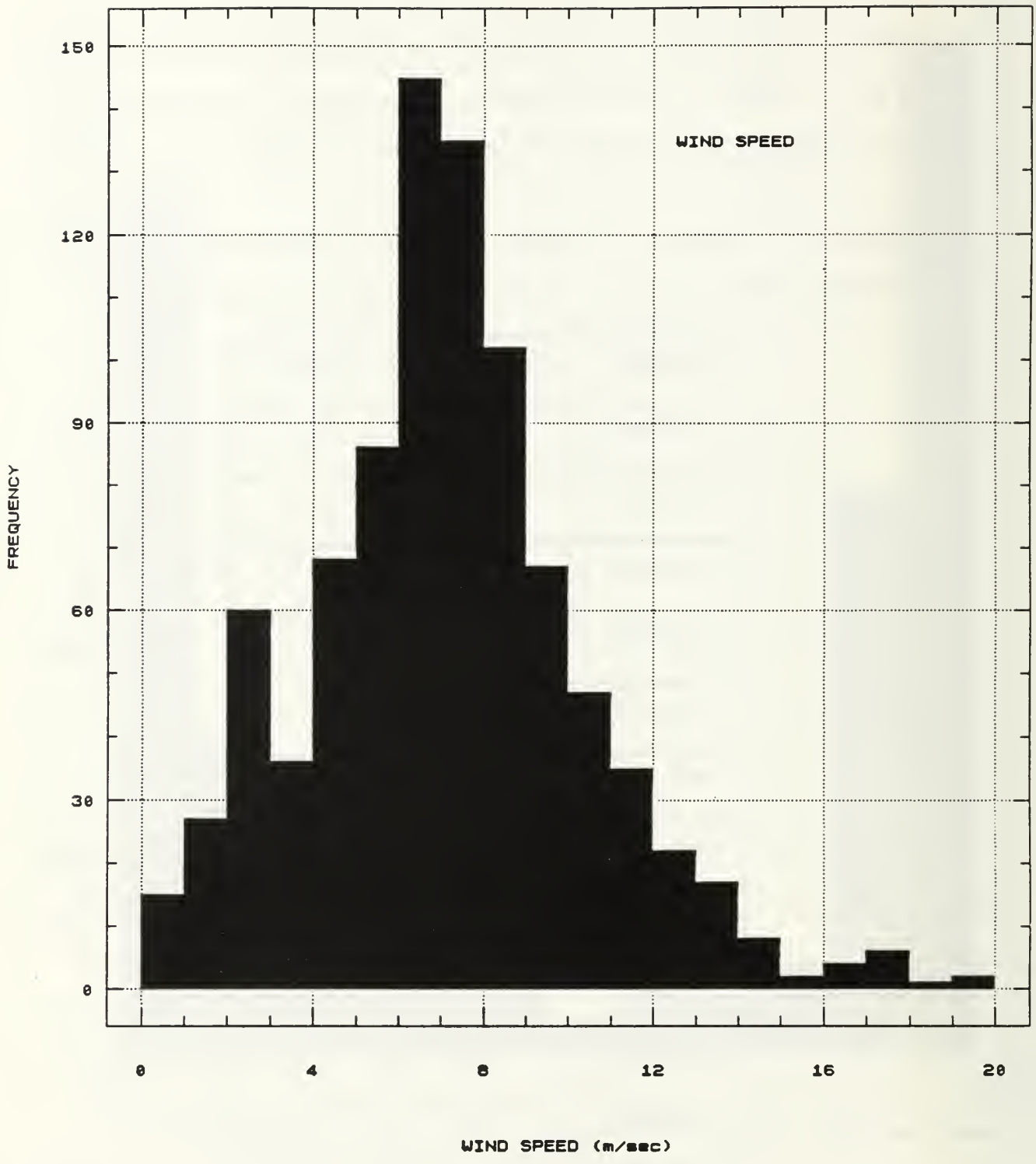

Figure 3.11 Histogram of wind speed reveals that the wind varied from 0-20 m/s with a mean of about 7 m/s.

the wind during this period can be characterized as being from the north at 6-8 m/sec. A three dimensional display of wind speed versus wind direction clearly demonstrates this in Figure 3.12.

TABLE 3. STATISTICAL DATA FOR WIND SPEED, TEMPERATURE, AND ICE SPEED. CALCULATED FROM HOURLY AVERAGED DATA.

VARIABLE	WIND SPEED (m/s)	TEMPERATURE (°C)	ICE SPEED (cm/s)
SAMPLE SIZE	913	913	913
MEDIAN	7.0	-22.3	12.5
MEAN	7.0	-22.3	14.2
STANDARD DEVIATION	3.4	5.0	10.5
MAXIMUM	20.1	-7.7	81.3
MINIMUM	0.0	-31.9	0.1

Figure 3.13 is the hourly-averaged time series of wind speed from 11 October to 18 November. Significant events include the strong winds (20 m/sec) associated with the passage of a synoptic low on days 285-286 (Hamilton, 1991), the period of relatively light winds from Julian day 308 to 312, and the periodic fluctuation of the winds on days 312 to 320. An autocorrelation of wind speed, Figure 3.14, revealed

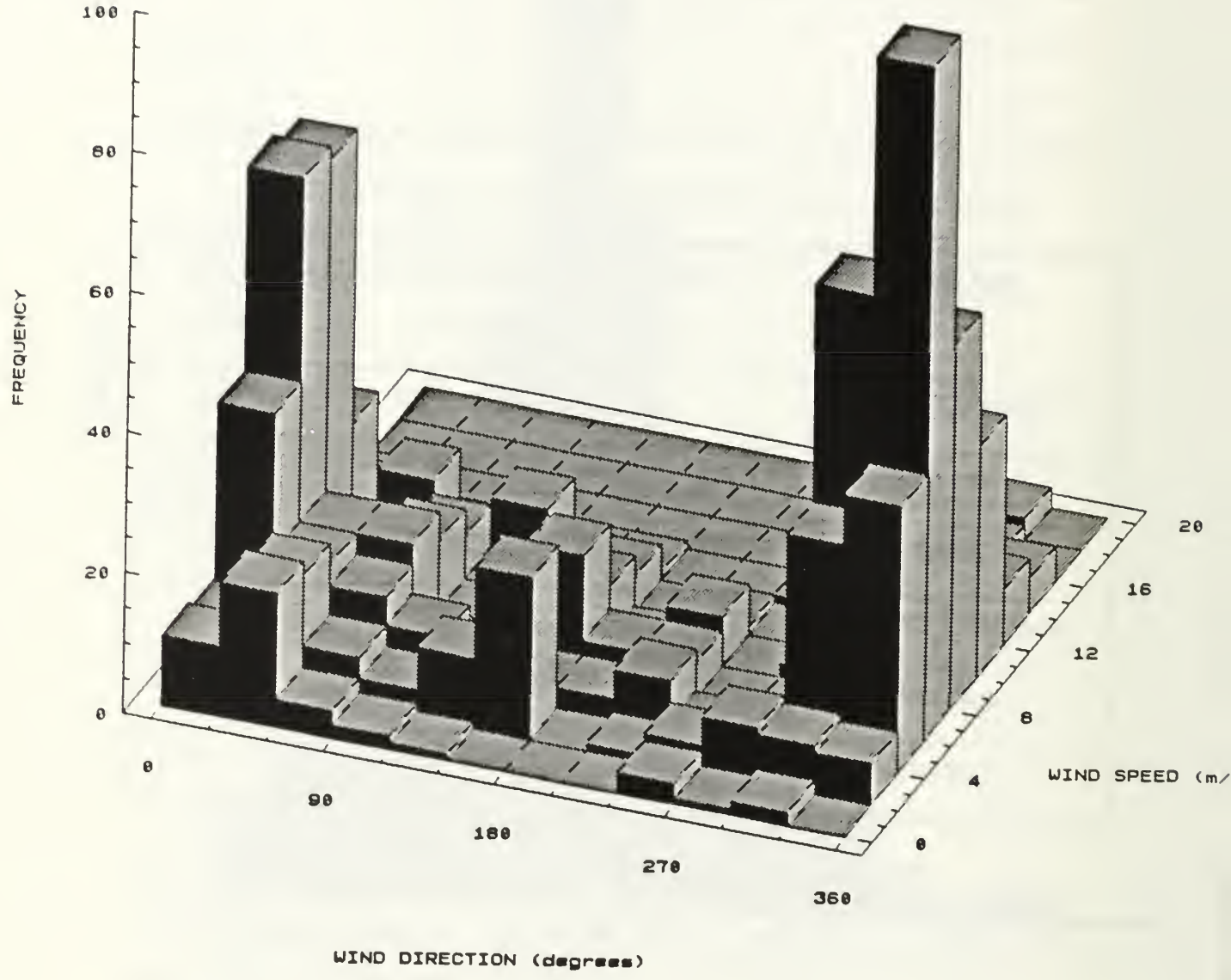

Figure 3.12 Three dimensional histogram of wind speed and wind direction reveals that the wind was generally from the north at 6-8 m/s.

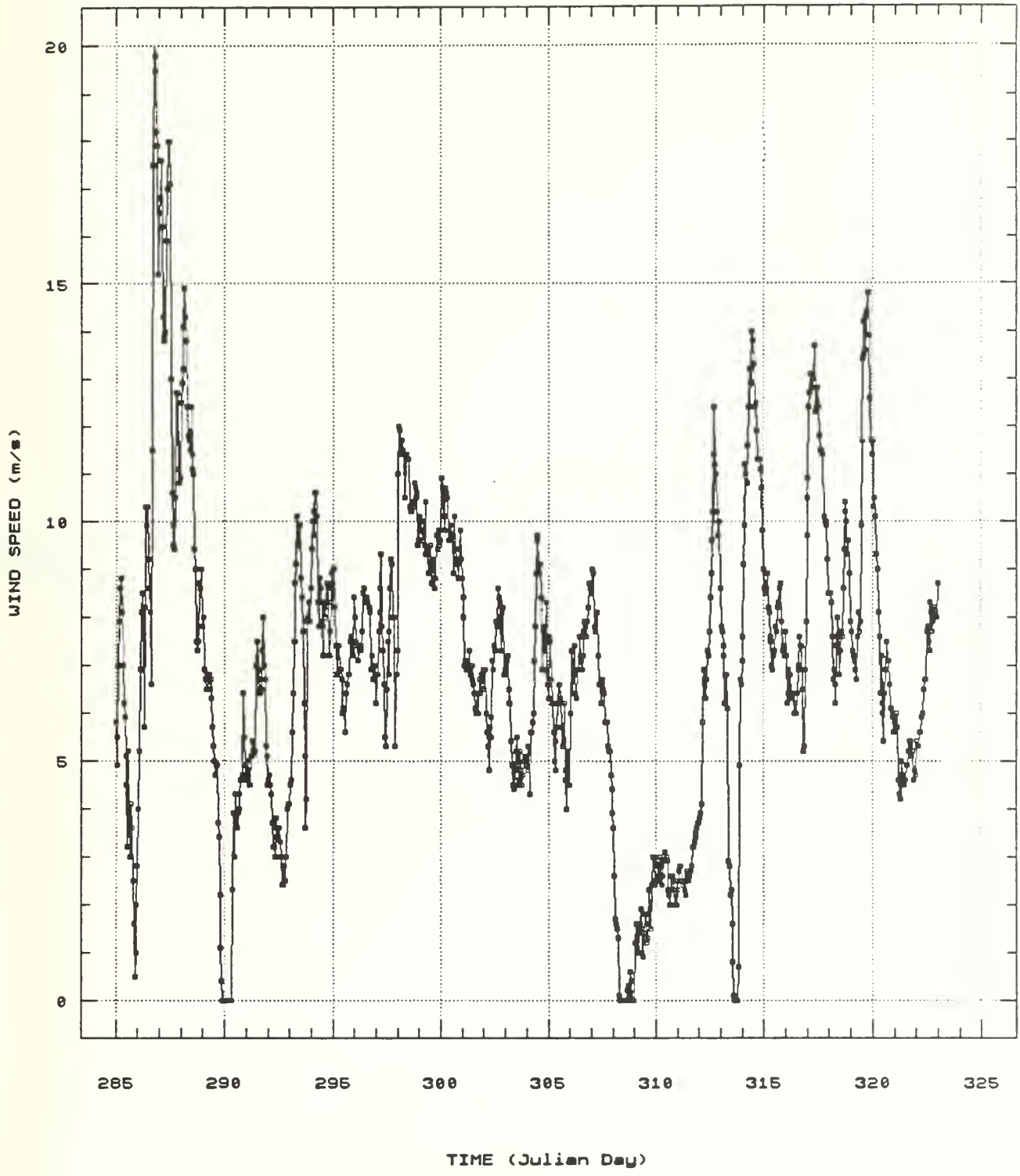

Figure 3.13 Time series of hourly-averaged wind speed that was recorded from 11 October to 18 November 1988 (Julian day 285-323) onboard the *Polarbjoern*.

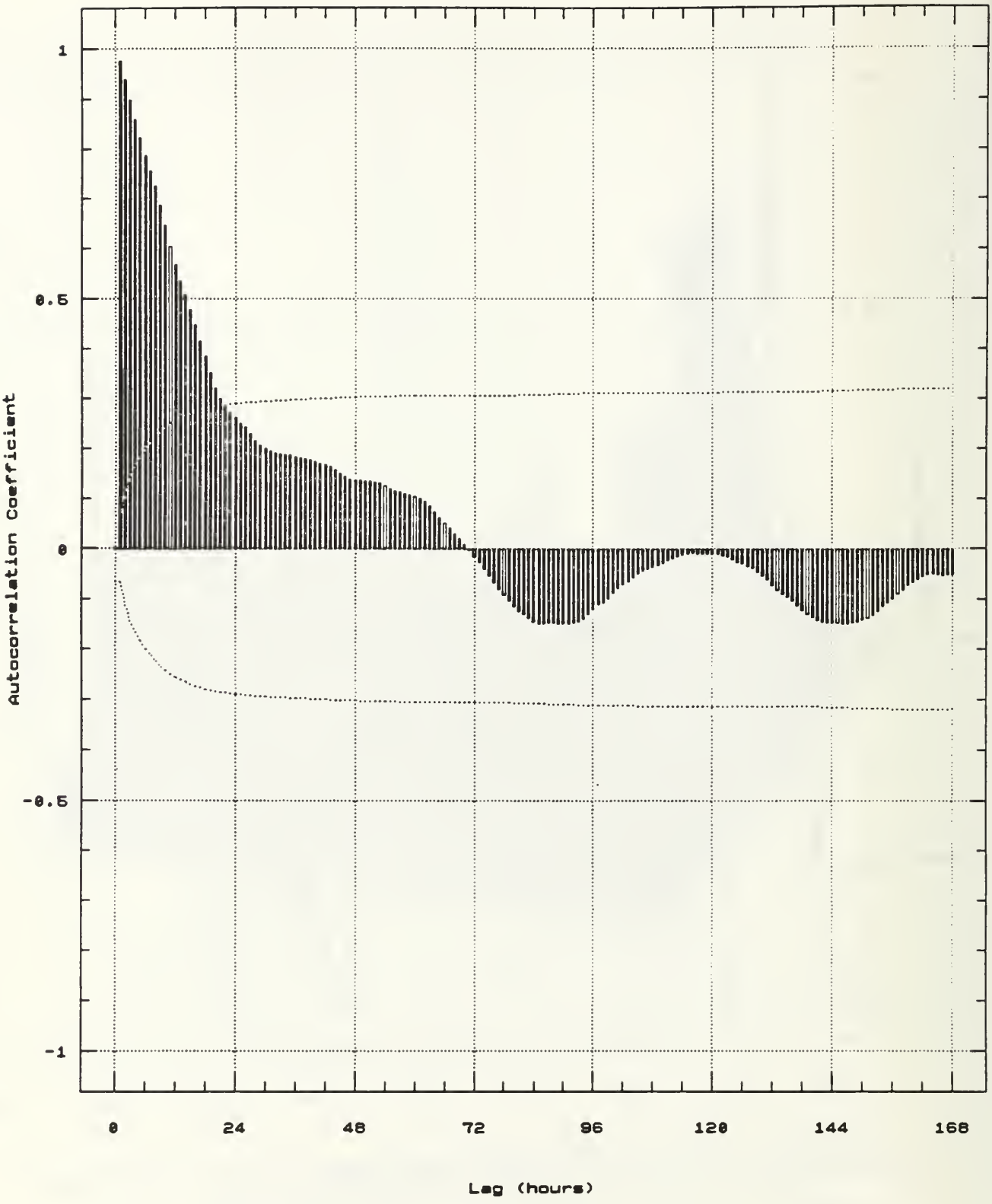

Figure 3.14 Autocorrelation of wind speed reveals no significant periodicities with lags of up to 72 hours.

no statistically significant periodicities in the first 24 hours. The correlation coefficient gradually declines for the first 72 hours with an e-folding time of about 17 hours.

2. Temperature Data

The temperature varied from a high of -7.7°C on Julian day 286 to a low of -32°C on day 310. Table 3 gives the relevant statistical information. While the temperature median was -22.3°C, Figure 3.15, a temperature histogram with one degree bins, reveals that there was no predominant temperature, but rather a broad range of values centered about the mean. Figure 3.16 displays the temperature time series during this period. An overall cooling trend is observed from day 287 to 307, which is followed by a period of rapid warming from day 311 to 313 when a shift to southerly winds occurred. With the return of northerly winds on Julian day 313, the cooling trend resumed and continued to dominate the remainder of the record. Superimposed on these long term trends are 1-2 day fluctuations in temperature that may exceed 10°C peak-to-peak.

An autocorrelation of the temperature, Figure 3.17, revealed no periodicities. However, the autocorrelation does support the strength of persistence beyond 48 hours and establishes an e-folding lag time of about 60 hours.

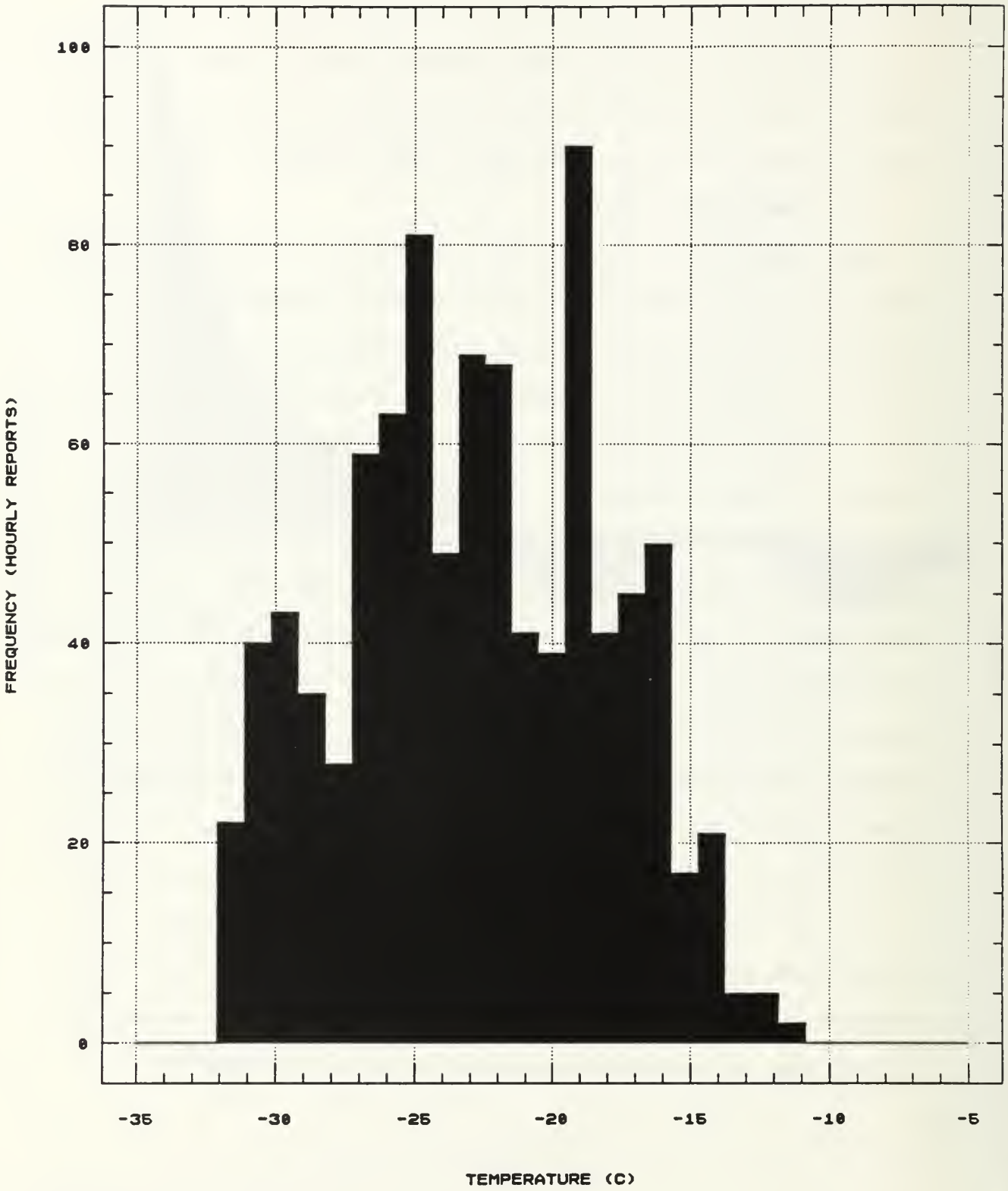

Figure 3.15 Frequency histogram of temperature (°C) reveals a broad range of temperatures from -8°C to -32°C.

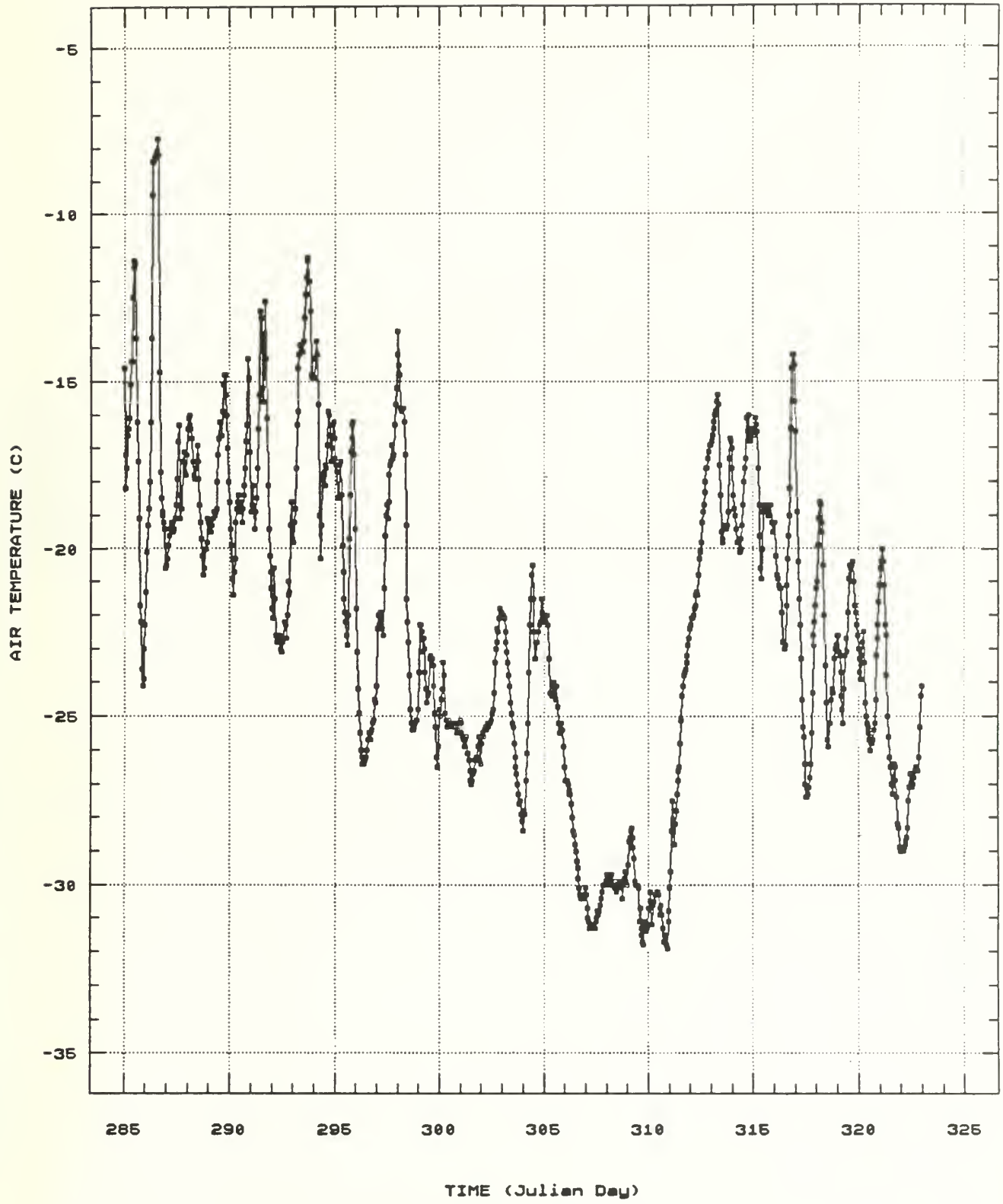

Figure 3.16 Time series of hourly-averaged temperatures (°C) that were measured onboard the *Polarbjoern* from 11 October to 18 November 1988 (Julian days 285-323).

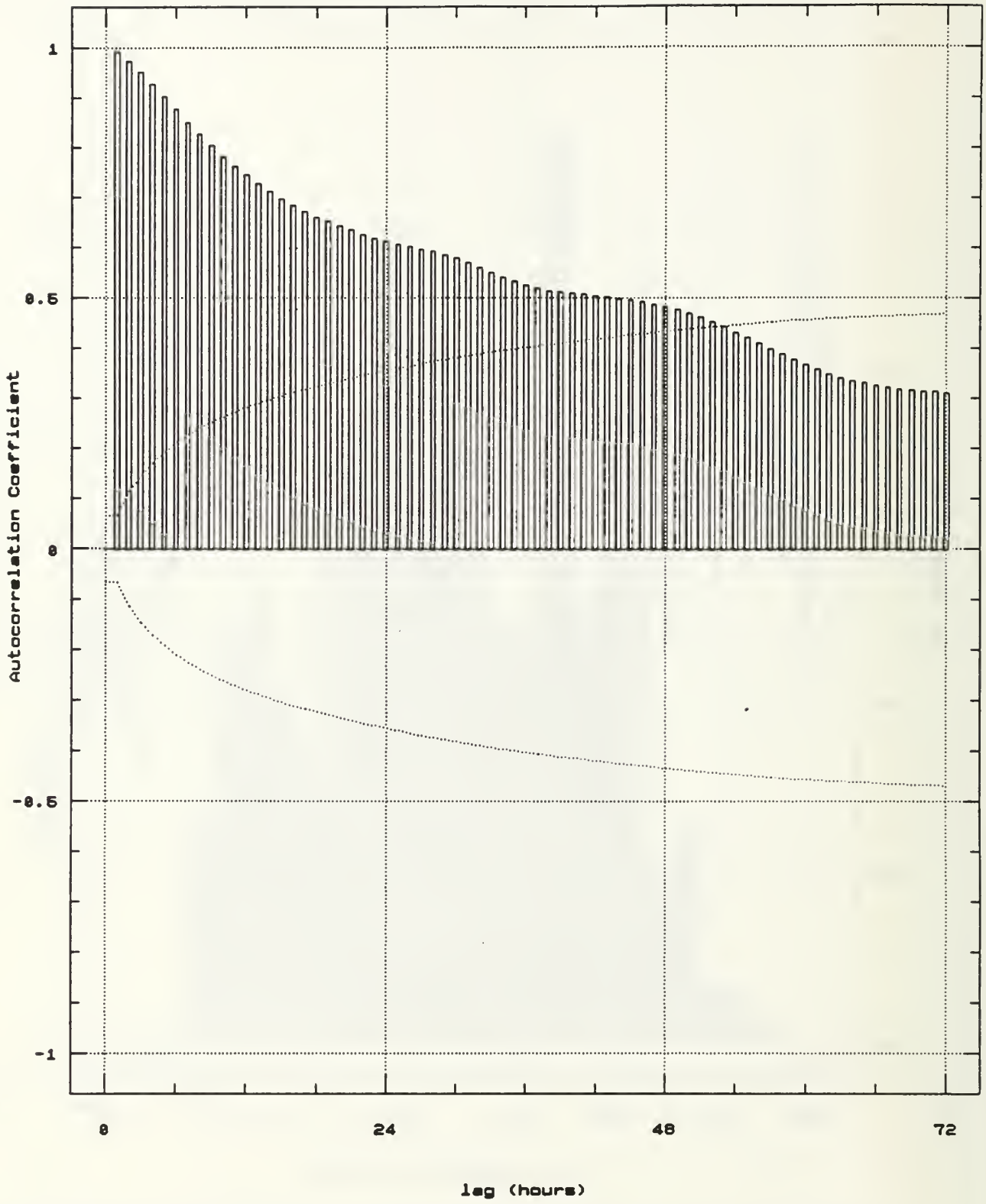

Figure 3.17 An autocorrelation of temperature (°C) revealed no periodicities and a temporal coherency of 60 hours.

C. ICE MOTION ANALYSIS

Previous studies have highlighted the strong relationship between ice flow speed and ambient noise (Lewis and Denner, 1988a). Therefore, substantial effort was devoted to examining the drift speed statistics and their relationship to ambient noise. The time series of ice speed is plotted in Figure 3.18a and is partitioned into its U (east) and V (north) components (Figures 3.18b and 3.18c). The ice speed varied from 0 to 81 cm/sec, with a mean of 14.2 cm/s and a standard deviation of 10.5 cm/sec. Two basic scales of motion are evident, a low frequency trend that changes on the order of days to weeks, and a higher frequency oscillation that varies every 12 hours. The low frequency trend acts as a background variation on which the high frequency oscillations are superimposed. This low frequency trend varies from about 0-20 cm/s while the high frequency oscillations range from 10-40 cm/s. The most noticeable features of Figure 3.18a are the extremely high ice speeds (81 cm/s) recorded on Julian day 287, the lack of ice motion on days 308-309, and the bi-modal nature of the ice speed peaks which are most apparent during the last ten days of the record. Figure 3.19 shows the overall distribution of ice speed and Table 2 the relevant statistics.

During Julian days 285-323, the mean direction of ice motion was predominantly to the southwest. There were,

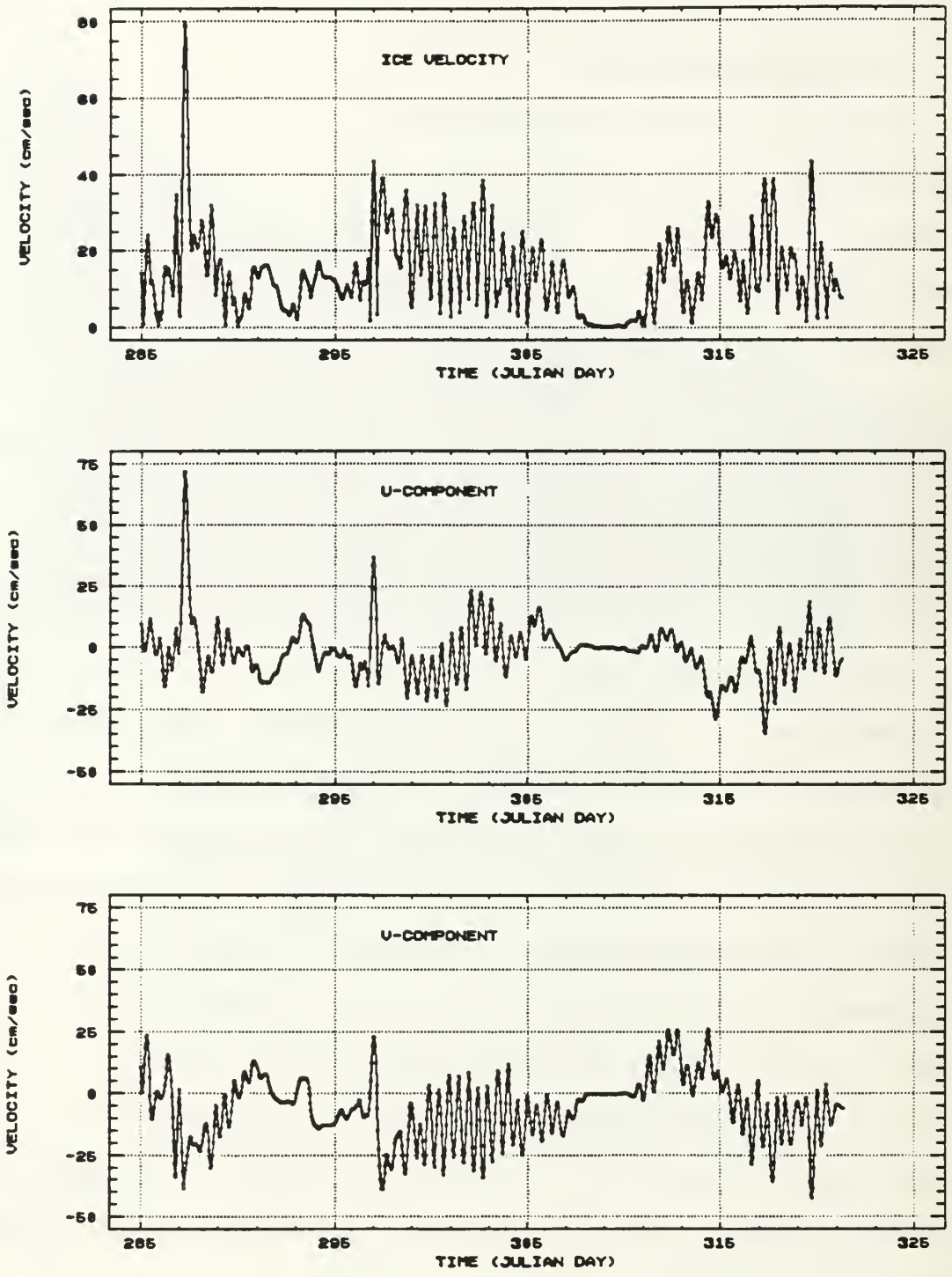

Figure 3.18 Time series of hourly interpolated ice speed and U & V-components of ice speed from 11 October to 18 November (Julian days 285-323).

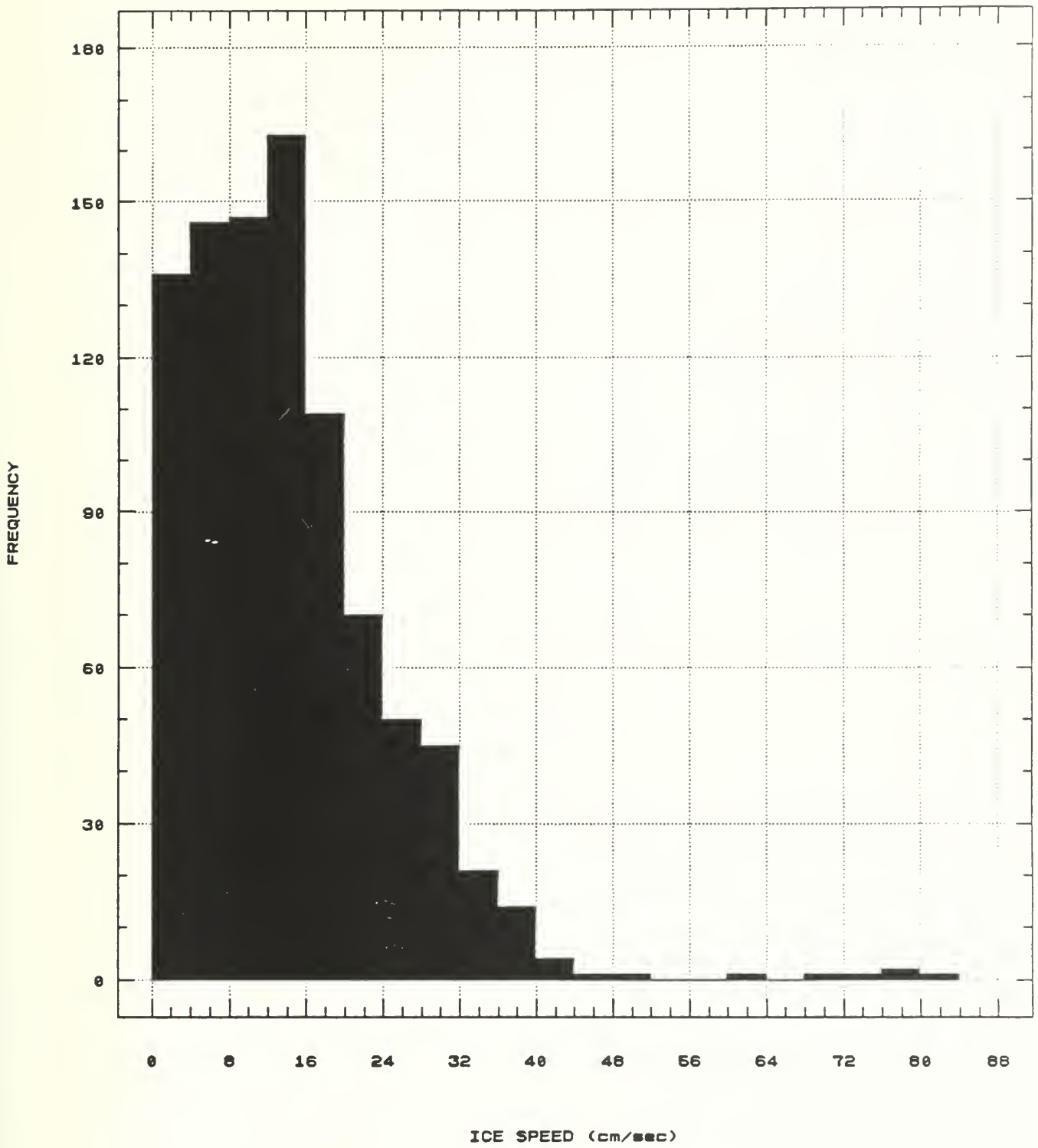

Figure 3.19 Frequency histogram of ice speed (cm/s) reveals a mean ice speed of about 14 cm/s.

however, four short periods when the mean direction of motion shifted and was to either the southeast or northwest. Figure 1.1, the track of the *Polarbjoern*, shows these movements. Segments a and d cover periods when the ship and ice floe moved to the southeast, sections b and c represent periods when the ship moved to the northwest.

Figure 3.20 reveals the ice motion on an hourly basis during Julian days 300 and 301. The speed barbs show the hourly speed and direction of the ice. Note the smooth 12 hour periodicity displayed by the clockwise rotation in ice direction. The ice direction steadily rotates from southward headings to northward headings over a 10 hour period and then quickly snaps around the remaining 180 degrees in the span of 1-2 hours. During this two day period, the ice speed varied from a few cm/s to 30-35 cm/s on a 12 hour cycle. The maximum ice speed was recorded when the ice direction was southwards and the minimum speed when the ice moved northwards. Thus, as the ice direction rotated clockwise from south to north, its speed decreased.

The autocorrelation of ice speed, Figure 3.21, demonstrates a strong 12 hour inertial/tidal influence. Determining whether this was inertial, tidal or a combination of the two proved to be impossible given the lack of current measurements. Previous Arctic studies were of little help in determining the nature of the oscillations on the continental shelf because the vast majority of these studies had been

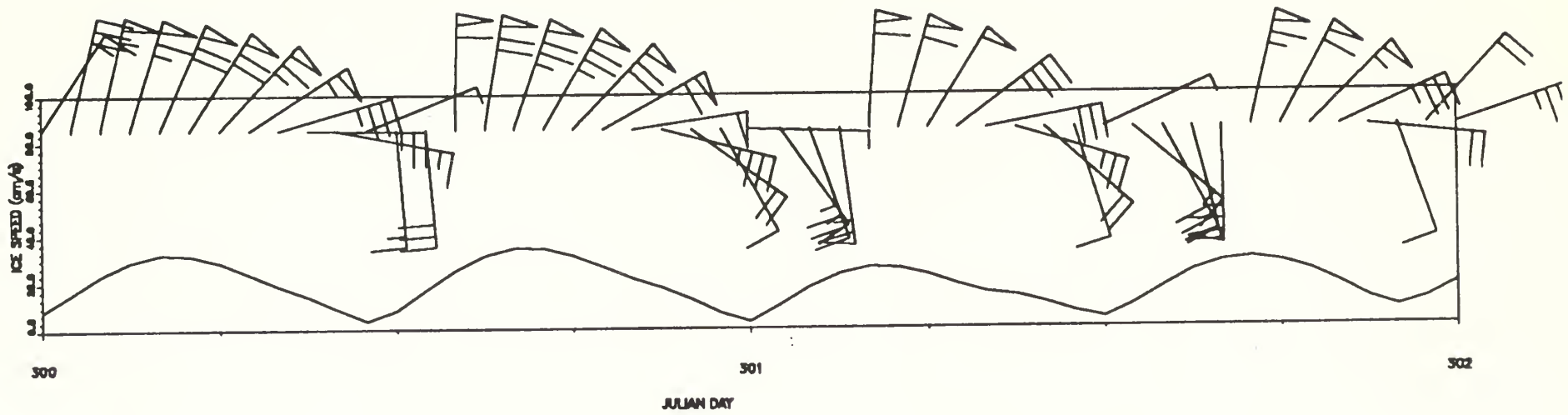

Figure 3.20 Hourly-averaged ice motion for Julian days 300 and 301. Speed barbs indicate speed and direction of motion while a continuous plot of ice speed (cm/s) reveals the smooth 12-hour periodicity. The ice direction steadily rotates clockwise from south to north over a 10 hour period before snapping around the remaining 180 degrees in 1-2 hours.

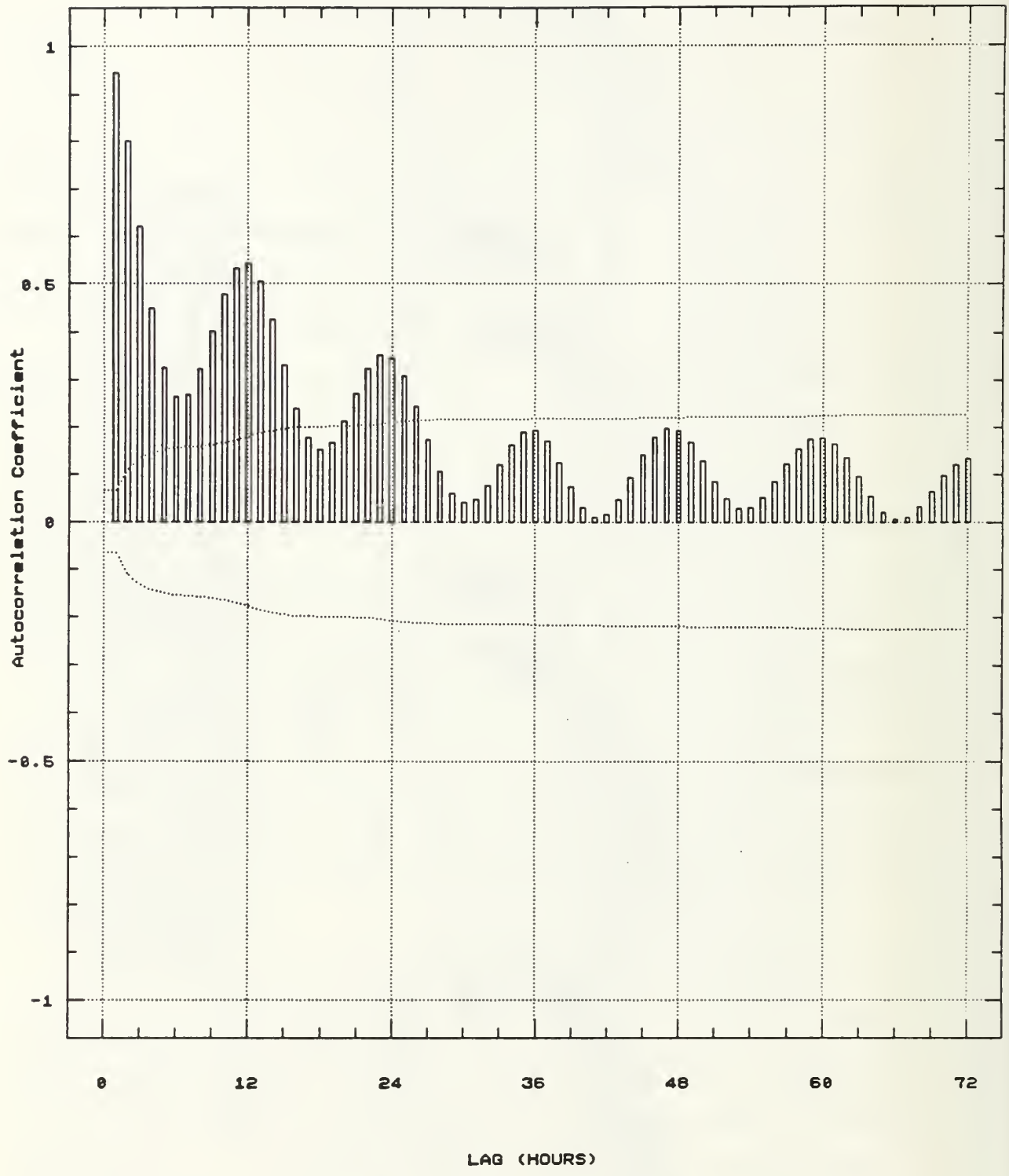

Figure 3.21 Autocorrelation of ice speed demonstrates a strong 12-hour tidal/inertial influence.

conducted in the deep waters of the central Arctic basin where tidal oscillations are negligible (Thorndike, 1986).

Tidal influences away from the central Arctic basin, i.e., on the continental shelves, are of much greater amplitude than in the central Arctic (Thorndike, 1986). Kowalik and Untersteiner (1978) determined that tidal influences may be an order of magnitude larger on the shelf than they are in the central basin. These tides are generally semi-diurnal rather than diurnal with semi-diurnal amplitudes of 20 cm and diurnal amplitudes of only 2-3 cm (Schwiderski, 1986). The lunar semi-diurnal (M_2) component has a period of 12.47 hours and is reinforced by the solar semi-diurnal (S_2) component which has a period of 12 hours (Neuman and Pierson, 1966).

Inertial motions in the region northeast of Svalbard vary from 12.06 hours at 83°N to 12.15 hours at 81°N. Thorndike (1986) determined that inertial amplitudes of 20 cm/s are possible in the Arctic. Thus, given the extremely similar amplitudes and periodicities of both the tidal and inertial oscillations, a conclusive determination of the nature of the oscillations may not be possible. Without additional current and ice speed measurements a final classification would be premature.

The cross-correlations of the U and V components of ice velocity, Figure 3.22, show the characteristic 3 hour lag in peak correlation described by Thorndike (1986) that characterizes a 12-hour clockwise oscillation. When a piece

of ice undergoing a tidal/inertial oscillation (period ~12 hours) moves in the positive U-direction, three hours later it will be moving in the negative V-direction. This relationship is what dictates the initial negative correlation peak with a lag of 3 hours. The negative and positive correlation peaks have initial lags of 3 hours and 9 hours, respectively. Subsequent positive/negative correlation peaks follow every 12 hours.

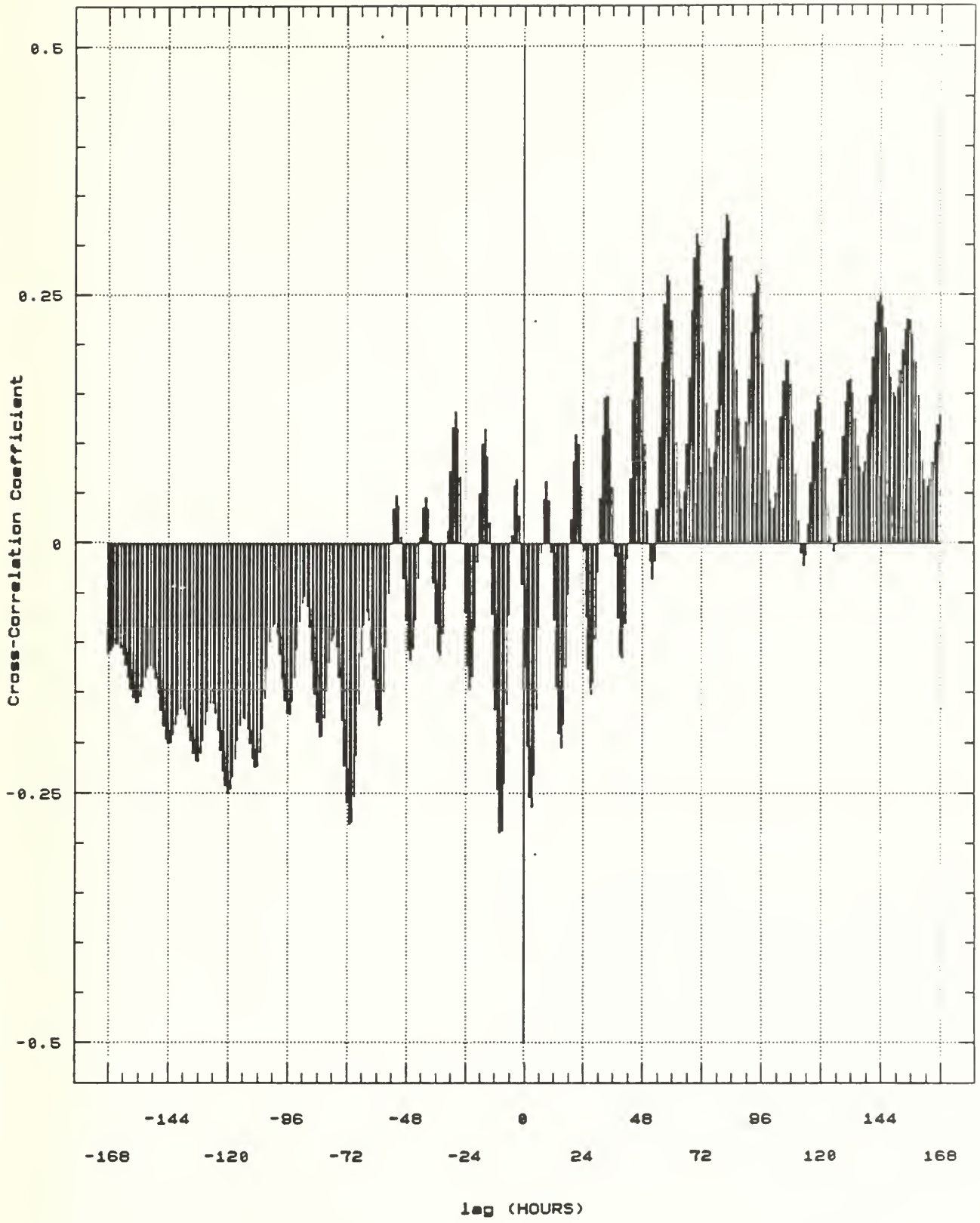

Figure 3.22 Cross-correlations of U & V components of ice speed demonstrate the characteristic 3-hour lag of maximum correlation for a 12-hour clockwise oscillation.

IV. CROSS-CORRELATIONS

This chapter will discuss the relationships between the various forcing functions (wind, ice motion, and air temperature) and ambient noise over the entire length of the record. Chapter V will examine the relationships for specific events or periods of time.

A. ICE MOTION FORCING FUNCTIONS

The primary driving forces for ice motion are the wind stress, the water stress, the coriolis force, the ocean dynamic height, and the internal ice stress (Hibler and Tucker, 1979). In free drift conditions, however, a close approximation of ice motion may be established by using only the two largest driving forces, the wind speed and the ocean current. For day to day ice motions, approximately 70 percent of the variance can be attributed to the winds (Thorndike and Colony, 1982). As the ice moves from the waters of the deep Arctic onto the continental shelf, tidal forces become increasingly important while inertial forces decrease in magnitude (Thorndike, 1986). When long term drift calculations are performed, the short term effects of the wind become less important while the ocean currents and coriolis force increase in importance (Hibler,1981). For these longer observations, approximately fifty percent of the ice motion

can be attributed to the wind while the other fifty percent must be derived from the ocean currents (Thorndike and Colony, 1982).

The two primary forces operating on the ice pack north of Svalbard, as revealed by ice motion analysis, are the wind stress and the tidal/inertial oscillations. Ocean current data, if it had been available, may have resolved the nature of the oscillations and revealed the relationship between the ocean currents and the ice motion in this region. One way to determine whether the oscillations were either tidally or inertially forced, without the benefit of current data, is to establish their periodicity. A regular period of oscillations that are in phase throughout the record might indicate a tidal origin because a tidal period remains essentially constant within a particular region. An inertial oscillation, while maintaining the same period at a particular latitude, is dependent on changes in wind and currents and tends to display a different phase for different forcing events and may disappear altogether if the forcing is removed. Thus inertial oscillations usually display a more irregular phase relationship between different portions of the record than a tidal oscillation.

As shown in Figure 4.1, the oscillations prior to day 297, particularly days 290-295, are fairly irregular in nature and are most likely inertial. The oscillations, after Julian day 297 when the *Polarbjoern* drifted onto the shelf (depth < 1000

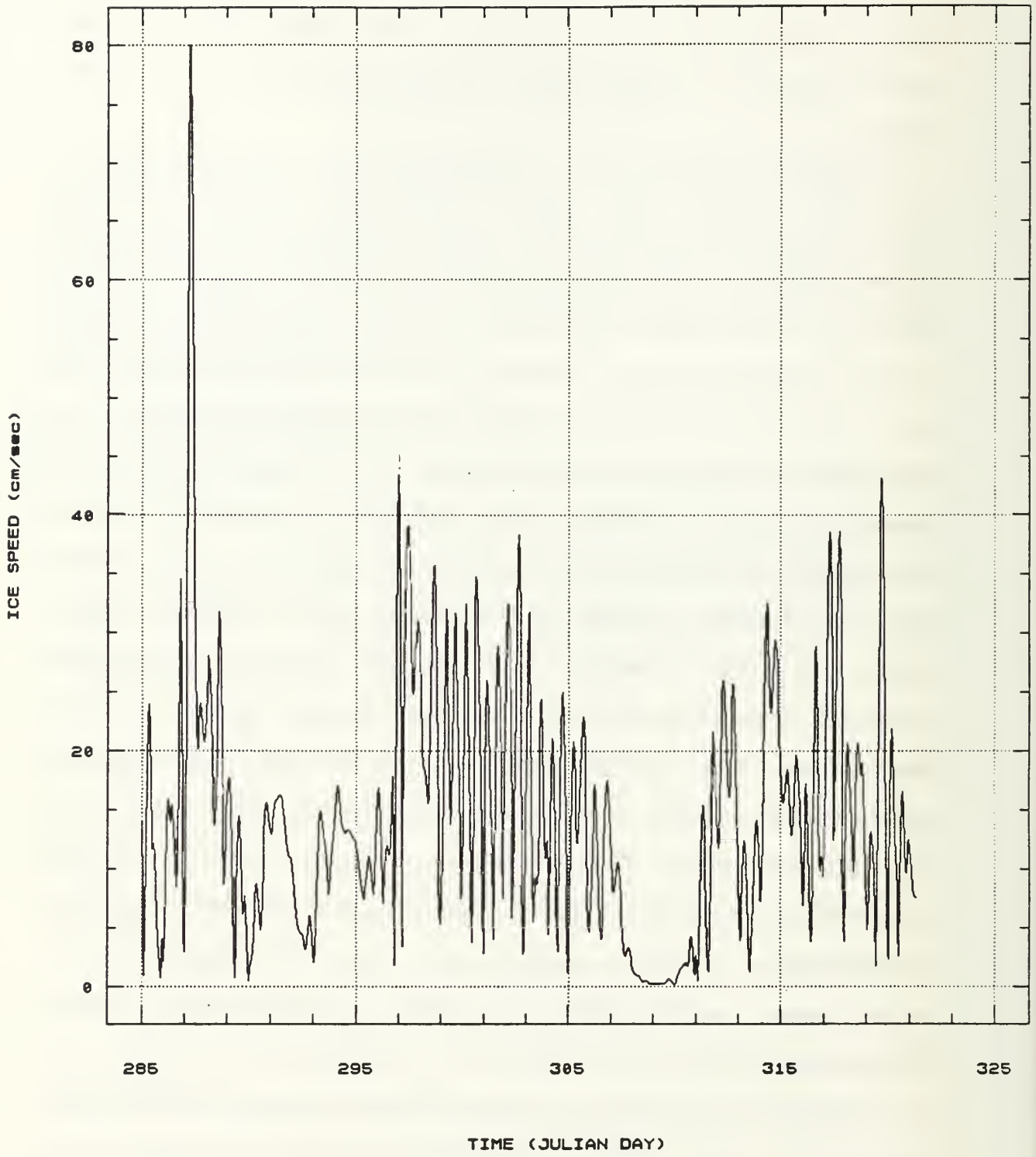

Figure 4.1 Hourly-averaged time series of ice speed (cm/s) from 11 October to 18 November 1988 (Julian days 285-323). The 12-hour oscillations vary throughout the record.

m), were extremely regular and might have indicated an increasing tidal influence were it not for the lack of oscillations during Julian days 308-310 when the ice drift speed was near zero. If tidal oscillations were present, then one would have expected to see them during this stationary period. Without additional investigation, the exact nature of the oscillations, be they tidal or inertial, can not be established. For the purposes of this study, an exact determination of the type of oscillation is not necessary and a simple classification of tidal/inertial will be sufficient.

As stated previously, the two primary forces acting on the ice are the wind stress and the tidal/inertial oscillations. The effects of these two forces can be most readily observed during an 11-day period in early November. Figures 4.2a and 4.2b present a time series of wind speed and ice speed during this period. The wind speed maxima that are observed on days 312, 314, and 317 can be directly correlated to the ice speed maxima that are present six hours later on the same day. Close analysis of Figures 4.2a and 4.2b reveals that each wind speed peak is associated with a bi-modal ice speed peak. This bi-modal nature in ice speed can be attributed to the influence of the tidal/inertial oscillations which are superimposed over the effects of the wind. When the oscillations are in phase with the wind direction, they serve to increase the wind-generated ice speed maxima; conversely when they are out of phase, i.e., oppose the wind direction,

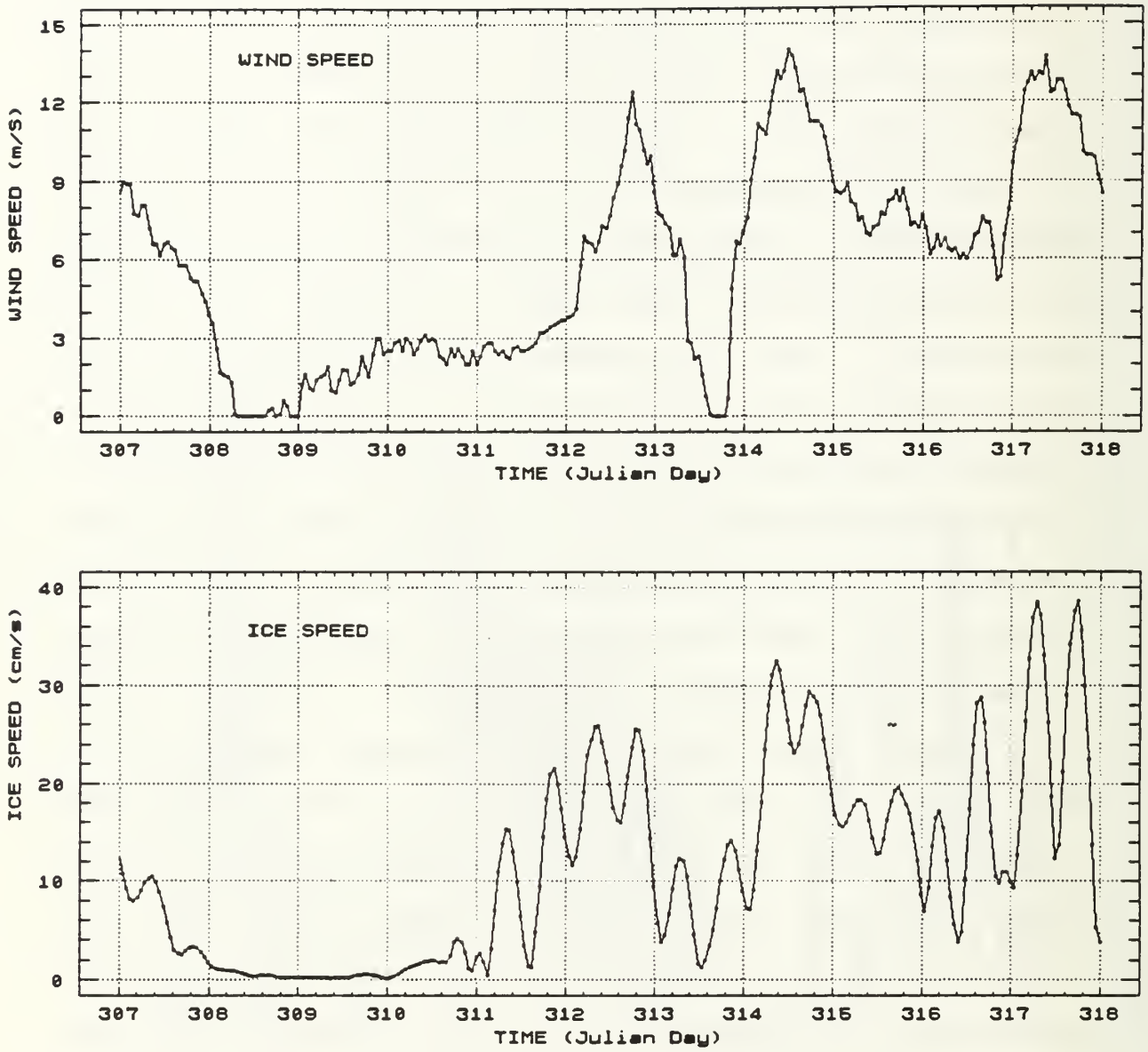

Figure 4.2 Hourly-averaged time series of wind speed and ice speed for Julian days 307-318. Note the bi-modal nature of the ice speed peaks and the six hour lag between wind speed and ice speed maxima.

they serve to decrease the ice speed. Thus, the ice speed maxima are generally bi-modal with the two peaks occurring 12 hours apart. Each peak is separated by a relative minimum occurring six hours after the first peak.

B. WIND and ICE MOTION

1. Wind Speed and Ice Speed

A cross-correlation between wind speed and ice speed was conducted on the 38-day record in order to verify the strong relationship between the wind and ice that was discussed above and to determine how these correlations compare with historical results. Figure 4.3 presents the cross-correlation between these two parameters. The direct correlation between wind speed and ice speed reveals a correlation coefficient of 0.62. Thus, a large portion of the variance of the ice speed, over the length of this analysis, can be accounted for by the wind speed. As the lag increased, the correlation steadily decreased out to the e-folding time of 24 hours. While the temporal coherence is relatively short, it is similar to the temporal scales obtained by Lewis and Denner (1987b) and Poffenberger, Bourke, and Wilson (1988). Lewis and Denner observed e-folding time scales of about 10-30 hours for the frequencies of 10, 32, and 1000 Hz that were based on measurements collected from 1975-1976 in the Beaufort Sea as part of the project AIDJEX. Poffenberger et al. computed e-folding time scales of 1.0 to 2.5 days from

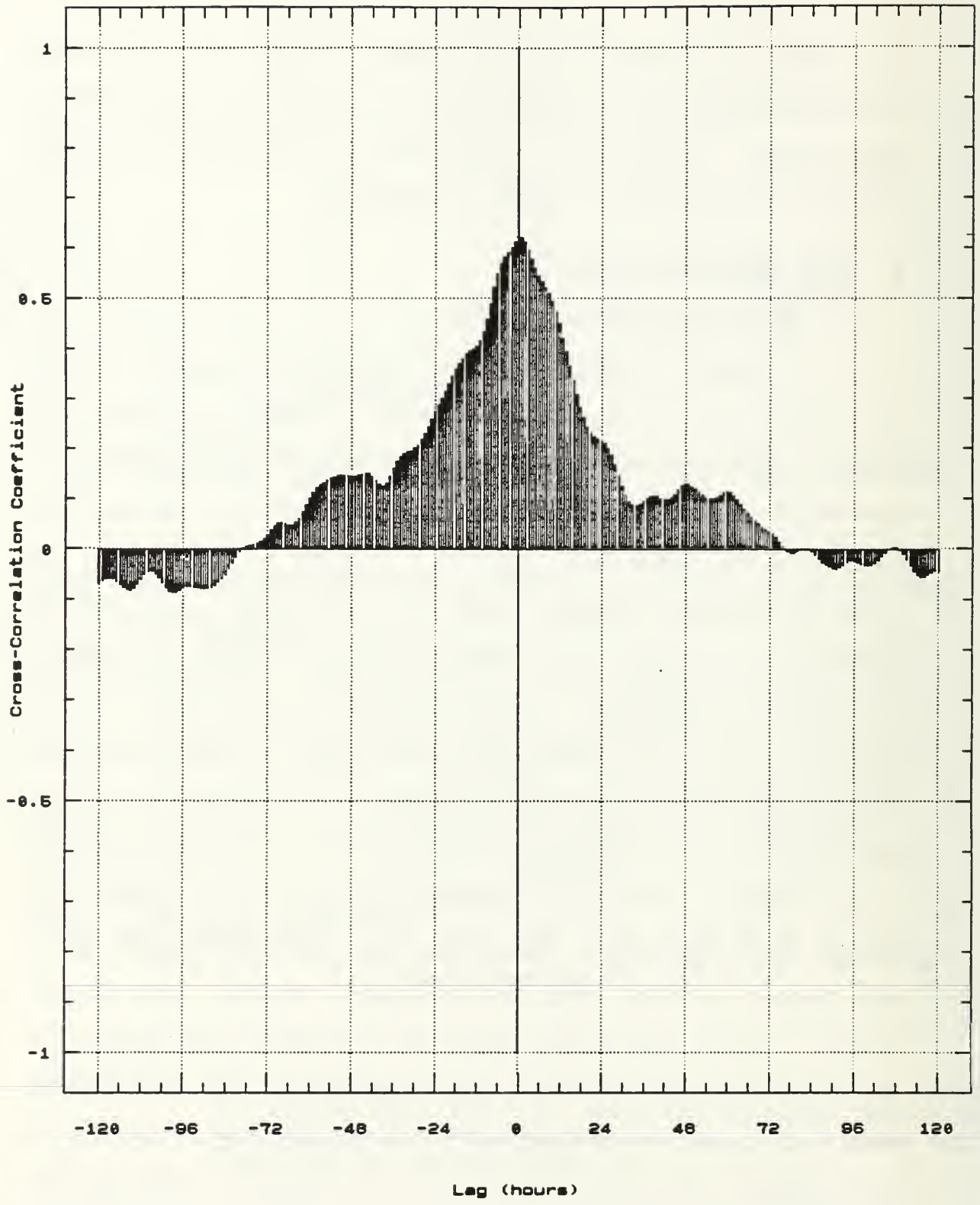

Figure 4.3 Cross-correlations between the 38-day wind speed and ice speed records.

Arctic ambient noise buoy measurements (10-315 Hz) collected in the Eurasian Basin during 1981-1984.

The high correlation between wind speed and ice speed is not just a statistical phenomena, but a proven relationship based on physics. It is a known fact that increases in the wind speed result in similar, but smaller, increases in the ice speed. This relationship was confirmed by early free-drift models based on the physics of the momentum balance. Zubov's rule (1943) states that ice drifts approximately 28 degrees to the right of the surface wind at 2 percent of the surface wind speed.

When the results of the Barents Sea wind speed/ice speed cross-correlations are compared with more recent statistical studies, the data compare quite favorably. Thorndike and Colony (1982) reported a high correlation from drifting buoys in the central Arctic basin ($r = 0.8$-0.9), with over 70 percent of the variance in the ice speed accounted for by the wind speed. The lower correlation from the Barents Sea data may reflect that the ice was not in free drift, as the buoys in the central Arctic basin were. The increase in internal ice stress, manifested by the increased ridging observed in this area (Figure 3.8), reduces the ability of the ice to freely respond to the variable wind forcing.

2. Wind Direction and Ice Direction

The mean direction of ice motion from Julian day 285 to 323 was predominantly to the southwest. There were, however, four short periods when the mean ice direction changed to either the southeast or northwest. These periods of anomalous ice motion correlate almost perfectly with shifts in the wind direction and are described below.

The path of the *Polarbjoern* from day 285 to 323 can be segmented into seven major sections that are labeled a-g in Figure 1.1. This drift path was derived from daily interpolated data which averaged out the 12-hour tidal/inertial oscillations and hence represents predominantly a wind-forced drift. Sections a and e cover periods when the ship and ice floe moved to the southeast, sections c and f represent periods when the ship moved to the northwest, and sections b, d, and g denote movement to the southwest.

Figure 4.4 shows the hourly-averaged wind and ice velocity time series for Julian days 285 to 323. Wind and ice directions are revealed by the barbs at the top of the plot, while the wind and ice speeds are plotted below the barbs. Since the ice motion was derived from hourly interpolated data, the 12 hour tidal/inertial oscillations that were averaged out in Figure 1.1 become apparent. While the oscillations can be discerned throughout the time series, they are most readily apparent during Julian days 299 to 305.

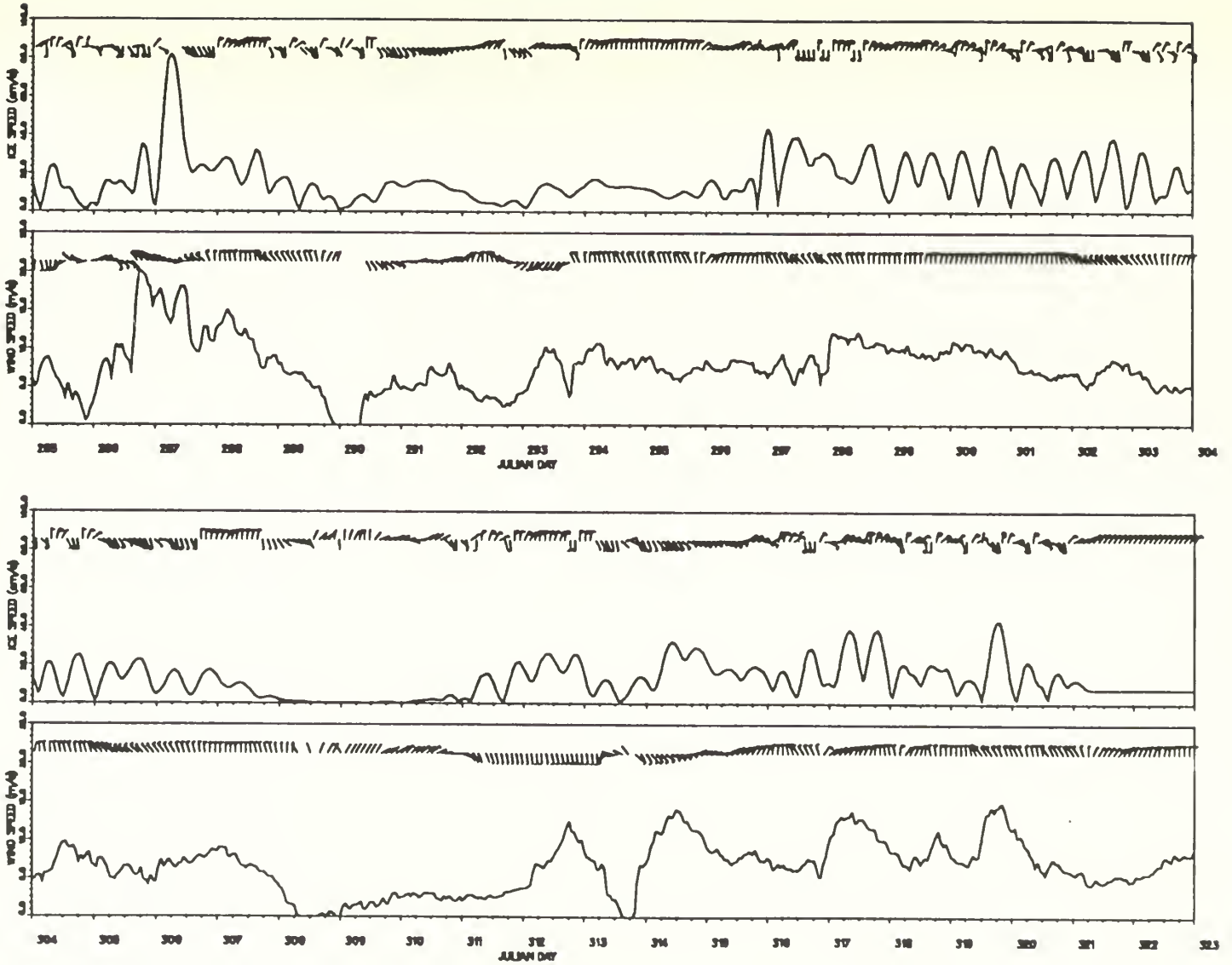

Figure 4.4 Hourly-averaged wind and ice motion time series for Julian days 285-323. Mean directions of ice and wind motion correlate well.

Another factor that is readily observable is the strong relationship between wind and ice speed. The maximum wind speed was recorded during the late evening hours on Julian day 286 while the maximum ice speed occurred 12 hours later on day 287. Conversely, periods of weak winds, Julian days 308-311, can be correlated with periods of slow ice speed. Similar wind speed/ice speed relations occur throughout the record.

The strong correlation between the wind and ice motion extends to their respective directions of movement as well. During periods of ice motion to the northwest (sections c and f), southeasterly winds are evident during the hours immediately preceding the shift in ice motion. Similarly, southeasterly ice motion (sections a and e) and southwesterly ice motion (sections b, d, and g) are preceded by appropriate shifts in the wind direction. Thus on a daily or longer time frame, the ice movement is heavily dependent on the wind direction.

Figure 4.5 reveals the strong tidal\inertial oscillations of the ice when subjected to the steady forcing of northerly winds during days 300 to 302. These type of oscillations occurred at various times throughout the record irrespective of the mean direction of ice motion. While the ice motion displayed a strong clockwise rotation due to tidal/inertial forcing, the southerly components were larger than the northerly motions and resulted in a net southerly motion.

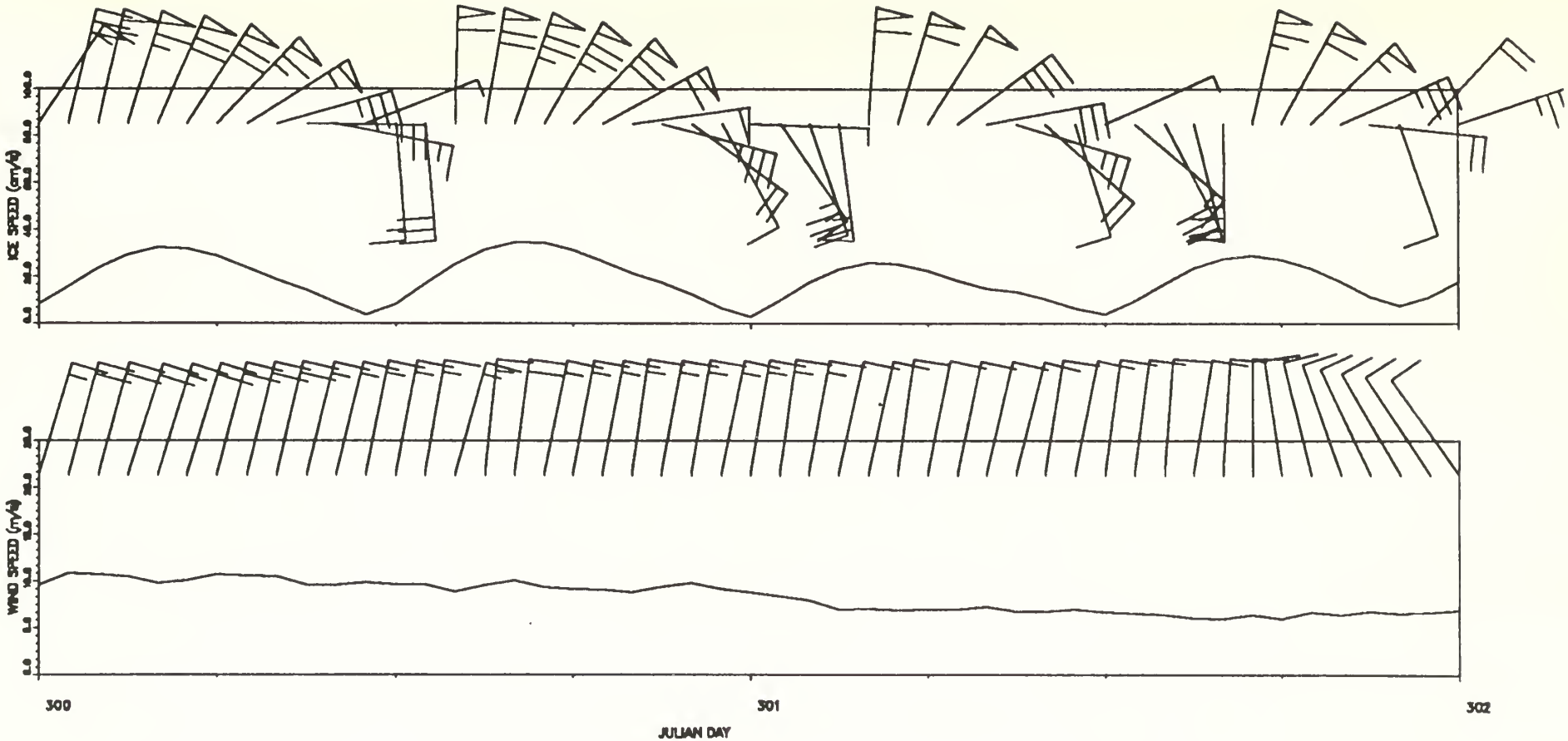

Figure 4.5 Hourly-averaged wind and ice motion (direction and speed) time series for Julian days 300 and 301 (26-27 October). The speed barbs at the top of each of the plots indicate the ice direction and wind direction. The ice speed (cm/s) and wind speed (m/s) are displayed below the barbs. The tidal/inertial oscillations display a strong rotational influence on the ice motion throughout the period. The ice speed decreases as the ice rotates clockwise reaching its minimum speed when it opposes the mean direction of ice motion. The wind remains relatively constant throughout the period.

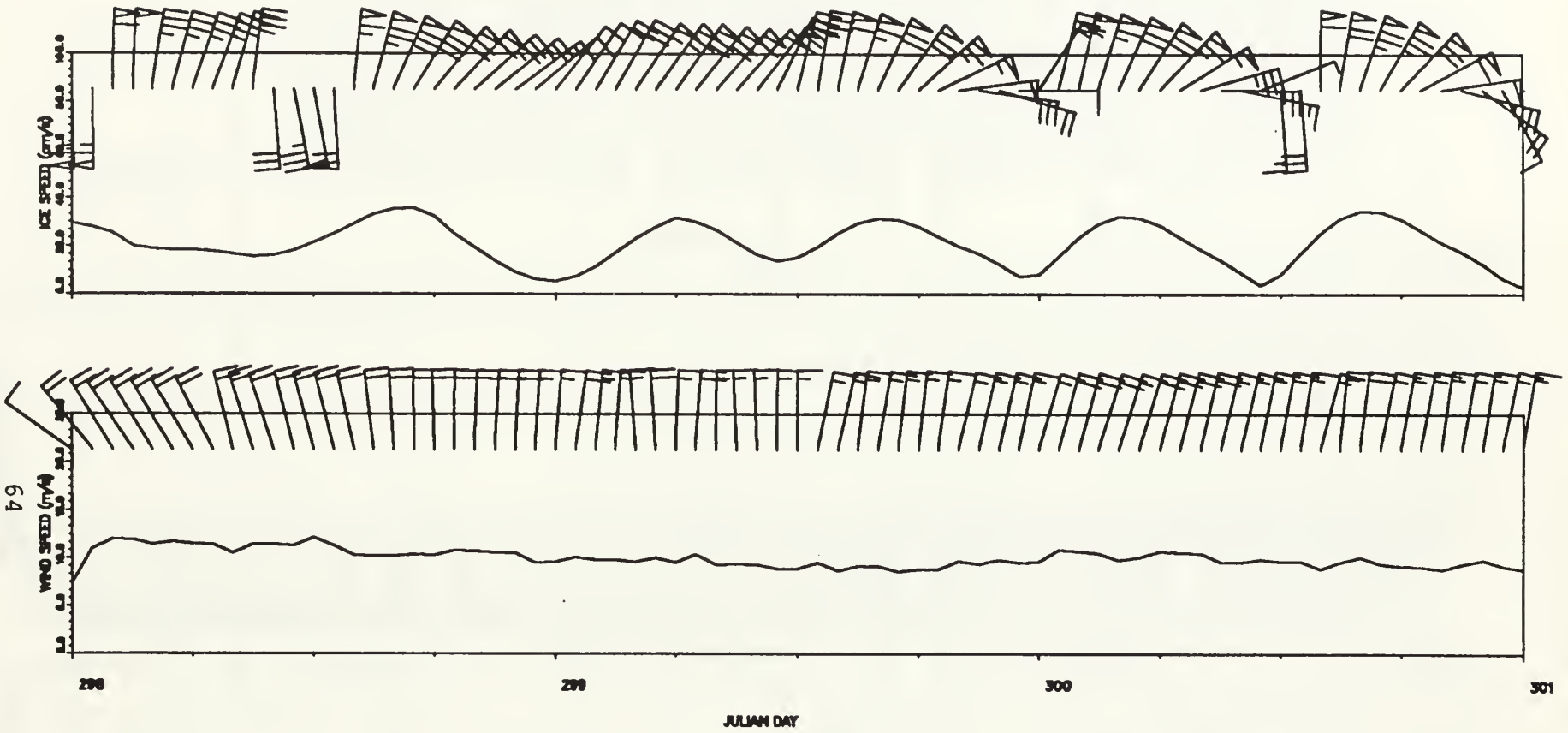

Figure 4.6 Hourly-averaged wind and ice motion time series for Julian days 288-301 (24-27 October). The speed barbs at the top of each of the plots indicate the ice direction and wind direction. The ice speed (cm/s) and wind speed (m/s) are displayed below the barbs. The tidal/inertial oscillations display an increasing rotational influence on the ice motion throughout the period. The ice speed decreases as the ice rotates clockwise reaching its minimum speed when it opposes the mean direction of ice motion. The wind remains relatively constant throughout the period.

During other portions of the record (Figure 4.6), the northerly oscillations were sufficient to reduce the southerly speed of the ice drift but were not strong enough to reverse the ice flow direction. This may be observed during Julian day 299. The ice direction rotates from the south to the southwest as the ice speed decreases from 35 cm/s to 5 cm/s. Note the increase in rotation in subsequent oscillations from day 299 to 301.

C. WIND SPEED and AMBIENT NOISE

Buck and Green (1978) correlated changes in large-scale atmospheric pressure gradients with ambient noise levels in the Beaufort Sea and obtained a correlation of about 0.6. Thus the close relationship between large-scale wind forcing and ambient noise has been known for many years. However, when only the local wind speed is considered, the cross-correlation between wind speed and ambient noise is significantly reduced. This reduction in correlation comes about because the ambient noise is dependent upon distant sources of wind-generated noise as well as local sources (Colony and Thorndike, 1980; Serreze, 1989).

The result of the cross-correlations between wind speed and ambient noise in the Barents Sea, which are based only on the local winds, are presented in Figure 4.7. All three frequencies display a complex shape with three peaks of

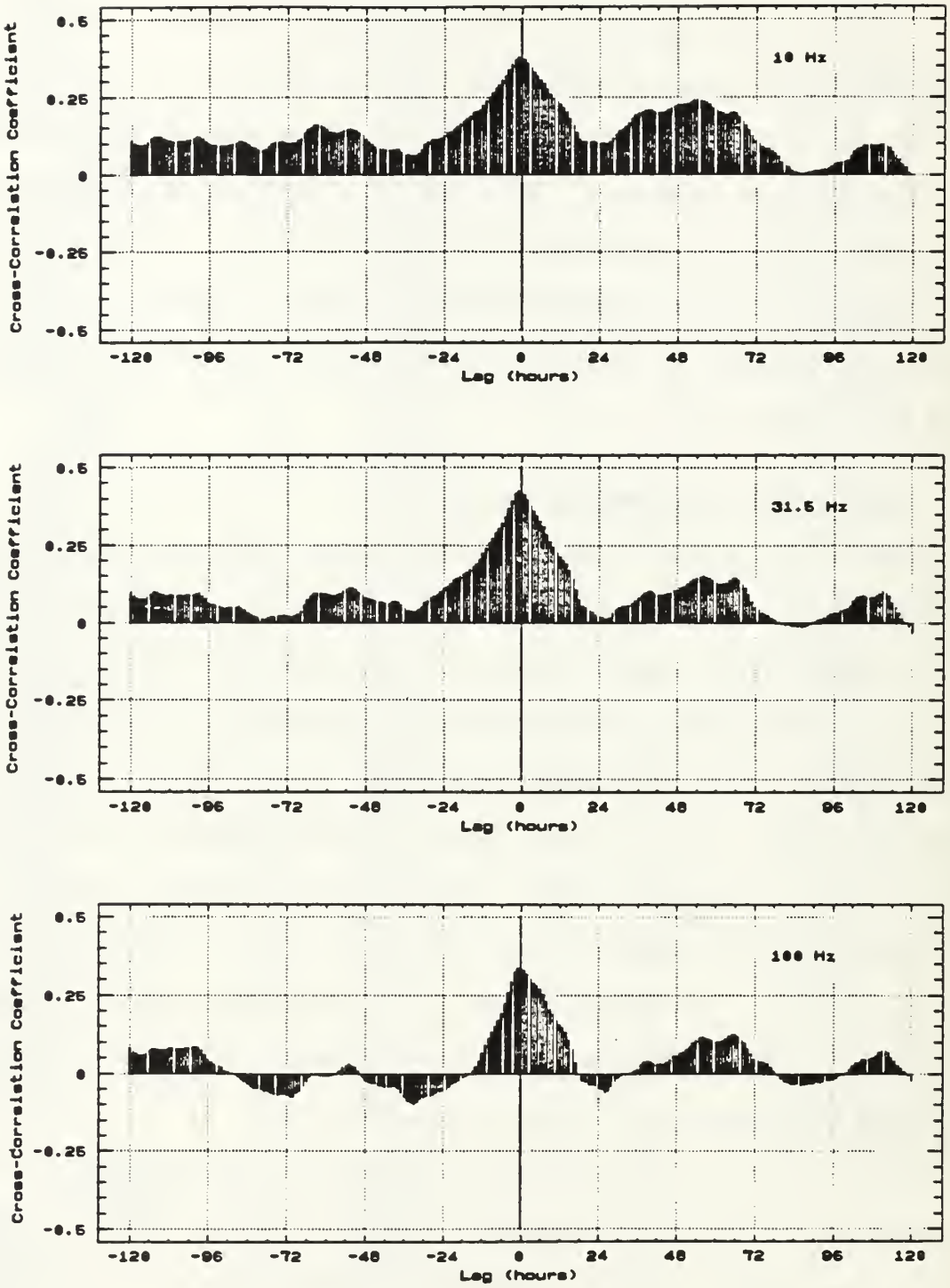

Figure 4.7 Cross-correlations between wind speed and ambient noise for frequencies of 10, 31.5, and 100 Hz.

decreasing magnitude. At 10 Hz the direct correlation between wind speed and ambient noise shows a relatively modest correlation coefficient of 0.38. The other two peaks are found at lags of 54 and 108 hours with coefficients of 0.25 and 0.1, respectively. The intervening minima are at 24 hours, where the correlation coefficient dips to 0.1, and at 84 hours and 120 hours where the correlations are zero. At 31.5 Hz, the coefficient plot is similarly shaped with a direct cross-correlation coefficient of 0.43 and secondary maxima of 0.15 and 0.1. The correlation coefficients at 100 Hz are less than those found at the lower frequencies with a direct cross-correlation coefficient of 0.34. The temporal coherency (e-folding time) for all three frequencies is about 15 hours.

While the autocorrelation of wind speed (Figure 3.14) revealed no periodicity, the increased cross-correlations displayed between the wind speed and ambient noise with lags of 54 and 108 hours may represent distant sources of wind-generated ambient noise. The propagation of low frequency ambient noise due to the periodic passage of synoptic scale cyclones can not be discounted.

D. ICE SPEED and AMBIENT NOISE

Previous ambient noise studies by Buck (1966), Lewis and Denner (1987a), and Higgins (1990) have revealed a close relationship between ice motion and low frequency ambient

noise. The Barents Sea data analyzed in this study also demonstrated a strong association, with ice speed accounting for a large portion of the ambient noise variability. Figure 4.8 displays the cross-correlations between hourly-averaged ice speed and the 10, 31.5, and 100 Hz ambient noise time series for the 38-day record. The maximum correlation between ice speed and ambient noise occurred with a lag of six hours. At 10 Hz the maximum correlation coefficient was 0.4 with subsequent correlation maxima occurring at 12 hour intervals until well beyond the e-folding time of 21 hours. The cross-correlations for 31.5 and 100 Hz are similar to the 10 Hz correlation described above. They retain the same periodicity, while the overall magnitude of the correlation coefficients decrease with increasing frequency. The six hour lag time and the 12 hour correlation peaks will be discussed in greater detail in subsequent paragraphs.

As previously stated, ice speed is primarily controlled by two factors in the waters northeast of Svalbard, wind speed and tidal/inertial oscillations. Thus, these two influences will be key factors in the correlation between ice speed and ambient noise. When the wind stress is increased, the ice speed will increase resulting in a higher ambient noise level and a positive cross-correlation between the two. When the 12-hour tidal/inertial oscillations are introduced, they serve to either increase the ice speed, when they are in phase with the mean direction of motion, or decrease the ice speed, when

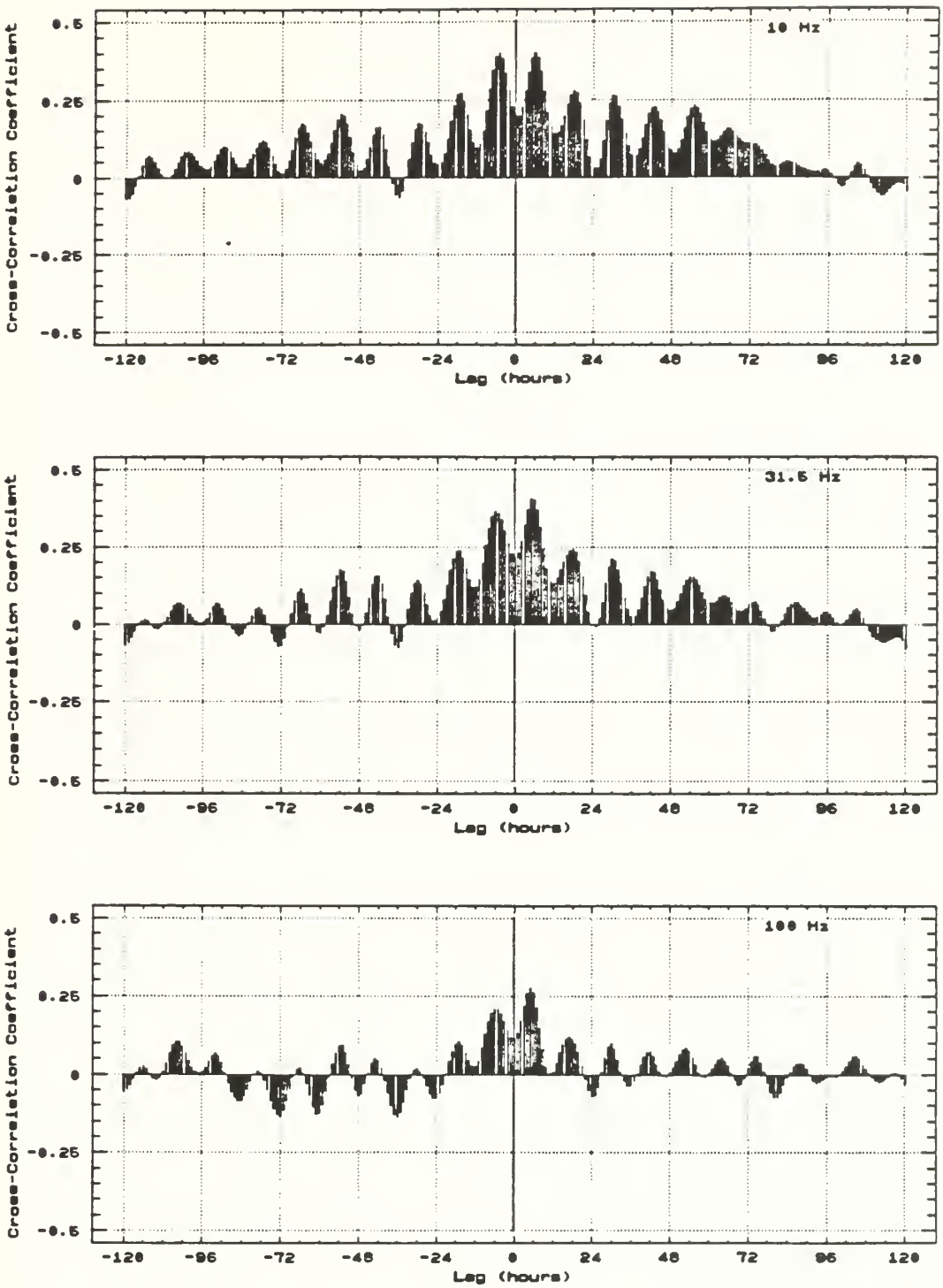

Figure 4.8 Cross-correlations between ice speed and ambient noise for frequencies of 10, 31.5, and 100 Hz. Note the strong 12-hour periodicity displayed.

they oppose the mean direction of ice movement. This oscillatory fluctuation in the net ice drift motion results in a complimentary oscillatory fluctuation in ambient noise.

The basic premise being put forth is that when the 12 hour tidal/inertial oscillation of the ice opposes the mean direction of ice movement, the ambient noise level increases. Initially, when an oscillation is in phase with the mean direction of motion, the ice speed increases. This increased ice speed in turn results in greater divergence of the ice field and a slight increase in the ambient noise level. The maximum noise level, however, occurs 6 hours later when the tidal/inertial oscillation opposes the mean direction of ice movement. When the net ice speed is reduced, increased convergence of the ice field results and the noise level increases markedly above the mean noise level. As explained above, this unexpected correlation is most likely the result of increased convergent forcing. When an ice floe oscillates such that its northward motion opposes the mean southward motion of the ice pack, greater convergent forces are generated in the ice pack, increased fracturing and ridging of the ice occurs and greater ambient noise levels are observed.

Figure 4.9, time series for Julian days 307-318, can be used to demonstrate the relationship between ice speed and ambient noise. Peaks in ambient noise occur during the relative minima of the ice speed peaks. These relative minima lie between the bi-modal ice speed peaks and mark the

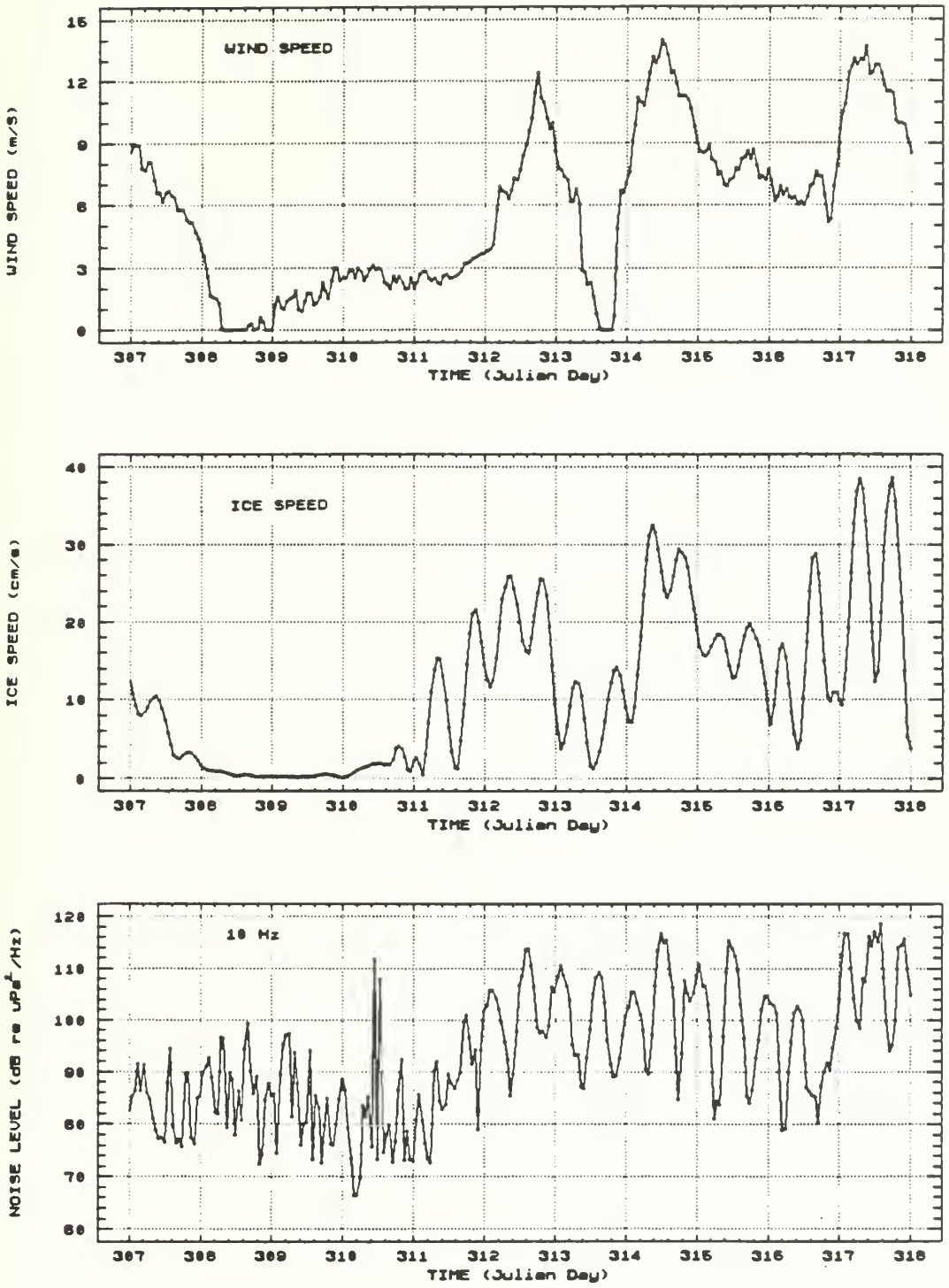

Figure 4.9 Hourly-averaged time series for wind speed, ice speed, and ambient noise (10 Hz). Maximum ambient noise levels coincide with the relative minima that lie between the bi-modal speed peaks.

northerly phase of the tidal/inertial oscillation. These ambient noise maxima occur six hours after the first peak of an ice speed maximum and validate the six hour lag found in the ice speed/ambient noise cross-correlation.

E. TEMPERATURE and AMBIENT NOISE

The cross-correlation between temperature and ambient noise (Figure 4.10) is quite different from the previous correlations performed with the wind and ice speed. The coefficient gradually decreases as the lag is increased and does not display any strong periodicity. Additionally, the correlaticn between temperature and ambient noise decreases with increasing frequency. The maximum correlation is found at 10 Hz where the coefficient gradually decreases from a high of 0.38 at 3 hours, to a low of 0.15 at the e-folding time (120 hours). Three relatively minor peaks possess lags of 36, 72, and 108 hours. The correlation is still relatively high at 31.5 Hz where a coefficient maximum of 0.27 is also found at the 3 hour lag point. The correlation between temperature and ambient noise is virtually zero at 100 Hz. This may indicate that the forcing at 100 Hz is significantly different from that found at 10 or 31.5 Hz. The relatively weak correlation between the air temperature and ambient noise may be an indication that the relation between the two may be associative and not causative, i.e., the correlation between the temperature and the ambient noise may be associated with

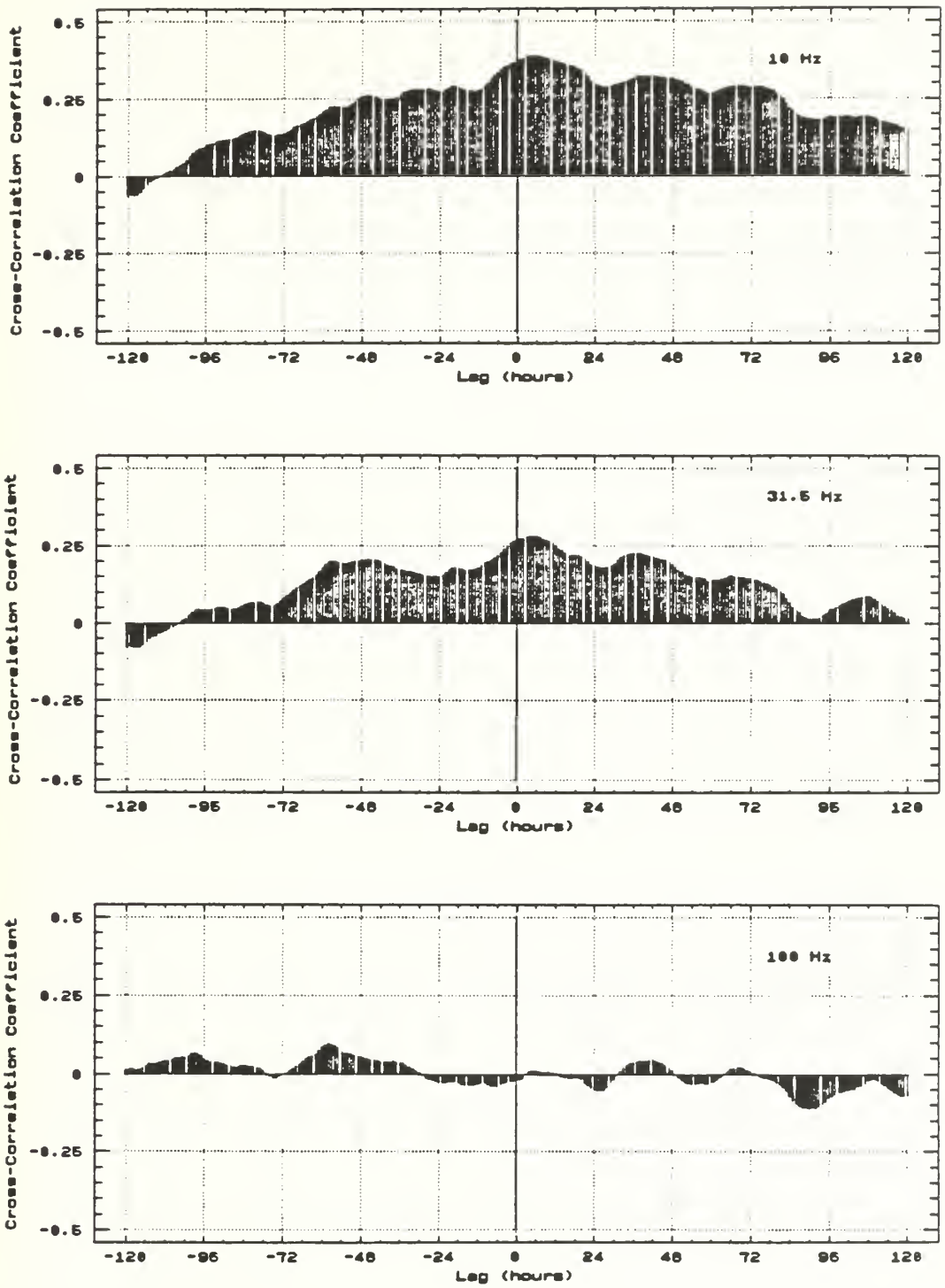

Figure 4.10 Cross-correlations between temperature and ambient noise for frequencies of 10, 31.5 and 100 Hz. Note that the correlation is negligible at 100 Hz.

warm southerly winds and the increased convergence that they entail. This association will be discussed in greater detail in Chapter V. Additional manipulation of the temperature record beyond that performed during this study might be beneficial. If the temperature record had been detrended, it may have eliminated any masking of high frequency periodicities.

F. FREQUENCY COMPARISONS

Cross-correlations were performed between the hourly averaged 10 Hz, 31.5 Hz, and 100 Hz ambient noise time series in order to determine whether the same forces were at work on each frequency. All displayed strong cross-correlations with correlation coefficients greater than 0.5 and exhibited some form of a tidal/inertial influence. As one might expect, adjacent octave bands (10 and 31.5 Hz; 31.5 and 100 Hz) displayed higher correlations than more distant bands (10 and 100 Hz).

The direct cross-correlation between 10 and 31.5 Hz, Figure 4.11a, proved to be the greatest with a correlation coefficient of 0.84. The lagged correlation displayed a strong tidal/inertial influence with correlation peaks at 12 hour intervals out to 60 hours. The e-folding time was about 14 hours.

The cross-correlation between 31.5 and 100 Hz, Figure 4.11b, also displayed a strong correlation (0.81) with a

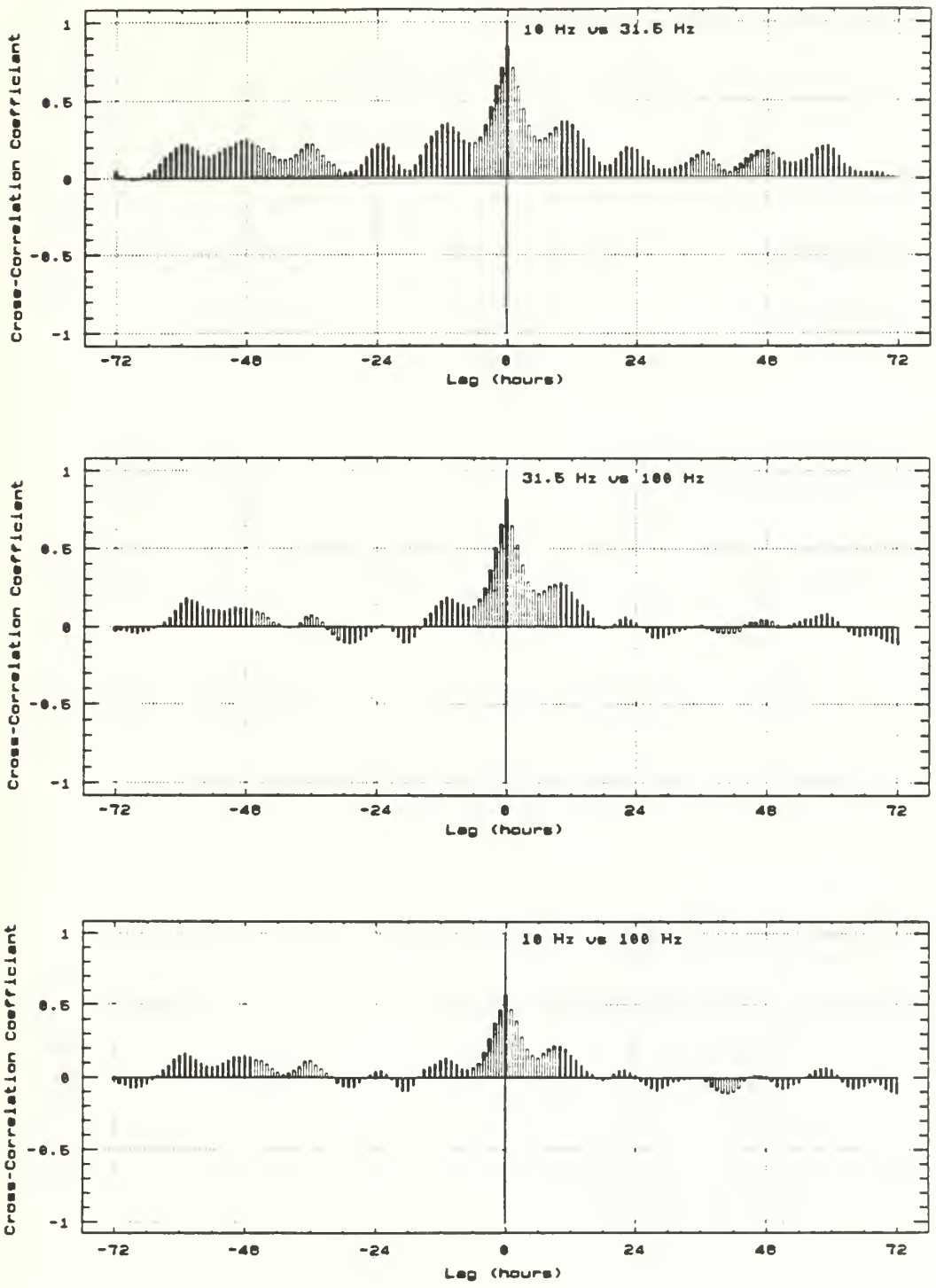

Figure 4.11 Cross-correlations between the hourly-averaged 10, 31.5, and 100 Hz time series. The 10 Hz/31.5 Hz cross-correlations display a strong 12-hour period.

secondary peak at 10 hours. No other significant peaks are present at longer lag times. The cross-correlation between 10 and 100 Hz (Figure 4.11c) is similar in shape to the 10 and 31.5 Hz cross-correlation with a direct correlation of only 0.6. The e-folding time was only 4 hours indicating a rapid decoupling of the two frequencies.

The cross-correlation between 10 Hz and 100 Hz is similar to previous measurements in the region. Poffenburger, Bourke, and Wilson (1989), in an analysis of drifting buoy measurements in the Eurasian Basin, reported cross-correlation coefficients of 0.63 in the summer and 0.78 in the winter for frequencies of 10 and 100 Hz.

Hence, it is only the lower two frequencies which exhibit a strong forcing by tidal/inertial oscillations and temperature related phenomena. While 100 Hz still displays some tidal/inertial forcing (Figure 3.9), its effect is much diminished. Some other forcing, not revealed in this analysis, provides the principle forcing at 100 Hz.

V. EVENT ANALYSIS

Statistical analysis of ambient noise over a relatively long period, such as the 38-day record of this study, can only reveal a limited amount of information. Long term averaging may in fact confuse matters by blurring the effects of various forcing parameters. If, however, the various trends can be successfully identified and separated, then additional information concerning the influence of these forces on ambient noise can be ascertained. This chapter will attempt to separate the statistical record in various ways in order to more clearly delineate the driving forces for ambient noise.

A. MOTION vs AMBIENT NOISE

The entire 38-day, 10 to 100 Hz, ambient noise record was divided into two classes, those reports that were acquired while the ice was moving northwards and those acquired while the ice drifted southwards. The hourly observations that displayed northerly motion included both northerly inertial/tidal oscillations which during periods of mean southerly motion, as well as the more abundant observations obtained during periods of mean northerly motion. Table 4 gives the statistical results for the three frequencies and Figure 5.1 is a spectral plot of the ambient noise levels

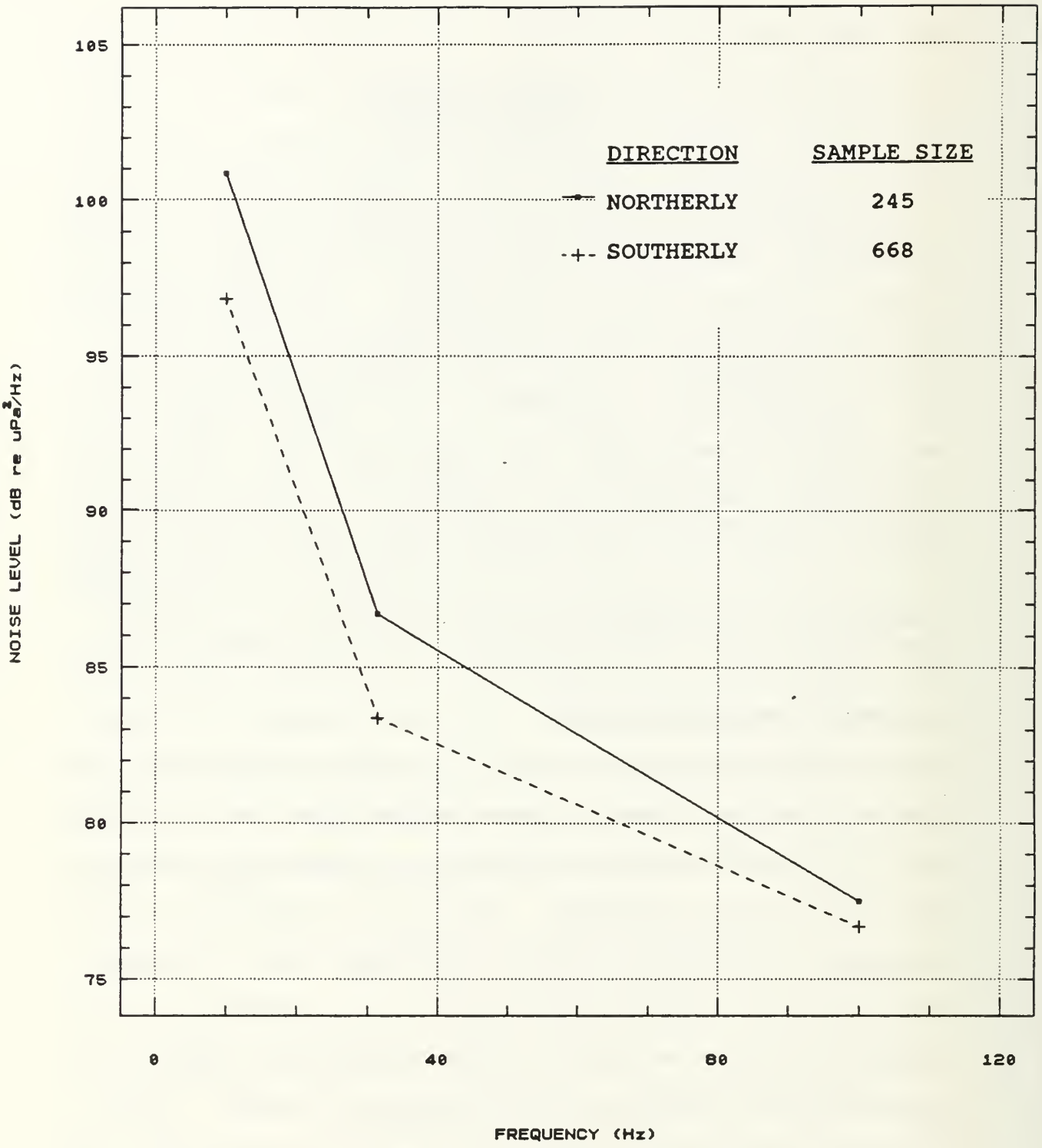

Figure 5.1 Spectral plot comparing the ambient noise levels recorded during northerly and southerly ice motion.

recorded under northerly and southerly flow conditions. Note that when the ice motion was to the north, the ambient noise was consistently higher. Northerly motion resulted in noise levels 4 dB noisier than southerly motion at 10 Hz and decreased to a 1 dB difference at 100 Hz.

TABLE 4. ICE MOTION vs AMBIENT NOISE

FREQUENCY DIRECTION	10 NORTH	10 SOUTH	31.5 NORTH	31.5 SOUTH	100 NORTH	100 SOUTH
SAMPLE SIZE	245	656	245	668	245	668
MEAN	98.8	95.3	87.0	84.4	78.5	77.5
MEDIAN	100.9	96.8	86.7	83.4	77.5	76.7
STANDARD DEVIATION	10.1	11.1	6.4	7.0	5.4	5.8
MAXIMUM	118.5	124.1	106.9	115.8	114.6	106.6
MINIMUM	66.3	64.3	64.8	64.4	63.9	63.9

There are two possible explanations for the difference in these ambient noise levels. The first possible explanation is that the increased ambient noise for northerly ice motion may be a result of the increased convergence associated with northerly tidal\inertial oscillations. This explanation is supported by the fact that throughout the noise record

increases in ambient noise were directly correlated to northerly oscillations in ice motion. The second and more influential factor in increased ambient noise (since more than 2/3 of the northerly observations were obtained during periods of mean northerly ice motion) is the increased convergence that occurs when local forcing drives individual ice floes northwards against the large unyielding ice pack. This convergence would also result in an increase in the ambient noise. Thus, when the local ice motion is southward, i.e., in phase with the large scale divergence, ambient noise levels decrease. When the local ice motion opposes the large scale motion (whether it is due to local wind forcing or tidal/inertial oscillations) the ambient noise levels increase. This relationship between convergence and increased ambient noise will be explored further in the paragraphs below.

Figures 5.2a and 5.2b display contrasting directions of mean ice motion during two different periods of the ambient noise record. Julian days 291 and 294 represent an early portion of the drift south while the *Polarbjoern* was still several hundred kilometers north of the Svalbard Archipelago. Julian day 291 displayed a mean northerly drift while day 294 displayed a mean southerly drift. Figure 5.2a reveals an almost uniform 12-13 dB increase in ambient noise during the period of mean northerly motion. It is postulated that the shift in ice direction is a purely regional phenomena that is

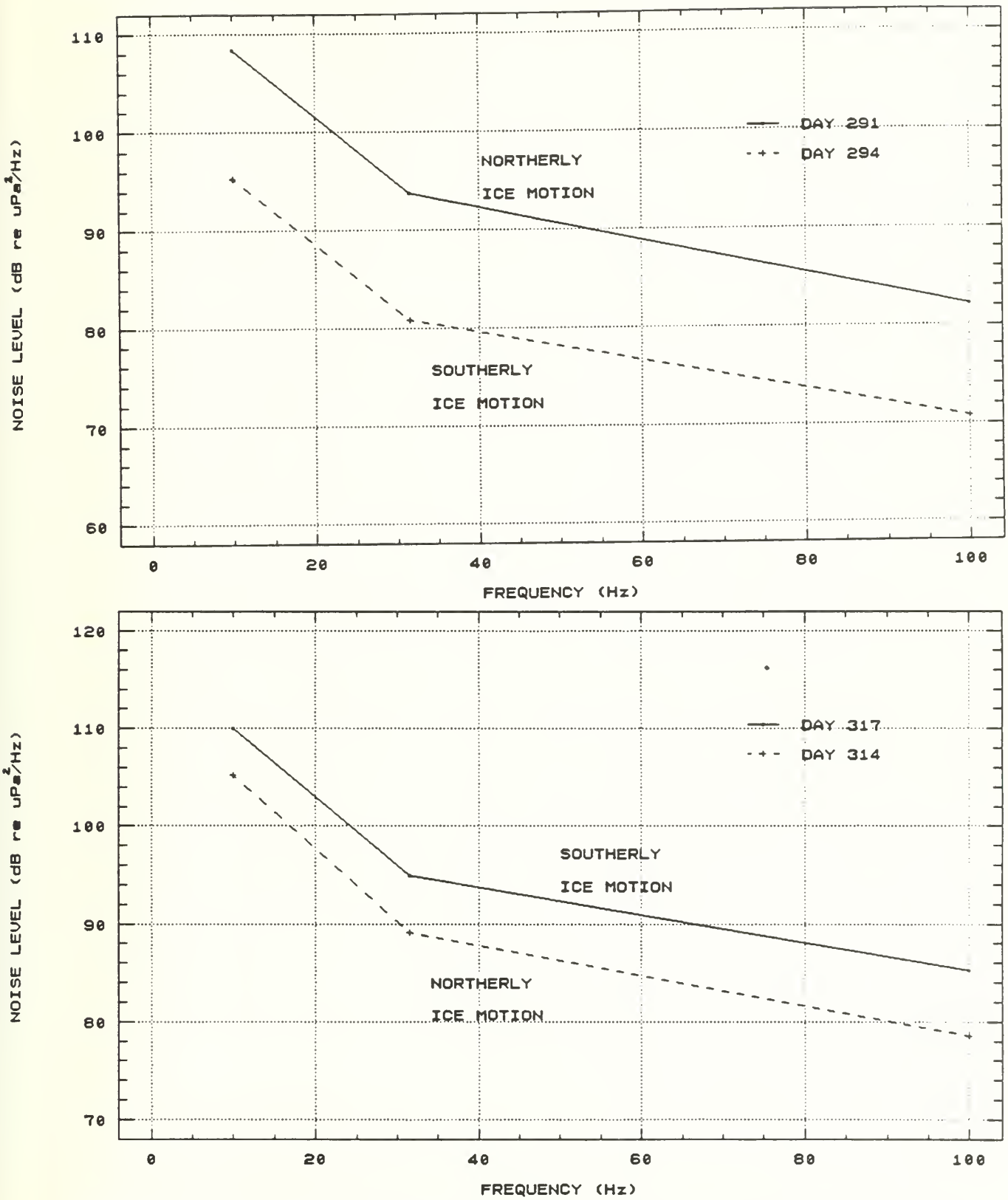

Figure 5.2 Spectral plots comparing ambient noise levels for northerly and southerly motion during two different periods of the record. The top plot displays contrasting motion in deep water while the second plot displays spectra in the vicinity of active ridging north of the island of Kvitoya.

limited in its extent by local wind forcing. Thus, the local northerly ice motion opposes the large scale southward motion of the ice pack resulting in increased convergence, ridging, and ambient noise.

The second period of contrasting ice motion was on Julian days 314 and 317 (Figure 5.2b). The ambient noise measurements collected during this period were in the immediate vicinity of active ridging north of the island of Kvitoya. The mean direction of ice motion was to the north during day 314 and to the south on day 317. Southerly ice motion during this portion of the study was associated with ambient noise levels that were 4-7 dB higher than during northerly motion. The difference in ambient noise levels for the contrasting directions of motion are most likely the result of the relative magnitudes of convergence. While some convergence would occur with northward ice motion, as explained in the previous example, greater levels of ridging/convergence were experienced with motion to the south against the unyielding island of Kvitoya. While the northerly ambient noise level is lower than the southerly level, it is still quite loud. It is only about 3-4 dB less than the levels of ambient noise measured during northerly motion in deep water (Julian day 291).

The two periods discussed above, Julian days 290/294 and 314/317, represent two different periods of convergence that resulted in increases in ambient noise. The first period of

convergence was generated by a mean northerly ice motion that opposed the macro-scale drift to the south. The second period represented increased convergence as the ice encountered the unyielding islands to the south.

B. AMBIENT NOISE vs. WIND SPEED

Another means of verifying the correlation between wind speed and ambient noise previously shown in Chapter IV is to divide the ambient noise record into wind speed groups. The overall wind speed record varied from 0-20 m/sec. The data record was then sorted into five bins of 4 m/sec each. Figure 5.3 shows the related frequency spectrum for these five wind speed classes. As expected, the ambient noise level increased with increasing wind speed. A critical wind speed at 31.5 and 100 Hz occurs at wind speeds greater than 12 m/s. Once this threshold is reached, the ambient noise spectrum becomes largely insensitive to further increases in wind speed. A possible explanation for this saturation level is that once the wind has reached 12 m/s, all of the relatively thin and young ice has been fractured and ridged. Further increases in the wind speed only serve to cause micro-fracturing in the ice (as opposed to large scale fracturing/ridge building) which results in only a limited increase in ambient noise with wind speed. A similar feature is observed in ambient noise/wind speed plots in the Barrow channel (Milne and Ganton, 1971). It must be noted that a relatively small number of samples,

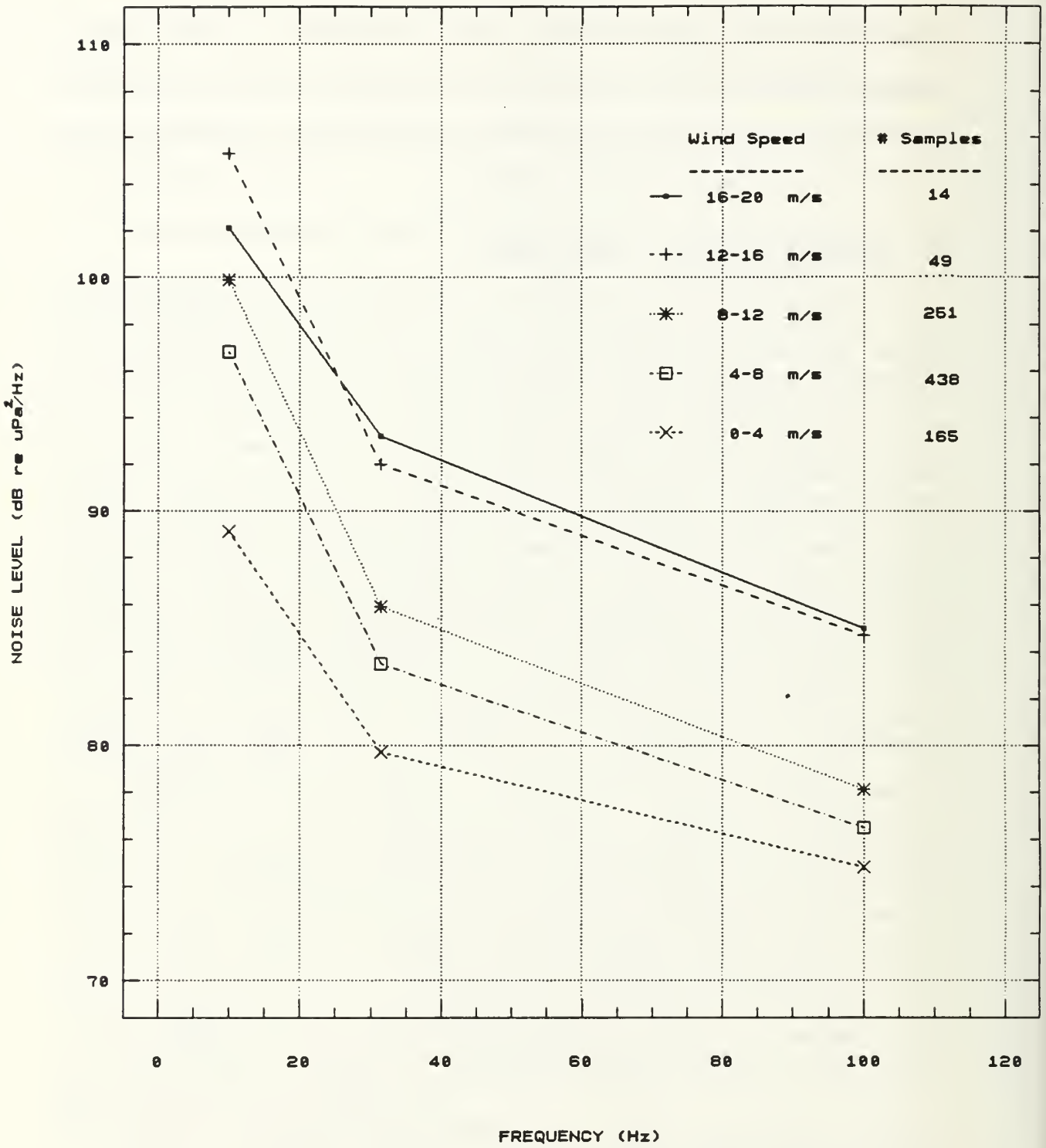

Figure 5.3 Spectral plots comparing the ambient noise at different wind speeds from 0 to 20 m/s.

14, were contained in the 16-20 m/s class and the assumption is that these values are representative of the class as a whole.

C. WARMING vs. COOLING TRENDS

A cooling trend present during Julian days 305-307 was compared to a warming trend from days 311-313 over the frequency range 10-100 Hz (Figure 5.4). The ambient noise levels during the warming period were 2-7 dB higher with the lower frequencies experiencing the largest increase. One possible explanation for the increased ambient noise found during the warming trend is that warmer temperatures decrease both the tensile and compressional strength of ice making it easier to fracture (Weeks and Mellor, 1984).

Another, more likely explanation for the increased ambient noise observed during a warming trend is that the increased noise may be only indirectly related to the temperature. Warming trends in the Arctic are generally associated with southerly winds while cooling trends are often synonymous with northerly winds. This association holds true for this experiment. During the period of cooling, days 305-307, the winds were from the north and during the warming trend of days 311-313, the winds were from the south (Figure 5.5). The critical factor in the warming trend may actually be the southerly winds and their associated convergence. As discussed previously, southerly winds have been correlated

with northerly ice motion and increased levels of ambient noise.

D. ANALYSIS OF SHALLOW WATER RIDGING ENVIRONMENT

1. Time Series Analysis

During the last week of data collection, the median ambient noise measurements were significantly higher than during the rest of the record. This is most likely attributable to the increased ridging activity brought about by close proximity to land. As mentioned previously, ridging activity was extremely high after Julian day 317 and forced the repeated reconnection of the hydrophone cables and their eventual removal from the ice on day 324.

The water depth steadily decreased from 175 m to 90 m during this period. Figure 5.6 shows the wind speed, ice speed, and temperature time series for Julian days 317-323. Northerly winds were present throughout this period with wind speeds varying from 4 to 15 m/s. The temperature ranged from -14°C at the start of the period to a low of -29°C on day 322. Temperatures increased by 7°C when the local pressure gradient decreased, resulting in weaker northerly winds that displayed a slight westerly component on days 318, 320, and 321. The ice speed displayed a strong 12-hour oscillation with ice speed maxima on days 317 and 319 correlating well with wind speed peaks on these same days.

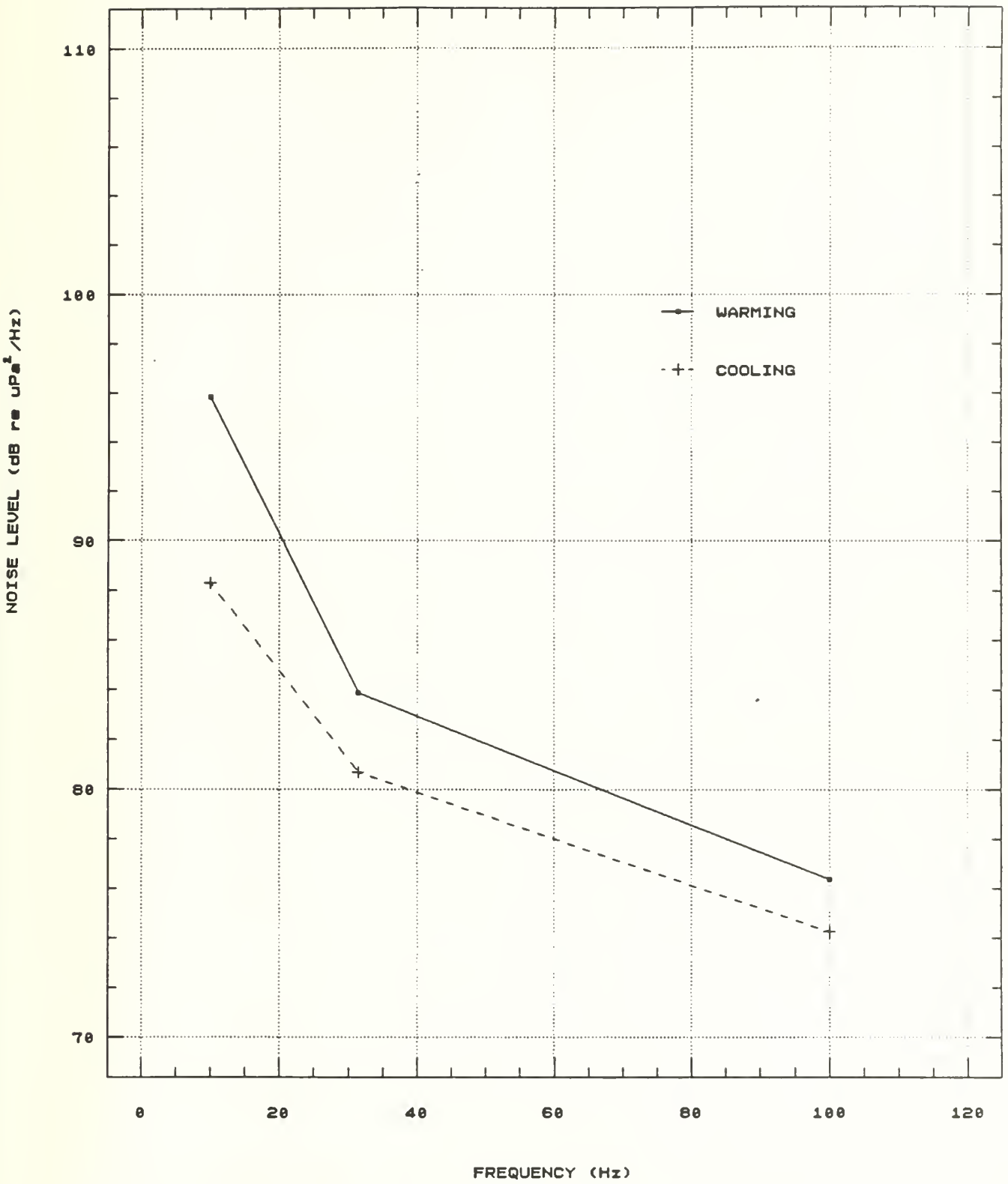

Figure 5.4 Spectral plots comparing the ambient noise levels recorded during a warming trend and a cooling trend.

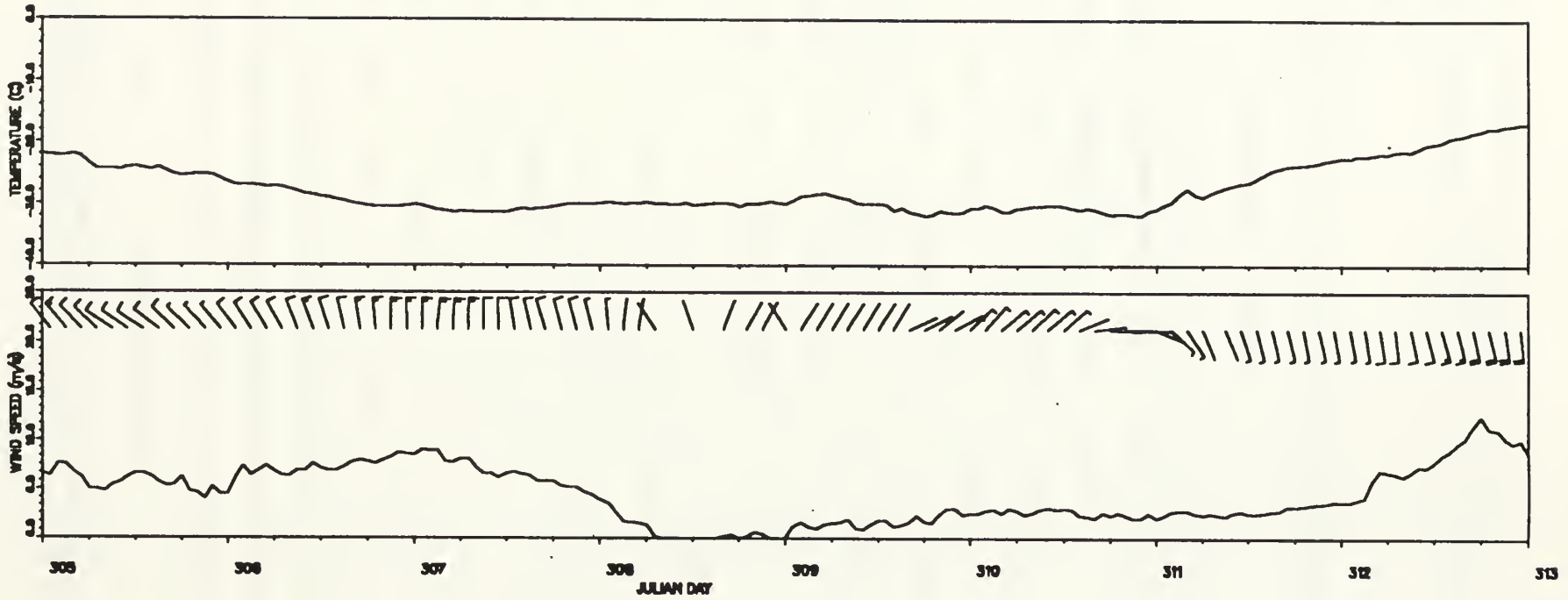

Figure 5.5 Hourly-averaged time series of wind and temperature. The cooling trend corresponds with northerly winds while southerly winds result in a warming trend.

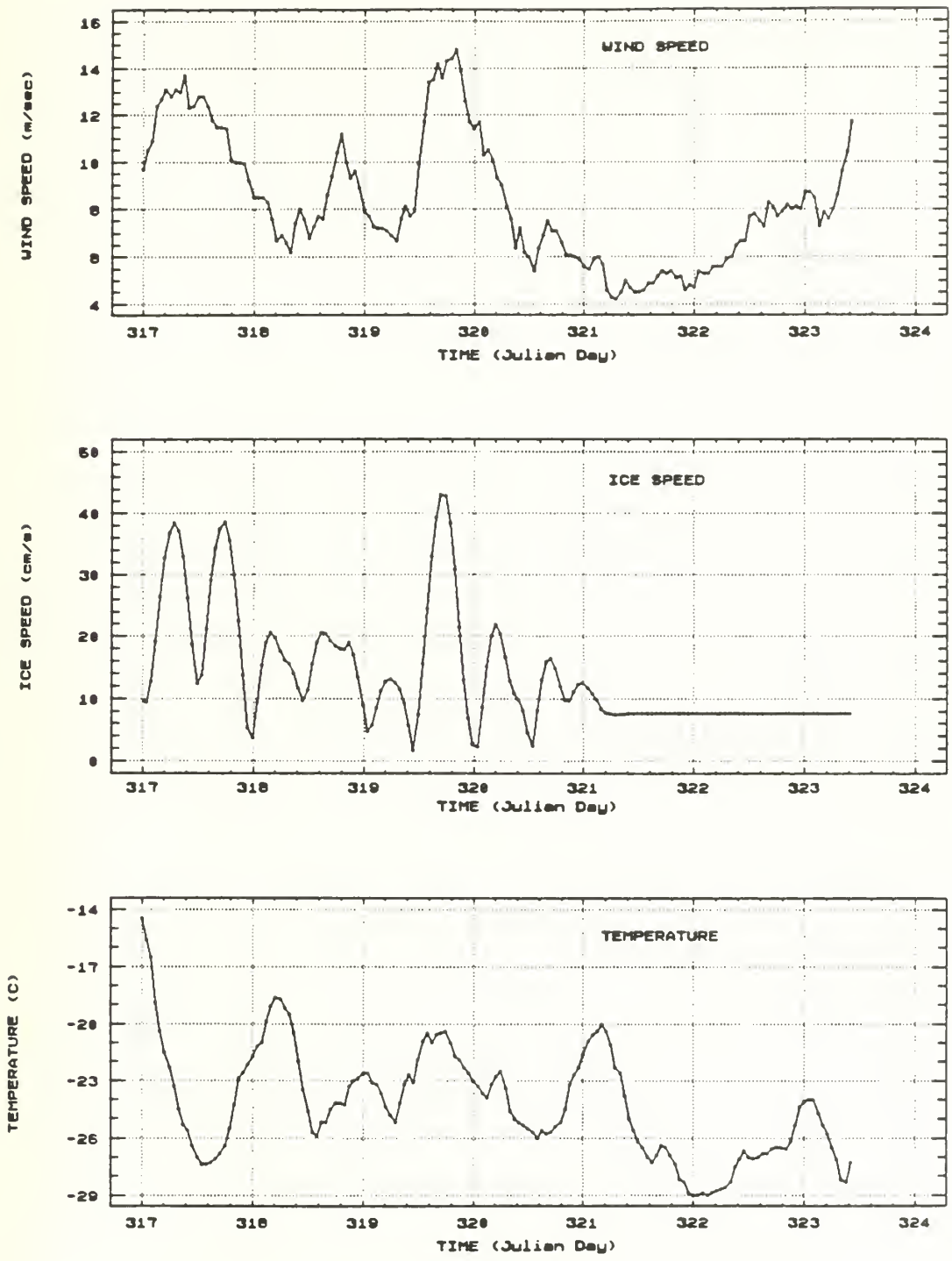

Figure 5.6 Hourly-averaged time series for wind speed, ice speed, and temperature on Julian days 317-324.

During the last week of ambient noise measurements, the median noise level decreased smoothly from 101 dB at 10 Hz to 73 dB at 1000 Hz (Figure 5.7). Figure 5.8 presents the ambient noise time series for 10, 31.5, 100, 315, 630, and 1000 Hz. Table 5 presents the statistical information for the six frequencies.

TABLE 5. AMBIENT NOISE STATISTICS FOR JULIAN DAYS 317-324

	10 Hz	31.5 Hz	100 Hz	315 Hz	630 Hz	1000 Hz
SAMPLE SIZE	102	155	155	155	155	155
MEAN	96.5	87.1	80.4	76.8	74.7	73.4
MEDIAN	100.8	88.2	80.6	75.8	74.7	73.0
STD DEV	14.6	9.3	7.1	6.0	5.6	4.9
MAXIMUM	118.6	106.0	101.3	91.8	88.2	86.9
MINIMUM	64.3	64.4	63.9	64.7	64.1	64.6

Twelve hour inertial oscillations are distinct at 10 and 31.5 Hz and are discernable at 100 Hz. The oscillations are most likely inertial since the established period on day 317 does not match the 12 hour period on days 321-323. If these oscillations were tidal, then the period would remain constant throughout the record. As the frequency increases, the

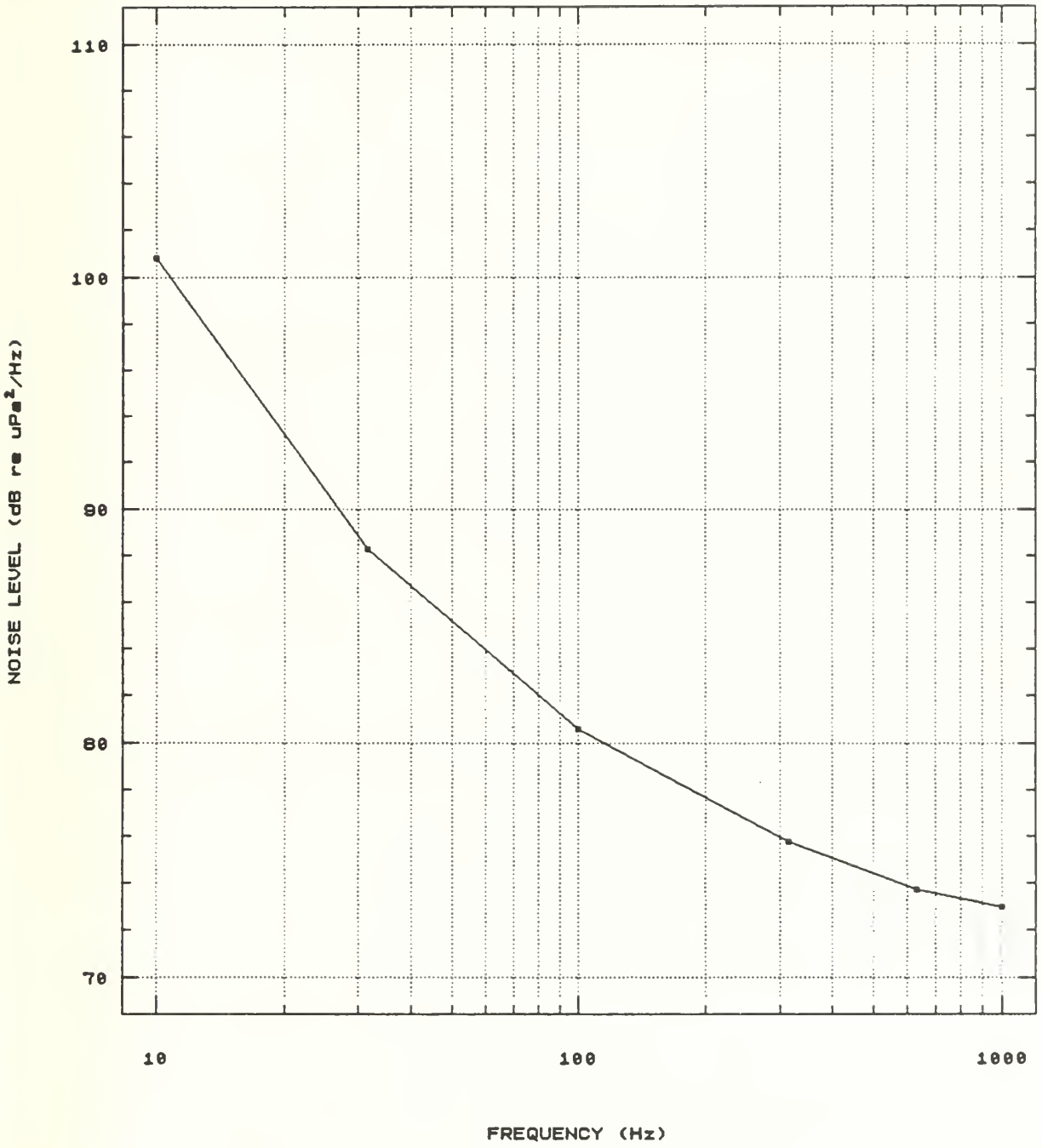

Figure 5.7 Median ambient noise levels in a region of active ridging north of Kvitoya for Julian days 317-324.

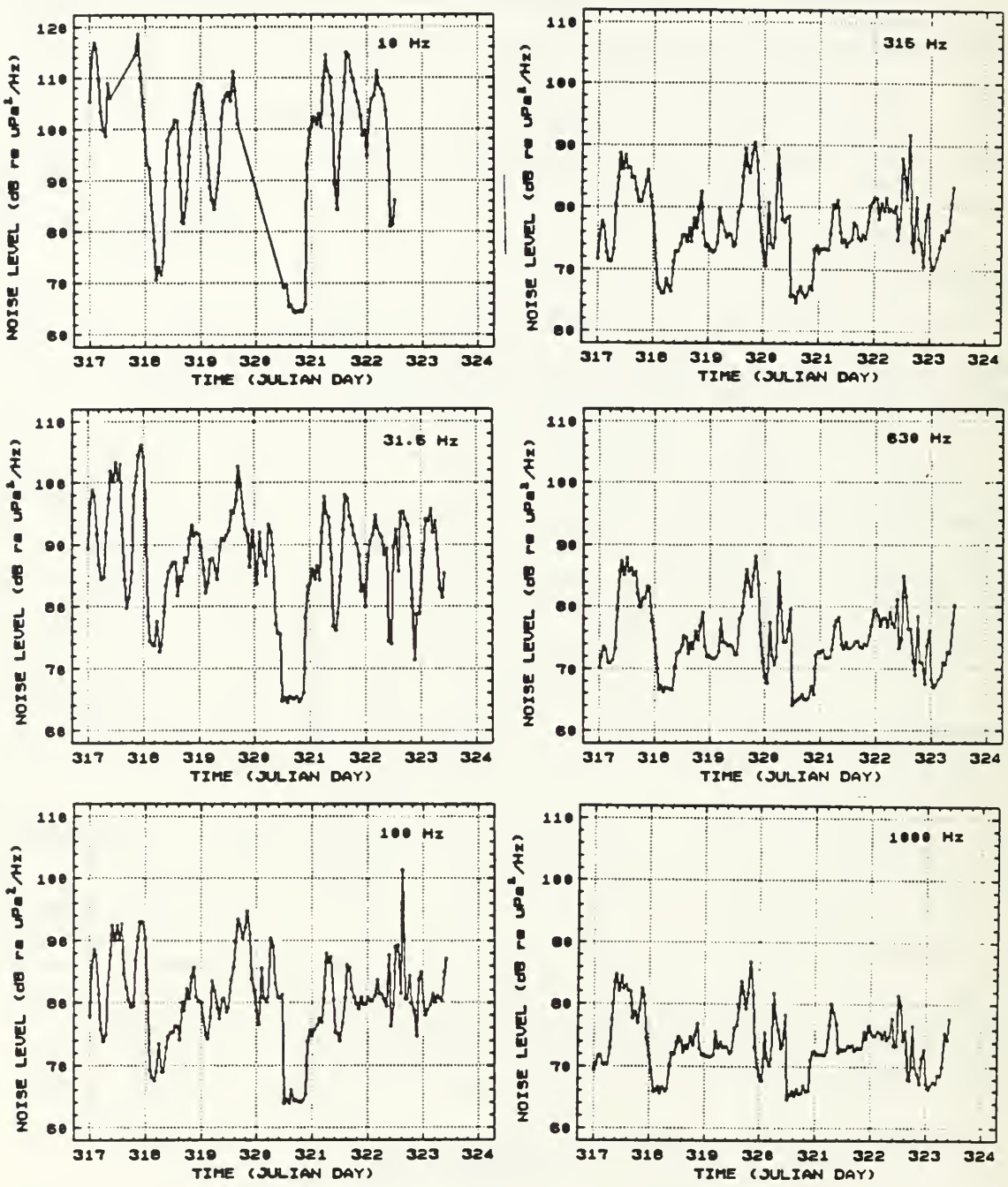

Figure 5.8 Hourly-averaged ambient noise time series for frequencies of 10, 31.5, 100, 315, 630, and 1000 Hz in a region of active ridging (Julian days 317-324).

inertial influence appears to decline. A high frequency oscillation is superimposed on the smooth inertial oscillations at 31.5 Hz while an inertial influence can be observed in the high frequency fluctuations at 100 Hz. The high frequency, 315-1000 Hz, time series are extremely similar and resemble the 100 Hz time series. While the shape of each of the time series are virtually identical, their overall mean and standard deviation decrease with increasing amplitude.

In summary, the active ridging environment encountered during the last week of observations, while displaying significantly higher ambient noise levels than the rest of the record, still displayed many of the same characteristics. Thus the processes that are responsible for ambient noise generation in a region of active ridging are similar to those found throughout the noise record.

A similar argument can be made for the noise-generating mechanisms at work in the higher frequencies (315-1000 Hz). The ambient noise spectra measured in this range were all virtually identical, indicating that the same noise generating mechanisms were at work. While the high frequency spectra bear a close resemblance to the 100 Hz spectrum, there are obviously significant differences in spectra and noise generation at 10 and 1000 Hz.

2. Cross-correlations

Cross-correlations were performed between ambient noise and wind speed, ice speed, and temperature measurements collected during Julian days 317-324. These correlations were performed in order to determine what the correlations were at the higher frequencies (315, 630, and 1000 Hz) and to contrast the shallow water, active ridging environment with the rest of the record. Cross-correlations involving the 10 Hz ambient noise measurements collected during the last week of the study (days 317-324) correlate poorly due to gaps in the record on Julian days 317, 320, and 322. Cross-correlations at 10 Hz will not be discussed in the text but will be retained in subsequent cross-correlation figures for comparison purposes only.

The cross-correlations between wind speed and ambient noise, Figure 5.9, display relatively high direct correlations with cross-correlation coefficients ranging from 0.37 and 0.44 for frequencies 31.5-1000 Hz. All frequencies display a large secondary maxima with cross-correlation coefficients of 0.20 to 0.30 (2.5 day lag) and an intervening negative maxima with correlation coefficients of -0.25 to -0.50 (24 hour lag). There is no physical explanation for why increasing winds would cause a decrease in ambient noise 24 hours later, so this negative correlation is assumed to be related to a different forcing. No obvious trends are discernable between

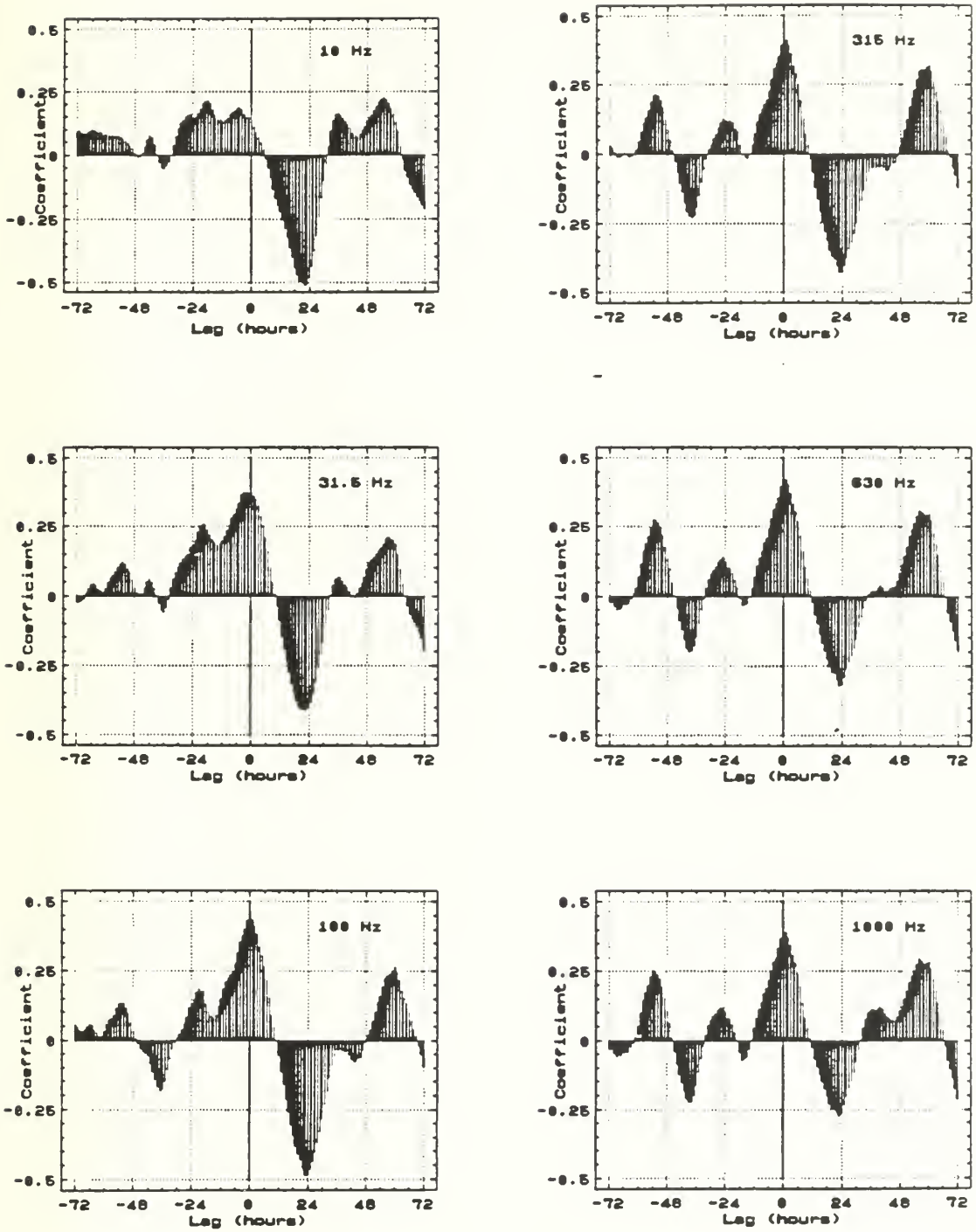

Figure 5.9 Cross-correlations of 7-day wind speed and ambient noise time series for 10, 31.5, 100, 315, 630, and 1000 Hz during Julian days 317-324 (12-19 November).

the high and low frequencies and all frequencies seem equally dependent on wind forcing as a source of ambient noise.

Comparisons between the wind speed and ambient noise cross-correlations performed on the entire record and the last week of observations reveal a close similarity (Figure 5.10). Both display the highest correlation with a lag of zero, a negative correlation maxima with a lag of 24 hours, and a secondary maxima with a lag of 2.5 days. The greatest difference between the two is in the magnitude of the negative correlation maxima which for the entire record has a coefficient of zero (no correlation) while the last week of observations reveals a strong negative correlation with a 24 hour lag. These differences may be attributable to the different types of forcing involved. The 38-day record contains many different, often opposing forces, over the entire record, while the 7-day record is subject to a more uniform forcing.

The next cross-correlations to be investigated are those between ice speed and ambient noise and can be viewed in Figure 5.11. Strong twelve hour inertial/tidal oscillations are evident at all frequencies in both the 7-day and 38-day records (Figure 5.12). All of the 7-day correlations (31.5 to 1000 Hz) display their maximum coefficients with a 2 to 4 hour lag (Figure 5.11). These maximum coefficient values increase with frequency from 0.35 at 31.5 Hz to 0.49 at 1000 Hz. The 2-4 hour lag revealed in the 7-day record is several hours

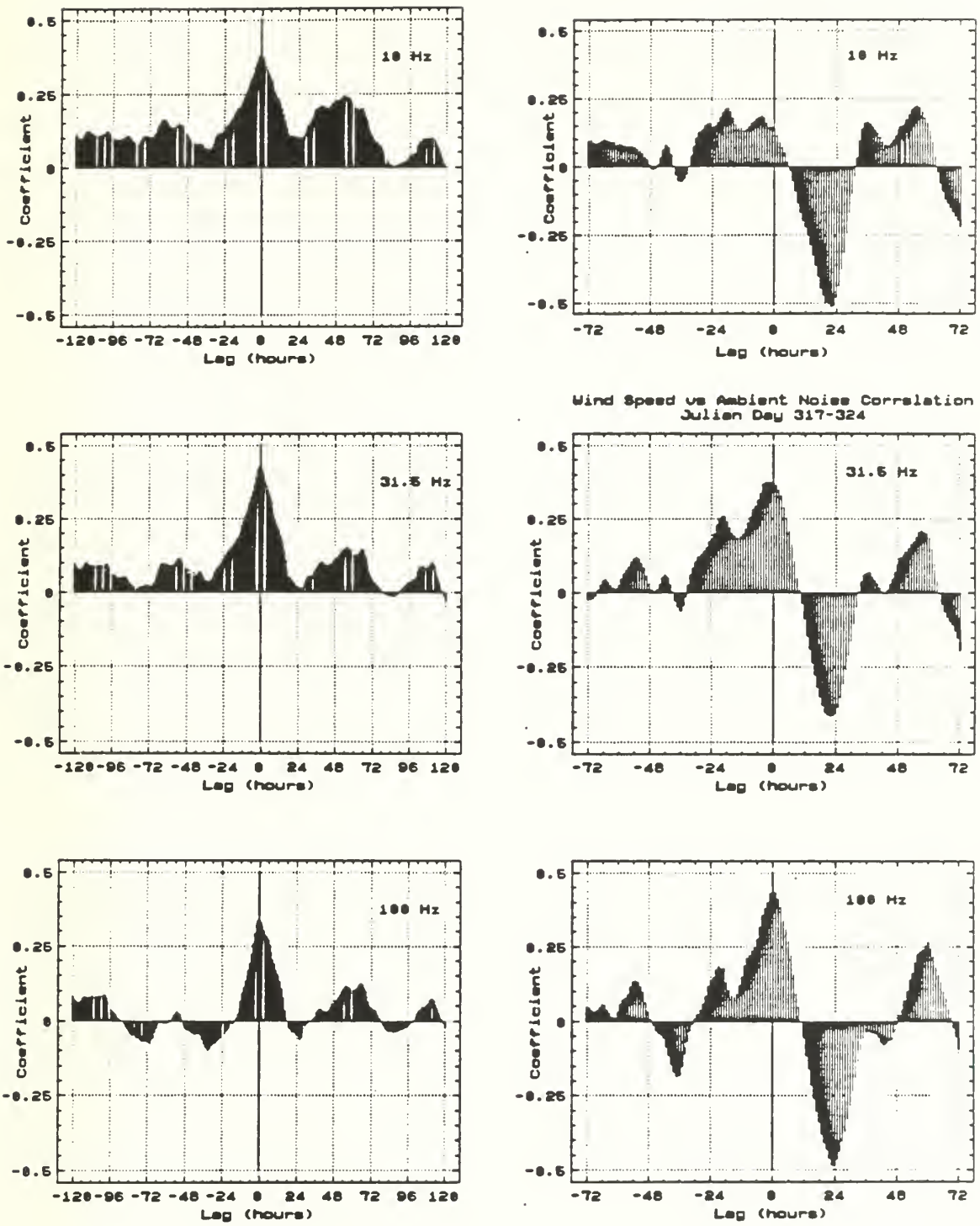

Figure 5.10 Comparison of 38-day (left) and 7-day (right) cross-correlations of wind speed and ambient noise time series for 10, 31.5, and 100 Hz.

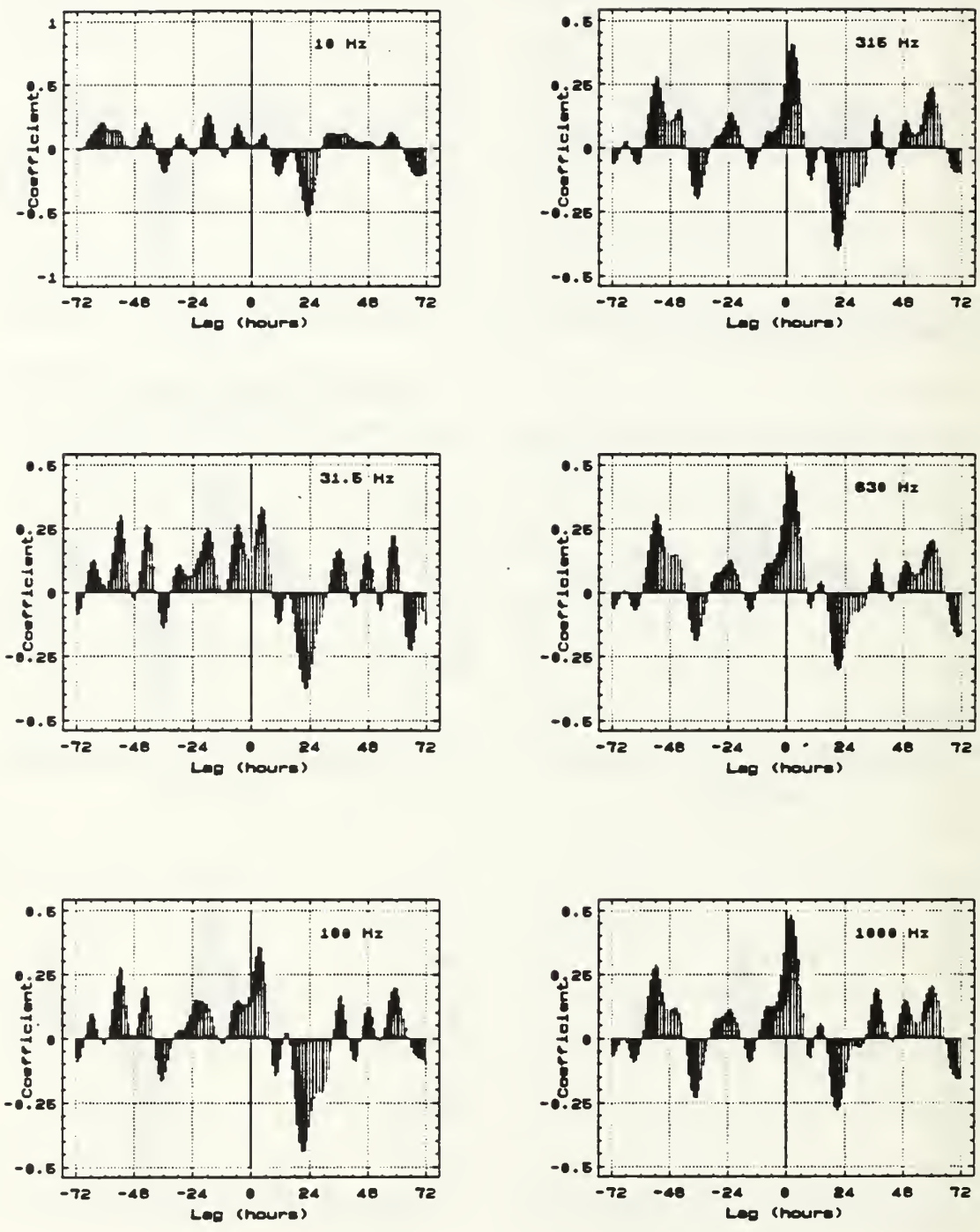

Figure 5.11 Cross-correlations of 7-day ice speed and ambient noise time series for 10, 31.5, 100, 315, 630, and 1000 Hz during Julian days 317-324 (12-19 November).

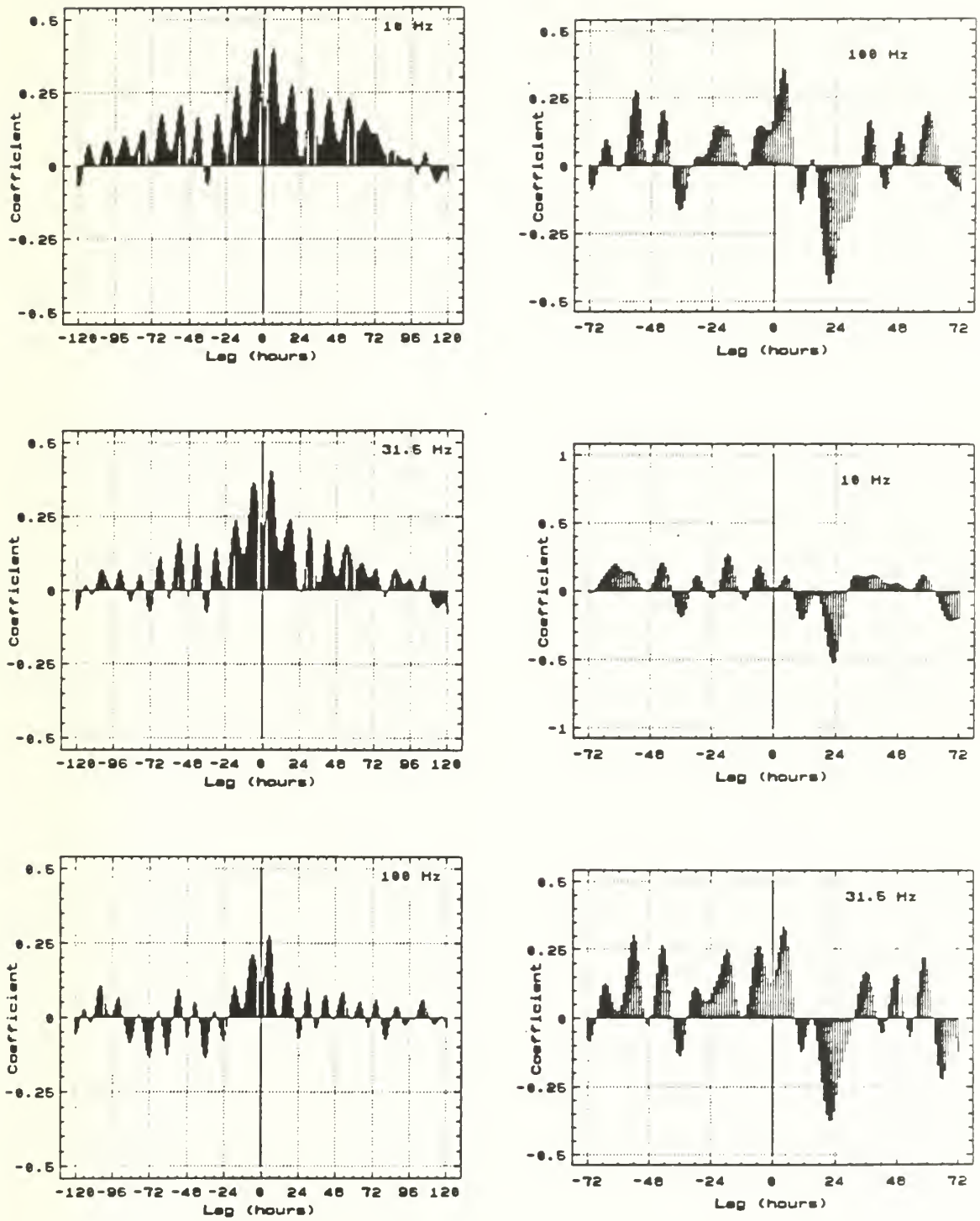

Figure 5.12 Comparison of 38-day (left) and 7-day (right) cross-correlations of ice speed and ambient noise for 10, 31.5, and 100 Hz.

shorter than the lag in maximum correlation found in the 38-day record. This difference may be attributable to the decreased importance of convergence due to tidal/inertial oscillations and the increased importance of Kvitoya-induced convergence. In the latter case, the maximum ambient noise is generated while the oscillation still has a southerly component and the ice is undergoing both an oscillatory stress and southerly convergence. Thus two important facts were derived from the ice speed/ambient noise correlations described above. The correlation between ice speed and ambient noise increases at higher frequencies; and the effects of tidal\inertial oscillations diminished in regions of active ridging.

Cross-correlations between 1/3 octave bands are presented in Figure 5.13. The highest direct correlations are found in the higher frequency bands where the cross-correlations approach 1.0. Even the lowest bands, 10 and 31.5 Hz, show a high direct cross-correlation coefficient of 0.75. All correlations display an e-folding time of between 4 and 5 hours with the correlation coefficient decreasing to zero with a lag of 12 hours. Secondary coefficient maxima are found in all plots with a lag of 2.5 days.

In comparing the 38-day frequency cross-correlations with the 7-day cross-correlations (Figure 5.14), several similarities and differences are noted. The 31.5 and 100 Hz cross-correlations are extremely similar. The only real

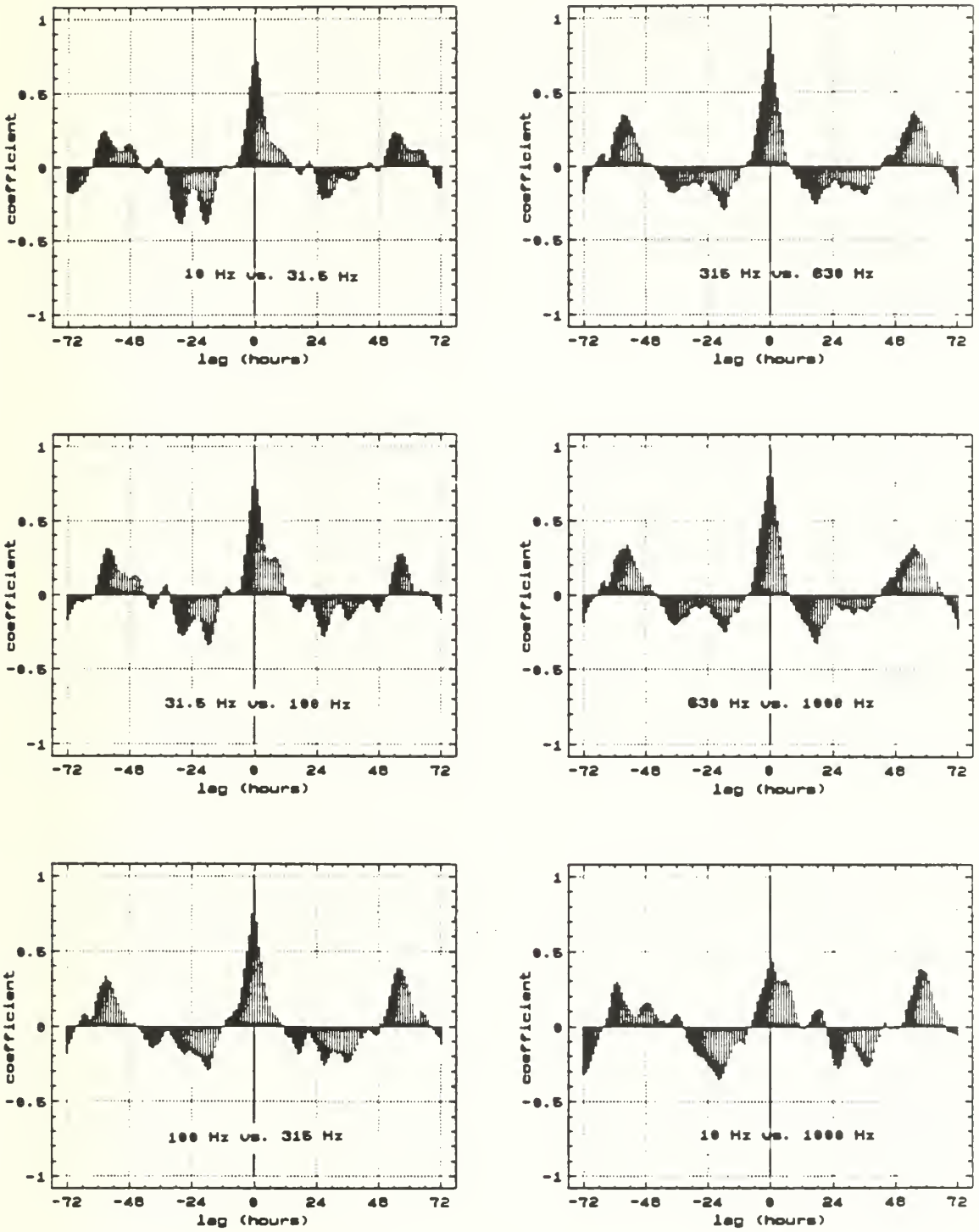

Figure 5.13 Cross-correlations between 7-day hourly averaged 1/3 octave bands measured during Julian days 317-324. Note the strong correlations at high frequencies.

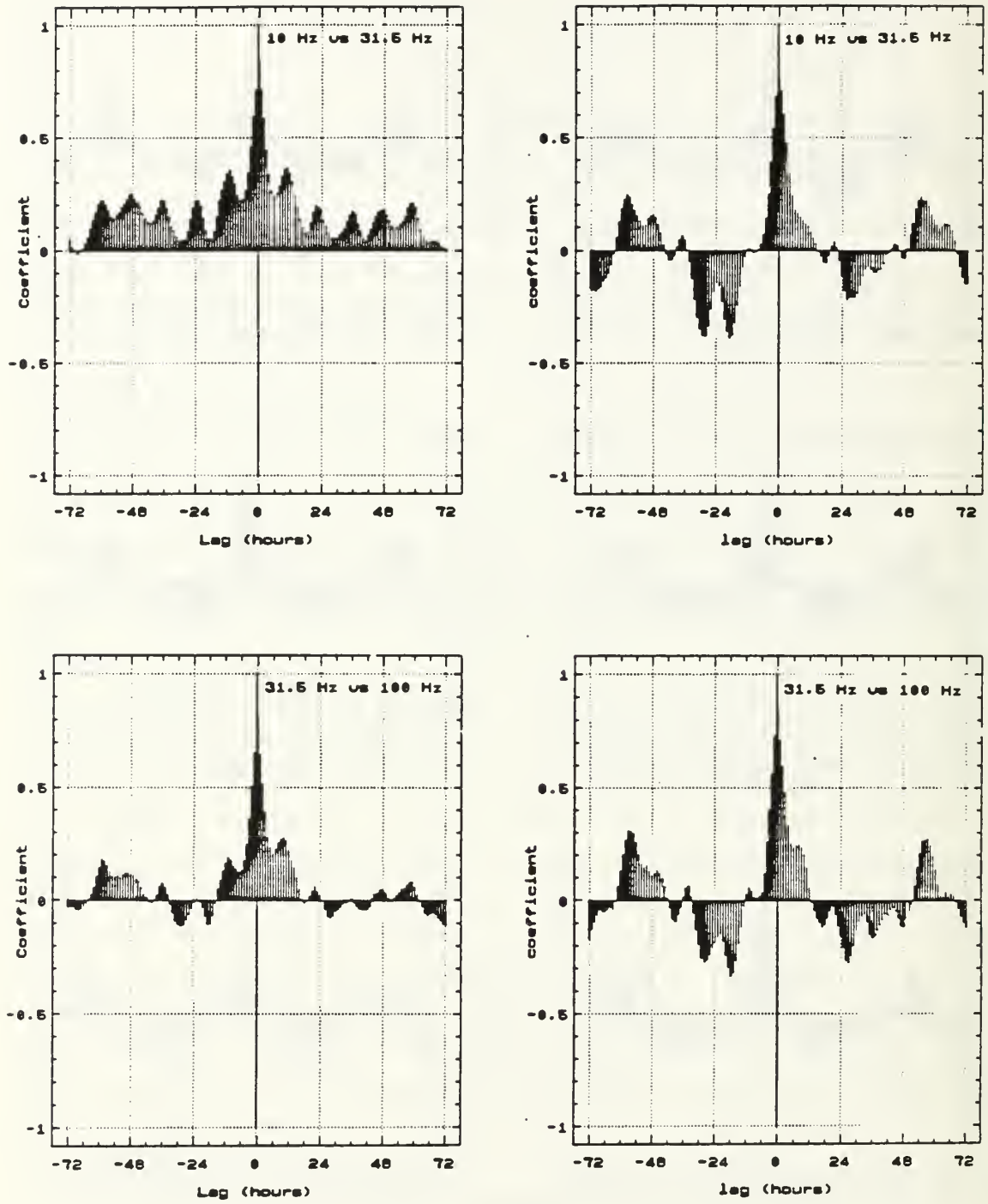

Figure 5.14 Comparison of 38-day (left) and 7-day (right) cross-correlations of hourly-averaged 1/3 octave bands.

differences lie in the relative magnitudes of the correlation peaks beyond 18 hours. The 10 Hz/31.5 Hz and 10 Hz/100 Hz cross-correlations do not compare quite as favorably, with the 7-day record displaying lower correlations and no tidal/inertial periodicities. As discussed previously, this difference is most likely the result of the gaps in the 10 Hz data record.

E. SHALLOW vs. DEEP WATER AMBIENT NOISE

Figure 5.15 compares the median ambient noise spectrums for deep water (days 284-291), shallow water (days 317-324), and the composite spectrum for the entire record (days 285-323). The deep water ambient noise spectrum was collected as the *Polarbjoern* drifted from the deep waters of the Arctic Basin (2300 m) until she reached the shallower waters of the continental rise (900 m) on Julian day 291. The shallow water spectrum was collected in waters between 90-175 m in depth in a region of intense ridging just north of Kvitoya (Figure 1.1).

The similarity between the deep water and composite noise spectra displayed in Figure 5.15 suggests that depth was not a controlling factor in this ambient noise study. While there is a 2 to 5 dB difference in ambient noise levels between the shallow and composite noise spectra, the difference may not be depth related. The difference may actually be the result of the relative proximity of the *Polarbjoern* to active ridging

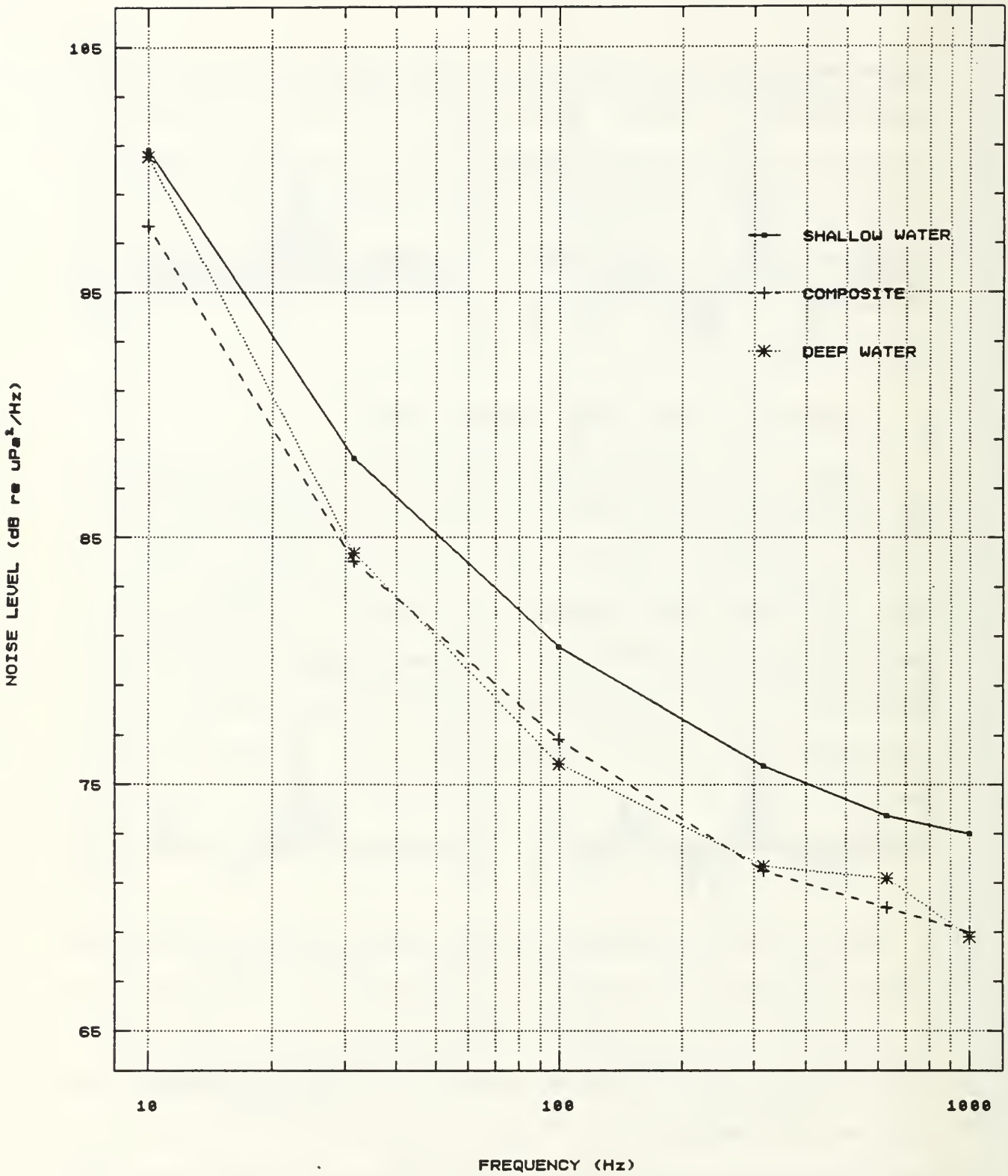

Figure 5.15 Comparison of deep water (days 284-291), shallow water (days 317-324), and composite (days 285-323) spectral plots.

areas. The first 32 days of ambient noise measurements were collected in a region where the intense ridging immediately north of the islands served as a distant source while the last week of measurements were recorded in a region of active local ridging. The actual effect of bathymetry on ambient noise levels will have to be resolved in future studies.

F. STANDARD DEVIATION COMPARISONS

In previous ambient noise studies conducted in the vicinity of Bermuda (Perrone, 1969) and Fiji (Bannister et al., 1979), large variations in standard deviation were recorded with changes in wind speed (Figure 5.16). In the ice covered waters northeast of Svalbard, no such variations were recorded. Figure 5.17 shows the effects of low (0-5 m/s), medium (5-10 m/s), and high wind speeds (10-20 m/s) on the standard deviation. The standard deviation displays a strong decrease with frequency similar to that found in Perrone's study (1979), but no wind dependency.

In the open water studies discussed above, the high winds acted as a broad frequency floor which dominated the ambient noise spectrum. Individual events and narrow band sources were effectively masked. As the wind speed decreased, these highly variable sources became unmasked and greatly increased the standard deviation. For the Barents Sea data, changes in wind speed directly effected the ambient noise level but not the standard deviation. Figure 4.9c, the 10 Hz ambient noise

time series for Julian days 307-318, displays 10 to 30 dB fluctuations throughout the period. These fluctuations can not be attributed to the 12 hour tidal/inertial oscillations since 20 dB fluctuations were still recorded when there were no oscillations (days 308 to 310).

An investigation of the standard deviation during periods of high ambient noise (days 317-324) and low ambient noise (days 304-312) did reveal a significant variation. Figure 5.18a shows the relative ambient noise levels during these two periods and Figure 5.18b their standard deviations. The standard deviation during the relatively noisy period of ridging was 3 to 5.5 dB higher than during the low ambient noise period. Thus, the fluctuations in the ambient noise record were not masked by increased noise levels as they were in Perrone's study (1969), rather, the overall amplitude of the fluctuations were increased. That is, noisy events in ice-covered waters are associated with large amplitude fluctuations indicating such events are not continuous in time nor space. A finite number of ridging events occur in the immediate vicinity of the hydrophone each lasting several minutes (Buck and Wilson, 1986). Unlike the open ocean where wave breaking and agitation of the sea surface is nearly continuous leading to saturation of the noise field, active ridging noise is more a series of discrete events.

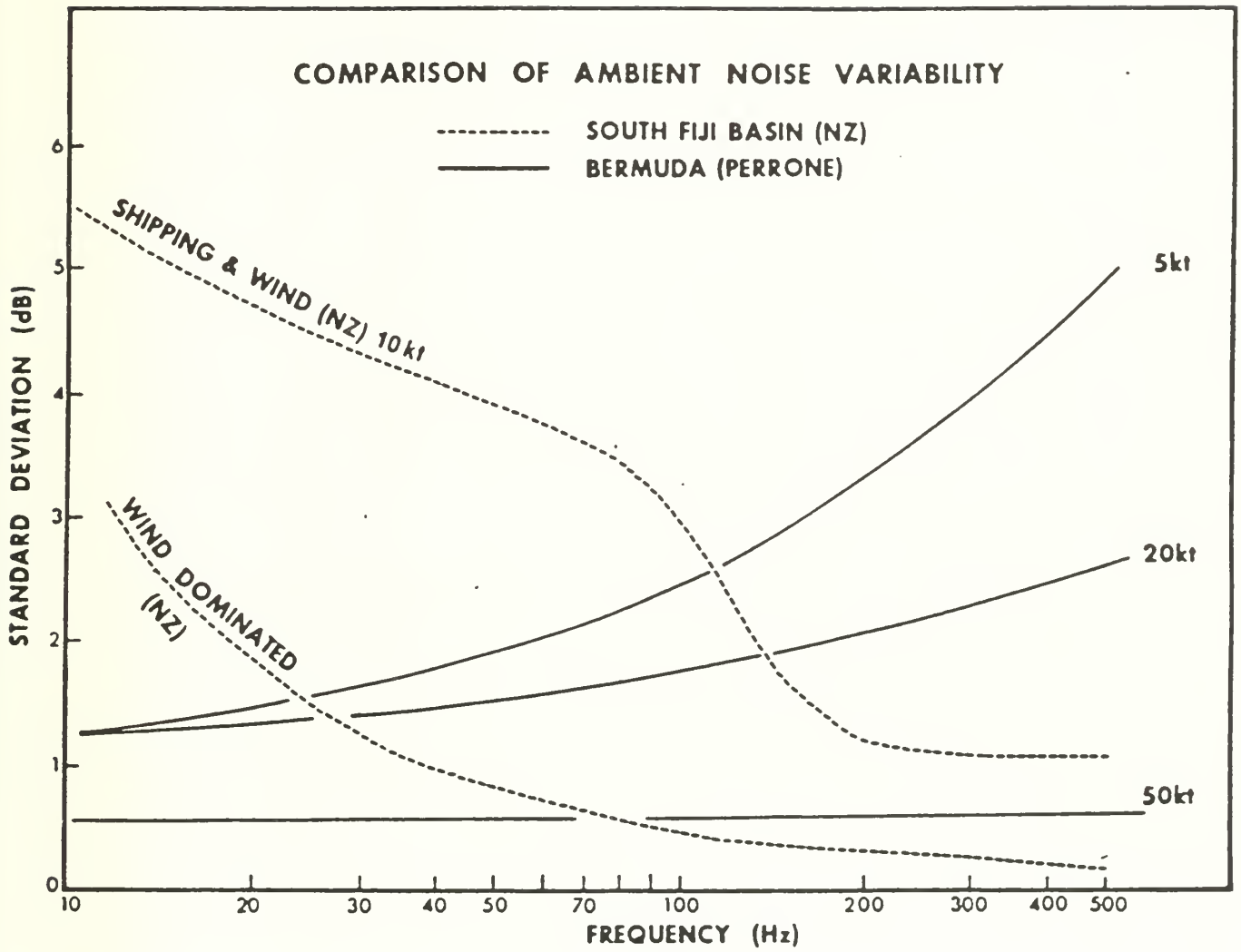

Figure 5.16 Variations in ambient noise standard deviations with increasing wind speed near Bermuda (Perrone, 1969) and Fiji (Bannister, 1979) (from Bannister, 1979).

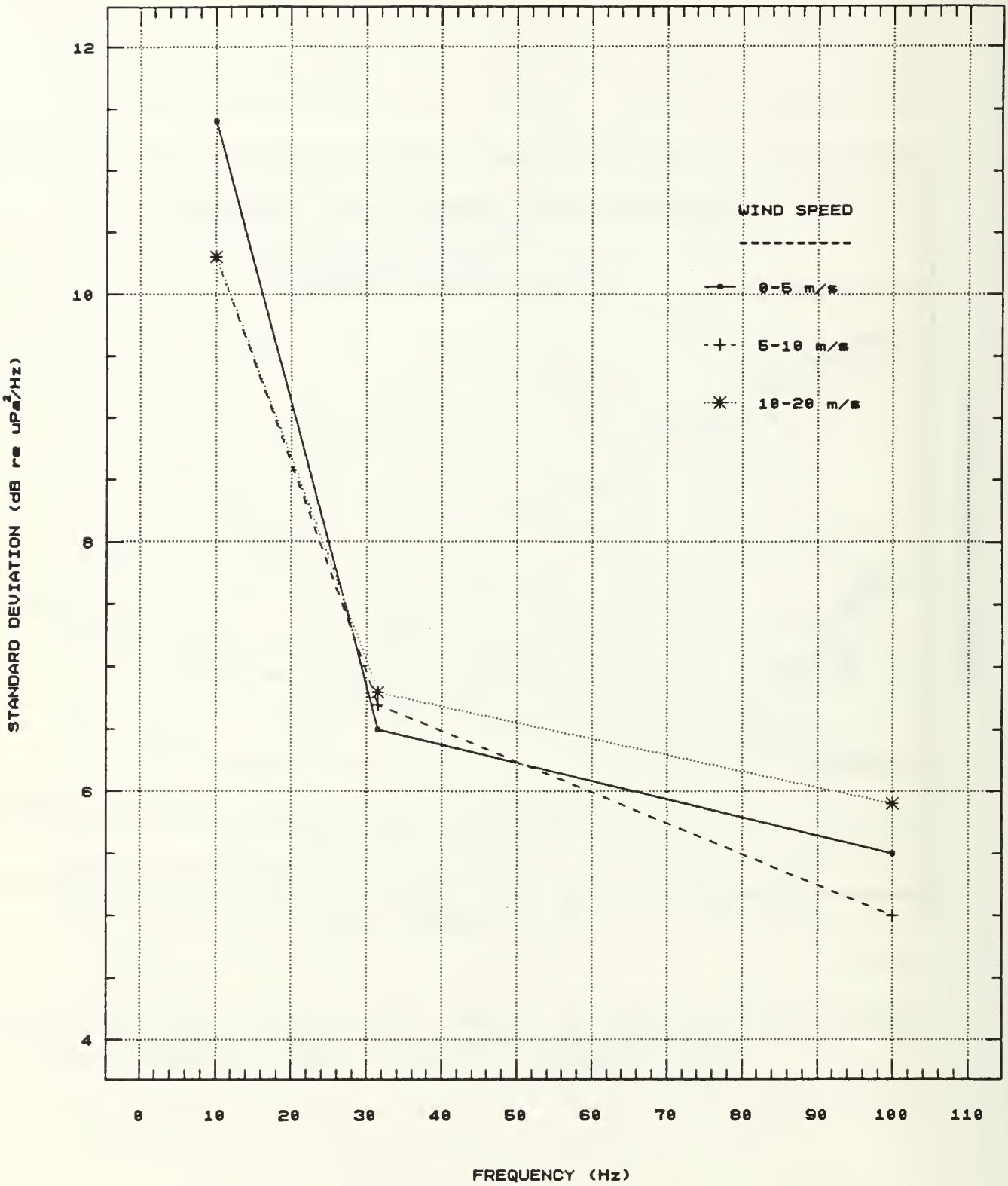

Figure 5.17 Comparison of ambient noise standard deviations in ice covered waters northeast of Svalbard. No wind dependency is demonstrated.

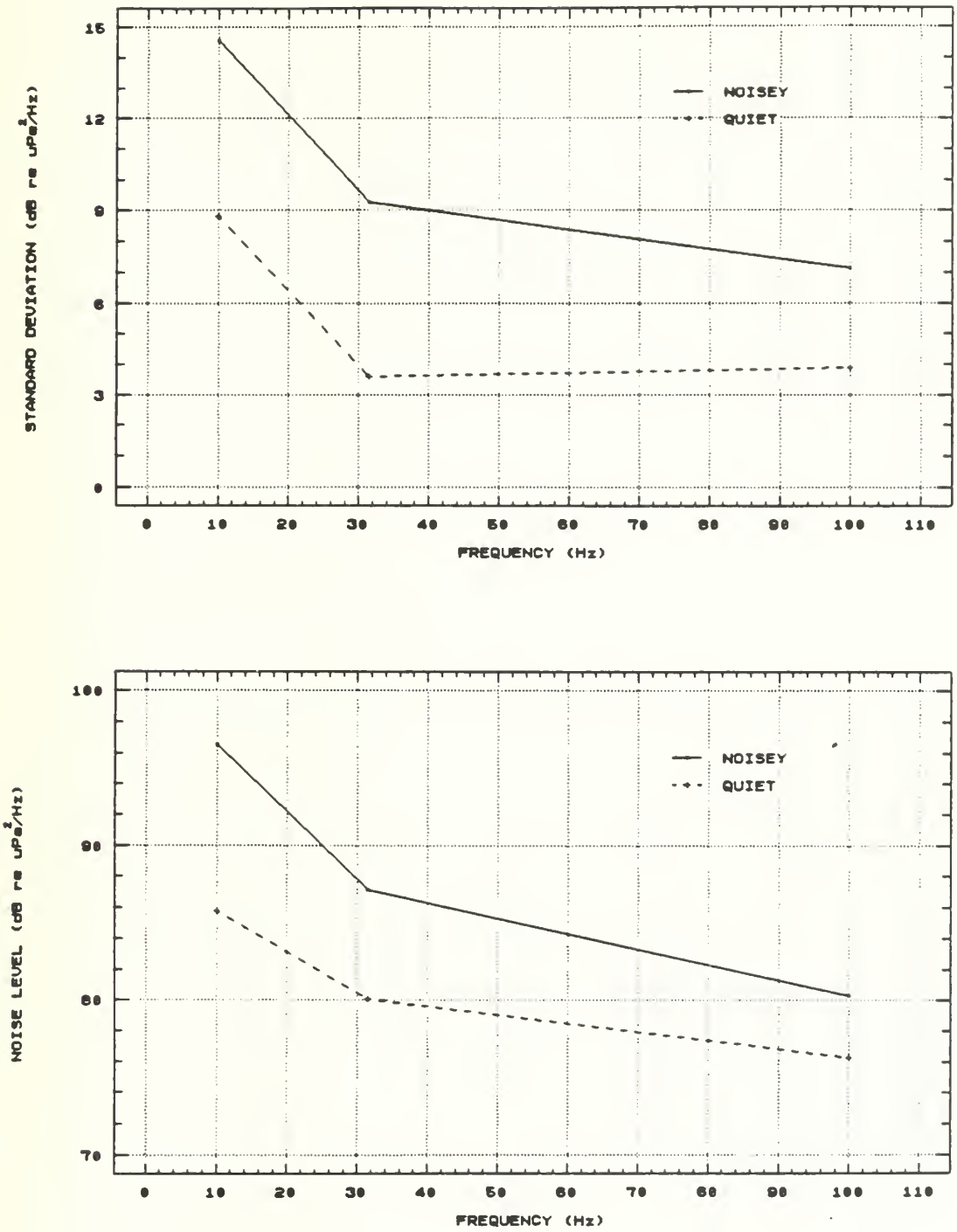

Figure 5.18 Comparison of standard deviations during periods of high ambient noise (days 317-324) and low ambient noise (days 304-312).

VI. SUMMARY, CONCLUSION, AND RECOMMENDATIONS

A. SUMMARY

Ambient noise measurements made northwest of Svalbard from two omni-directional hydrophones, deployed at 60 and 90 m beneath the ice, were acquired as the research vessel *Polarbjoern* drifted south from 11 October to 18 November 1988. The ambient noise data as well as the accompanying meteorological and ice motion data were collected as part of the Coordinated Eastern Arctic Experiment, CEAREX. The ambient noise measurements were composed of one and a half minute samples that were averaged hourly to provide a 38-day time series of 10, 31.5, and 100 Hz. Higher frequencies were considered valid only above the median level due to high system electronic noise. Measurements were obtained in deep and shallow water (<100 m) as the ship drifted generally southwestward with the ice pack towards the Svalbard Archipelago. The ambient noise time series were correlated with hourly-averaged wind, air temperature, and ice motion data in order to determine the major noise generating mechanisms. Both visual and numerical comparisons between the ambient noise and the environmental parameters revealed significant correlations.

B. CONCLUSIONS

■ The ambient noise levels northeast of Svalbard are extremely high, 20-30 dB higher than typical central Arctic basin values, but compare favorably to other dynamically active regions (MIZ, active ridging).

■ The time scales of the noise field varied on two basic levels. A high frequency oscillation varied on the order of 8-12 hours; this oscillation was superimposed on a more slowly varying trend of 2-10 days.

■ Ice motion analysis indicated that two primary forces were operating on the ice pack, wind stress and 12-hour tidal/inertial oscillations. Due to the proximity of the tidal and inertial periods, the nature of these twelve hour oscillations could not be conclusively determined. Initial indications are that these oscillations are inertial in origin. Inertial indicators included variations in phase at different points in the record, no oscillations during periods of negligible ice motion, and increased oscillation amplitude with increased ice speed.

■ A cross-correlation coefficient of 0.62 was observed for hourly averaged wind speed and ice speed measurements with a temporal coherency of about 24 hours. A visual inspection also revealed that the fastest periods of ice motion were found several hours after periods of peak wind speed. Similarly, when the winds were calm, the ice speed went to zero. The strong correlation between wind speed and ice speed was similarly observed in the relationship between wind direction and ice motion. Periods of southerly winds coincided with periods of mean northerly ice motion while northerly winds resulted in net southerly ice drift.

■ Moderate cross-correlations were established between the hourly-averaged, locally measured, wind speed and ambient noise. Cross-correlation coefficients of 0.38, 0.43, and 0.34 were obtained for the frequencies of 10, 31.5, and 100 Hz, respectively. The e-folding time between the wind speed and the ambient noise was about 16 hours. Additionally, a critical speed of 12 m/s was observed above which the ambient noise spectrum became largely insensitive to further increases in wind speed. Periods of peak wind speed were followed within hours by increased ambient noise levels.

■ Hourly-averaged ice speed and ambient noise levels displayed cross-correlations that were similar or slightly

greater than that between wind speed and ice motion. The cross-correlation coefficients for 10, 31.5, and 100 Hz were 0.4, 0.40, and 0.28, respectively. The e-folding time decreased from 21 hours at 10 Hz to 12 hours at 100 Hz.

- In general, the ambient noise level increased with ice speed. The exception to this rule occurred when the tidal/inertial oscillations opposed the mean direction of ice motion and resulted in a six hour lag in maximum correlation between ice speed and ambient noise. Ice speed maxima were bi-modal in nature due to these tidal/inertial oscillations and the ambient noise maxima were generally coincident with the relative minima located between these bi-modal ice speed peaks.

- The cross-correlations between adjacent octave bands, 10/31.5 Hz and 31.5/100 Hz, were extremely strong (coefficients of 0.84 and 0.81, respectively) while more distant bands, 10/100 Hz, displayed a lesser correlation coefficient of 0.60.

- A 7-day ambient noise record was examined while the ship was in a region immediately north of the island of Kvitoya where widespread active ridging was observed. Median ambient noise levels were 2-5 dB higher than during the composite 38-day record. The ice speed/ambient noise cross-correlations displayed maximum correlations at lags of 2-4 hours.

- Northerly ice motion was composed of two scales of motion. It consisted of either short term tidal/inertial oscillations imbedded in a net southerly drift or longer term, mean northerly motion that accounted for over two thirds of the northerly observations. Northerly ice motion observations displayed ambient noise levels that were up to 10 dB higher than southerly ice motions. These higher levels were observed for both oscillatory and mean northerly motion.

- In contrast to previous mid-latitude observations, the standard deviations obtained from the 38-day ambient noise record displayed no wind dependency. Standard deviations obtained from calm periods were virtually identical to those from gusty periods. There were, however, large differences in standard deviation displayed between relatively quiet and noisy periods. Standard deviations during periods of relatively loud noise levels were on the average 3 to 5.5 dB higher.

- Tidal/inertial oscillations resulted in increased convergence and higher levels of ambient noise when they opposed the mean direction of motion.

- In the region northeast of Svalbard, infrequently occurring southerly wind events resulted in northerly ice motion that opposed the mean southerly motion of the Arctic ice pack. During these periods of extended northerly ice drift, increased convergence and ridging of the ice field occurred and the ambient noise levels rose accordingly.

- Significant cross-correlations between temperature and ambient noise (10 to 100 Hz) were probably only indirectly related to temperature. Warm southerly winds resulted in increased ambient noise as stated above. Cooling trends were synonymous with northerly winds which were associated with divergent conditions and lower ambient noise levels.

- Separate and distinct noise generating mechanisms were responsible for the significant differences between the low (10 and 31.5 Hz) and high (100 Hz to 1000 Hz) frequency ambient noise time series. This is substantiated by the more than 5 dB difference in standard deviations displayed by the 10 and 100 Hz time series; the lack of correlation between air temperature and ambient noise at 100 Hz while the low frequencies (10 and 31.5 Hz) demonstrated significant correlations; and the strong tidal/inertial oscillations observed in the 10/31.5 Hz cross-correlations that were missing in the lower correlated 10/100 Hz cross-correlations.

C. RECOMMENDATIONS

- Due to the extremely complex relationship between the various ambient noise generating mechanisms, no definitive relationship between temperature and ambient noise was established. Additional investigation into this relationship using the Barents Sea air temperature/ambient noise record as well as other Arctic data sets would be beneficial.

- The effects of bathymetry on ambient noise was not conclusively resolved due to the widespread active ridging observed in the waters immediately north of the island of Kvitoya. This ridging complicated the shallow water ambient noise environment. Were the increased noise levels observed in this region a function of the active ridging, shallow water or a combination of the two? Additional ambient noise measurements in this or other shallow water ice covered regions that are not dominated by active ridging would help resolve this issue.

- The collection of detailed ocean current measurements, in concert with additional ice motion analysis, in the region northeast of Svalbard would help settle the debate over the nature of the 12-hour tidal/inertial oscillations found in

this region. This issue must be resolved if future ambient noise algorithms and models are to be successful. Ocean current measurements would also allow a more detailed determination of the relative influences of the wind, tides, and currents on ice motion and ambient noise.

LIST OF REFERENCES

Bannister, R. W., R. N. Denham, K. M. Guthrie, D. G. Browning, A. J. Perrone, "Variability of Low-frequency Ambient Sea Noise", *J. Acoust. Soc. Am.*, 65(5), 1156-1163, (1979).

Bradley, M. R., and S. B. Hartley, *The AEAS Arctic Ambient Noise Data Base (U)*, Planning Systems Inc., Slidell, LA., (1986). (SECRET document).

Buck B. M., "Arctic Acoustic Transmission Loss and Ambient Noise", in: *Arctic Drifting Stations*, edited by J. E. Sater, Arctic Institute of North America, 427-438, (1968).

Buck B. M., J. H. Wilson, "Nearfield noise measurements from an Arctic pressure ridge", *J. Acoust Soc. Am.*, 80(1), 256-264, (1986).

Davidson K. L., P. S. Guest, Personal Communication with the Author, Naval Postgraduate School, Monterey, CA, January (1991).

Diachok O. I., and R. S. Winokur, "Spatial Variability of Underwater Ambient Noise at the Ice-water Boundary", *J. Acoust. Soc Am.*, 55(4), 750-753, (1974).

Dyer I., "The Song of Sea Ice and Other Arctic Melodies", *The Robert Bruce Lecture: 2 March 1983, Arctic Technology and Policy*, edited by I. Dyer and C. Chryssostomidis, Hemisphere Publishing, Washington, D.C., 11-37, (1983).

Green C. R., B. M. Buck, "Influence of Atmospheric Pressure Gradient on Under-Ice Ambient Noise", *USN J. Underwater Acoust.*, 529-538, (1978). (CONFIDENTIAL Document).

Hamilton S. W., "Meteorological Features During Phase I of CEAREX from 17 September 1988 to 7 January 1989", Masters Thesis, Naval Postgraduate School, Monterey CA, March (1991).

Hibler W. D., and W. B. Tucker, "Some Results From a Linear Viscous Model of the Arctic Ice Cover", *J. Glaciol.*, 22: 293-304, (1979).

Hibbler W. D., "Ice Dynamics", in: *The Geophysics of Sea Ice*, edited by N Untersteiner, Plenum Press, New York, 577-640, (1986).

Higgins M. D., "Ambient Noise In the Arctic Ocean and its Relation to the Summertime Reversal of the Beaufort Gyre", Masters Thesis, Naval Postgraduate School, Monterey, CA, March (1990).

Hunkins K.,"The Oceanic Boundary Layer and Stress Beneath a Drifting Ice Flow", *J. Geophys. Res.*, 81: 3425-3433, (1975).

Johannessen O. M., K. V. Starke, S. S. Payne, "Ambient Noise in the Marginal Ice Zone", *Technical Report No. 14*, The Nansen Remote Sensing Center, Solheimsvik, Norway, (1988).

Kowalic Z., N. Untersteiner, "A Study of the M_2 Tide in the Arctic Ocean", *Dt. Hydrogr Z.*, 31, (1978).

Lackman G. M., P. S. Guest, K. L. Davidson, R. J. Lind, J. Gonzalez, "CEAREX/Polarbjoern Meteorology Atlas", *Naval Postgraduate School Data Report*, Monterey, CA, (1989).

Lewis J. K., W. W. Denner, "Arctic Ambient Noise in the Beaufort Sea, Seasonal Relationships to Sea Ice Kinematics", *J. Acoust. Soc. Am.*, 83(2), 549-565, (1987a).

Lewis J. K., W. W. Denner, "Arctic Ambient Noise in the Beaufort Sea: Seasonal Space and Time Scales", *J Acoust. Soc. Am.*, 82(3), 988-997, (1987b).

McPhee M. G., "CEAREX 1988 Polarbjoern Drift: Position and Velocity Analysis", *McPee Research Inc. Report*, Naches, Washington, (1989).

Makris N. C., I. Dyer, "Environmental Correlates of Pack Ice Noise", *J. Acous. Soc. Am.*, 79(5), 1434-1440, (1986).

Milne A. R., "Thermal Tension Cracking in Sea Ice: A Source of Underice Noise", *J. Geophys. Res.*, 77(12), 2177-2190, (1972).

Milne A. R., J. H. Ganton, "Noise Beneath Sea Ice and Its Dependence on Environmental Mechanisms", *USN J. Underwater Acoust.*, 21(1), (1971). (CONFIDENTIAL Document).

Neuman G., W. J. Pierson, *Principles of Physical Oceanography*, Prentice-Hall Inc., Englewood Cliffs, N.J., 298-325, (1969).

Prada K. E., "Real Time Ambient Noise Spectra Acquisition and Display", *Proceedings of Fourth Working Symposium on Oceanographic Data Systems*, Computer Society Press, San Diego, CA, 197-207, (1986).

Perrone A. J., "Deep Ocean Ambient Noise Spectra in the Northwest Atlantic", *J. Acoust. Soc. Am.*, 46, 762-770, (1969).

Poffenburger D. L., R. H. Bourke, J. H. Wilson, "Ambient Noise in the Eurasian Basin", *USN J. Underwater Acoust.*, 38(4), 433-455, (1988). (CONFIDENTIAL Document).

Pritchard, R. S., "Arctic Ocean Backgound Noise Caused by Ridging of Sea Ice", *J. Acoust. Soc. Am.*, 82(3), 988-997, (1987).

Pritchard, R. S., "Eastern Arctic Ambient Noise", *Oceans '89*, Vol. 4, 1246-1251, (1989).

Pritchard, R. S., Personal Communication With the Author, Naval Postgraduate School, Monterey, CA, (1991).

Serreze M. C., "Seasonal and Interannual Variations of Sea Ice Motion In the Canada Basin and Their Relationships with the Arctic Atmospheric Circulation", Ph.D. Thesis, University of Colorado, Boulder, Colorado, (1989).

Schwiderski E. W., "Tides", in: *The Nordic Seas*, edited by B. Hurdle, 219, New York, (1986).

Schwiderski E. W., "Global Ocean Tides, Part II: The Semidiurnal Principal Lunar Tide (M_2), Atlas of Tidal Charts and Maps", *NSWC TR 79-414*, Naval Surface Weapons Center, Dahlgren, Virginia, (1989).

Thorndike A. S., "Kinematics of Sea Ice", in: *The Geophysics of Sea Ice*, edited by N. Untersteiner, Plenum Press, New York, 489-550, (1986).

Thorndike A. S., R. Colony, "Large Scale Ice Motion in the Beaufort Sea During AIDJEX, April 1975 - April 1976", *Sea Ice Processes and Models*, edited by R. S. Pritchard, University of Washington Press, Seattle, Washington, 249-260, (1980).

Thorndike A. S., R. Colony, "Sea Ice Motion in Response to Geostrophic Winds", *J. Geophys Res.*, (87)(C8): 5845-5852, (1982).

Urick R. J., *Principles of Underwater Sound*, 3rd Edition, McGraw-Hill Book Company, New York, 224-227, (1983).

Weeks W. F., M. Mellor, "Mechanical Properties of Sea Ice in the Actic Seas", in: *Arctic Technology and Policy*, edited by I. Dyer and C. Chryssostomidis, Hemisphere Publishing, Washington, 235-260, (1986).

Zubov N. N., "Arctic Ice", *Izd. Glavsevmorputi*, Moscow, 1-360, (1943). (U.S. Navy Hydrographic Office, translation 217, 1963; available as AD426972, NTIS, Springfield, VA, (1963)).

INITIAL DISTRIBUTION LIST

		No. Copies
1.	Superintendant Attn: Library, Code 52 Naval Postgraduate School Monterey, CA 93943-5000	2
2.	Superintendent Attn: Chairman, Department of Oceanography (Code OCCo) Naval Postgraduate School Monterey, CA 93943-5000	1
3.	Superintendent Attn: Professor Robert H. Bourke (Code OCBf) Naval Postgraduate School Monterey, CA 93943-5000	3
4.	Commanding Officer Attn: Lt John D. Cousins Precommissioning Detachment Essex (LHD-2) Fleet Training Center, Code 30 Naval Station San Diego (32nd Street) San Diego, CA 92136-5035	1
5.	Commanding Officer Attn: Dr. William Jobst Naval Oceanographic Office NSTL Station Bay St. Louis, MS 39522	1
6.	Commanding Officer Naval Ocean Research and Development Activity NSTL Station Bay St. Louis, MS 39522	1
7.	Commanding Officer Naval Polar Oceanography Center, Suitland Washington, DC 20373	1
8.	IceCasting Inc. Attn: Dr. Robert S. Pritchard 11042 Sand Point Way N.E. Seattle, WA 98125-5846	2
9.	Superintendant Attn: Dr. John Newton (Code OC/Ne) Naval Postgraduate School Monterey, CA 93943-5000	1

10. Dr. Warren Denner 1
11650 McCarthy Road
Carmel, CA 93924

11. Professor Arthur B. Baggeroer 1
Room 5-326
Ocean Engineering Department
Massachusetts Institute of Technology
Cambridge, MA 02139

Thesis
C756783 Cousins
c.1 CEAREX ambient noise
data measured northeast
of Svalbard.

Thesis
C756783 Cousins
c.1 CEAREX ambient noise
data measured northeast
of Svalbard.

DUDLEY KNOX LIBRARY
3 2768 00014498 4